From the Institute of Epidemiology, Helmholtz Zentrum München
German Research Center for Environmental Health
and the Chair of Epidemiology, Ludwig-Maximilians-Universität Munich
Director: Prof. Dr. Annette Peters

Cardiometabolic Risk: Assessment by traditional and novel imaging-based markers

Thesis submitted for a Doctoral degree in Human Biology
at the Faculty of Medicine
Ludwig-Maximilians-Universität, Munich

by
Susanne Ina Rospleszcz
from Munich, Germany

2019

With approval of the Medical Faculty
of the Ludwig-Maximilians-Universität Munich

Supervisor:	Prof. Dr. Annette Peters
Co-Examiners:	Prof. Dr. Dirk-André Clevert
	Priv. Doz. Dr. Bernhard Bischoff
Dean:	Prof. Dr. med. dent. Reinhard Hickel
Date of oral exam:	09. 07. 2019

Eidesstattliche Versicherung

Rospleszcz, Susanne

Name, Vorname

Ich erkläre hiermit an Eides statt,

dass ich die vorliegende Dissertation mit dem Thema

Cardiometabolic Risk: Assessment by traditional and novel imaging-based markers

selbständig verfasst, mich außer der angegebenen keiner weiteren Hilfsmittel bedient und alle Erkenntnisse, die aus dem Schrifttum ganz oder annähernd übernommen sind, als solche kenntlich gemacht und nach ihrer Herkunft unter Bezeichnung der Fundstelle einzeln nachgewiesen habe.

Ich erkläre des Weiteren, dass die hier vorgelegte Dissertation nicht in gleicher oder in ähnlicher Form bei einer anderen Stelle zur Erlangung eines akademischen Grades eingereicht wurde.

München, 14.12.2018

Ort, Datum

Susanne Rospleszcz

Unterschrift Doktorandin/Doktorand

Für meine Eltern.

Contents

Abstract

Summary

Background. Cardiometabolic diseases are the major cause of mortality and morbidity worldwide. Diagnosis at a pre-pathological state, before irreversible damage has been imposed on the organism, is therefore essential to disease prevention. Risk assessment is important in clincial decison making to tailor therapeutic intervention to those who benefit most, but also fundamental for developing general treatment guidelines and public health care policies. Cardiometabolic risk can be assessed by an absolute percentage estimate, i.e. a risk score, or by a deeper phenotypic characterization of the pre-pathological disease state. Risk scores are mainly constructed from traditional cardiometabolic risk factors, such as blood pressure or lipid profile, and can be utilized for risk stratification. However, these traditional risk factors - and hence the risk scores - cannot provide a thorough depiction of the subclinical cardiometabolic phenotype.
Imaging-based markers of cardiometabolic disease, derived by Magnetic Resonance Imaging (MRI), are able to detailedly picture anatomical and physiological changes. Thus, they have the potential to characterize the subclinical cardiometabolic phenotype more acurately and hence advance risk assessment.
This thesis aims to identify temporal trends in the development of traditional cardiometabolic risk factors and the subsequent impact on established risk scores; and to quantify the association of imaging-based markers to cardiometabolic phenotypes.

Methods. We used data from the KORA study, which comprises several well-characterized population-based cohorts from the region of Augsburg, Southern Germany. Three cohorts enrolled in 1989/1990, 1994/1995 and 1999/2000, respectively, were analyzed for their cardiometabolic risk factor profiles and for the performance of two established risk scores regarding discrimination and calibration. Another sample of N = 400 individuals underwent whole-body imaging by MRI. For these individuals, we constructed multivariate longitudinal trajectory clusters of cardiometabolic risk factors and related them to a panel of MRI-derived abdominal and ectopic adipose tissue parameters. Furthermore, we assessed associations of prediabetes and type 2 diabetes to cardiac morphology as well as to a cluster of MRI parameters covering several organs. To this aim, an unsupervised fuzzy clustering algorithm and regularized LASSO regression for variable selection were employed.

Results. There were temporal trends in cardiometabolic risk factor profiles. For instance, mean Body Mass Index, mean systolic blood pressure, and mean total cholesterol significantly decreased; at the same time, intake of antihypertensive and lipid-lowering medication increased. This affected the performance of risk scores in a sex-specific way: while

the scores gained discrimination ability for women, performance for men dropped. However, discrimination ability was still adequate at all time points.
Longitudinal trajectory clusters of risk factors were significantly associated to MRI-derived adipose tissue compartments. The variation in adipose tissue that could be explained by these clusters varied to a substantial degree, with highest values for total abdominal adipose tissue and lowest values for intrahepatic fat. Furthermore, there were significant associations of prediabetes and type 2 diabetes to measurements of myocardial wall thickness as well as to a cluster of MRI parameters covering several organs. We identified specific diabetes-related combinations of MRI parameters, which included abnormal values of visceral adipose tissue and intrahepatic fat.

Conclusion. While risk scores based on traditional cardiometabolic markers still perform adequately and capture a major part of cardiovascular risk burden, imaging-based phenotyping has a substantial potential to early recognize pre-pathological cardiometabolic states.

Zusammenfassung

Hintergrund. Kardiometabolische Erkrankungen sind die Hauptursache für Mortalität und Morbidität weltweit. Es ist daher essentiell für die Krankheitsprävention, diese Erkrankungen zu einem prä-pathologischen Stadium zu diagnostizieren, bevor irreversible Schädigungen bereits aufgetreten sind. Risikoeinschätzungen sind für die klinische Entscheidungsfindung wichtig, um therapeutische Maßnahmen denjenigen zukommen zu lassen, die am meisten davon profitieren. Sie sind aber auch grundlegend, um allgemeine Behandlungsleitlinien festzulegen sowie öffentliche Gesundheitspolitik zu entwerfen. Das kardiometabolische Risiko kann anhand einer absoluten Prozentzahl eingeschätzt werden, d.h. durch einen sogenannten Risikoscore; es kann jedoch auch durch eine genauere Betrachtung des prä-pathologischen Krankheitsstadiums bewertet werden. Risikoscores werden üblicherweise aus klassischen kardiometabolischen Risikofaktoren gebildet, wie z.B. Blutdruck und Lipiden, und können zur Risikostratifizierung verwendet werden. Die klassischen Risikofaktoren, und somit auch die Risikoscores, können jedoch keine tieferen Einblicke in den subklinischen kardiometabolischen Phänotyp geben.
Bildgebungsbasierte Marker, die durch Magnetresonanztomographie (MRT) gewonnen werden, sind in der Lage, anatomische und physiologische Veränderungen detailliert darzustellen. Sie haben daher das Potential, die Einschätzung des kardiometabolischen Risikos durch die genauere Charakterisierung des subklinischen kardiometabolischen Phänotyps zu verbessern.
Ziel dieser Arbeit ist, zeitliche Trends in der Entwicklung klassischer kardiometabolischer Risikofaktoren und deren Einfluss auf die Leistung etablierter Risikoscores zu bestimmen;

außerdem soll die Assoziation bildgebungsbasierter Marker mit kardiometabolischen Phänotypen quantifiziert werden.

Methoden. Es wurden Daten der KORA Studie verwendet, die mehrere gut charakterisierte bevölkerungsbasierte Kohortenstudien aus der Region Augsburg umfasst. Drei Kohorten, die in den Jahren 1989/1990, 1994/1995 und 1999/2000 erfasst wurden, wurden auf ihr kardiometabolisches Risikoprofil untersucht; außerdem wurde die Leistung zweier etablierter Risikoscores hinsichtlich Diskrimination und Kalibrierung analysiert. Eine weitere Stichprobe von N = 400 Probanden unterzog sich einem Ganzkörper-MRT. Für diese Probanden wurden Cluster von multivariaten longitudinalen Trajektorien, basierend auf klassischen kardiometabolischen Risikofaktoren, konstruiert und die Assoziation dieser Cluster mit Parametern von abdominellem und ektopischem Fettgewebe bestimmt. Desweiteren wurden die Assoziationen von Prädiabetes und Typ 2 Diabetes mit kardialer Morphologie und mit einem Cluster verschiedener, mehrere Organe umspannender MRT Parameter berechnet. Dazu wurde ein Fuzzy Clustering Algorithmus sowie zur Variablenselektion eine regularisierte LASSO Regression verwendet.

Ergebnisse. Es gab zeitliche Trends in kardiometabolischen Risikoprofilen. Zum Beispiel nahmen der mittlere Body Mass Index, der mittlere systolische Blutdruck, und das mittlere Gesamtcholesterin über die Zeit ab; gleichzeitig stieg die Einnahme von Antihypertonika und Lipidsenkern über die Zeit an. Dadurch wurde die Leistung der Risikoscores in einer geschlechtsspezifischen Weise beeinflusst: während die Diskriminationsleistung der Scores bei Frauen anstieg, fiel die Leistung bei Männern ab. Dennoch war die Diskriminationsleistung zu allen Zeitpunkten immer noch ausreichend.
Cluster von multivariaten longitudinalen Trajektorien waren signifikant mit MRT-erfassten Fettgewebeparametern assoziiert. Die Variabilität in Fettgewebe, die von den Clustern erklärt werden konnte, schwankte stark. Die höchsten Werten erreichte das gesamte abdominelle Fett und die niedrigsten Werten das intrahepatische Fett. Darüber hinaus gab es signifikante Assoziationen des Prädiabetes und Typ 2 Diabetes zu Messungen myokardialer Wanddicke sowie zu einem Cluster verschiedener MRT Parameter, die mehrere Organe umspannten. Spezifische Diabetes-typische Kombinationen von MRT Parametern konnten identifiziert werden; diese beinhalteten anormale Werte von Viszeralfett und intrahepatischem Fett.

Schlussfolgerung. Während Risikoscores, die auf klassischen kardiometabolischen Markern basieren, nach wie vor genügende Leistung zeigen und den Großteil der kardiovaskulären Krankheitsbelastung erfassen, hat die Phänotypisierung durch bildgebungsbasierte Marker substantielles Potenzial, das prä-pathologische Stadium kardiometabolischer Erkrankungen frühzeitig zu erkennen.

List of Abbreviations

AHA American Heart Association

ARIC Atherosclerosis Risk in Communities

ARWMC Age Related White Matter Changes

AUC Area under the Curve

BMI Body Mass Index

BP blood pressure

CHD coronary heart disease

CI Confidence Interval

CT Computed Tomography

CVD Cardiovascular Disease

EDV end-diastolic volume

EF ejection fraction

EM Expectation-Maximization

ESV end-systolic volume

FHS Framingham Heart Study

FRS Framingham Risk Score

HDL High Density Lipoprotein

(i)-IFG (isolated) Impaired Fasting Glucose

(i)-IGT (isolated) Impaired Glucose Tolerance

KORA Cooperative Health Research in the Region of Augsburg

LASSO Least Absolute Selection and Shrinkage Operator

LDL Low Density Lipoprotein

LGE Late Gadolinium Enhancement

LV left ventricular

MESA Multi Ethnic Study of Atherosclerosis

MI myocardial infarction

MRI Magnetic Resonance Imaging

PAF Population Attributable Fraction

PCE Pooled Cohort Equations

PDFF proton-density fat fraction

PROCAM Prospective Cardiovascular Münster Study

ROC Receiver Operating Characteristic

SAT subcutaneous adipose tissue

SCORE Systematic Coronary Risk Evaluation

SHIP Study of Health in Pomerania

TAT total adipose tissue

VAT visceral adipose tissue

WC waist circumference

WHO World Health Organization

WML white matter lesions

1 Background

1.1 Concept of cardiovascular and cardiometabolic risk

Cardiometabolic diseases impose a major burden on global health. Cardiovascular Disease (CVD), specifically ischemic heart disease, is the major cause of mortality worldwide [1], although there is a decreasing trend in Europe. The prevalence of obesity, type 2 diabetes and related metabolic disorders is substantial, and steadily increasing. The prevalence of obesity has risen by 30% in the last decades [2] and although the increase rates in developed countries have been slowing down, obesity still presents a central public health challenge. In the same vein, the global diabetes prevalence is estimated to be over 10% by 2040 [3].

Cardiometabolic diseases are by definition complex and multi-factorial. Various extrinsic and intrinsic parameters contribute to the development of these disorders and act conjointly. Important parameters are lifestyle choices, such as nutrition habits, physical activity, sedentary behavior and smoking. Especially the rise in obesity has been attributed to an aggravation in these lifestyle choices and behaviors. Those parameters can theoretically be controlled by each person individually; however they are also affected by societal, cultural and economic influences [4]. Other environmental parameters, such as air pollution, noise, and stress can be influenced by an individual only to a limited degree. Finally, there are intrinsic genetic and epigenetic parameters which contribute to an individual's predisposition to cardiometabolic disease [5].

In a long-term process, an individual's phenotype manifests itself, defined by the traditional CVD risk factors: high blood pressure, high levels of total cholesterol and Low Density Lipoprotein (LDL) cholesterol, low levels of High Density Lipoprotein (HDL) cholesterol or high Body Mass Index (BMI). These factors were already established by early population-based studies such as the Framingham Heart Study (FHS) [6]. Unfavorable risk factor profiles are associated to a higher risk of cardiometabolic disease. The concept of cardiometabolic risk implies that an unfavorable risk factor profile that predisposes to a higher probability of experiencing cardiometabolic disease can be measured and used to determine who might benefit from an early intervention.

Usually, when cardiometabolic diseases are therapeutically treated, there is already irreversible damage to the organism, e.g. after a myocardial infarction (MI) or at the diagnosis of diabetes. Diagnosing these diseases at an earlier, pre-pathological level, before symptoms are emerging and irreversible damage has been imposed on the organism, is therefore essential to disease prevention. When cardiometabolic diseases are detected at earlier stages, lifestyle changes or treatment by medication might inhibit further disease

progression and damage.

Risk assessments are crucial for treating physicians to decide who might benefit most from therapeutic intervention. Communication of long-term CVD risk can also help to encourage individuals to initiate or maintain lifestyle changes and pharmacological treatments. Furthermore, community-based risk assessments are also essential to develop general treatment guidelines and broader health care policies. Societies like the American Heart Association (AHA) or the European Society of Cardiology recommend regular CVD risk assessment and communication [7, 8]. Some scientific reports indicate that periodical check-ups by general practitioners result in lower CVD mortality, though the evidence is not yet firmly established [9, 10].

Risk can be assessed in absolute percentage quantities, e.g. by a risk score which predicts an individual's risk to experience disease within a specified time span in the future. However, risk can also be assessed by a more detailed characterization of the intermediate, pre-pathological disease state. A better understanding of how traditional risk factors and metabolic phenotypes are connected can help to elucidate potential pathophysiological pathways and thereby potential cardiometabolic risk.

1.2 Traditional markers and CVD risk scores

Traditional CVD markers such as blood pressure, lipid profile and glycemic status are readily obtained in standard clinical practice. Traditional markers are the basis for various established risk scores that estimate an individual's CVD risk. These risk scores work with different risk factors as covariables for an underlying regression model - usually a Cox Proportional Hazards model- and predict the probability to experience a cardiovascular event within a specified time frame, e.g. five years or ten years. Patients can then be stratified according to their predicted risk and treatment, e.g. antihypertensive medication or statin therapy can be tailored accordingly.

For the estimation of CVD risk, a variety of published risk scores is available. Their usefulness is often questionable, as many are not properly documented, suffer from methodological shortcomings or have not been externally validated [11]. However, there are a number of established risk scores, which have been proven to be useful and are commonly employed. These risk scores have mostly been derived from population-based cohorts and also externally validated. The commonly used CVD risk scores are outlined in the following.

Framingham Risk Score (FRS). Derived from the FHS and its offspring cohorts, three main risk scores have been established. The first one was published in 1998 [12] and predicts coronary heart disease (CHD) and hard CHD outcomes for a 10 year time frame. It is

applicable to men and women in the age range of 30 to 74 years without prior CHD. Predictor variables comprise age, systolic and diastolic blood pressure (BP), HDL cholesterol, LDL cholesterol - or, in an alternative version, total cholesterol - , presence of diabetes and smoking behavior. Estimates for 10 year risk of CHD were obtained from a Cox regression model. By categorizing continuous variables, the well-known score sheets were created, which allow practitioners to easily calculate their patient's CHD risk by adding up points from the score sheets. Framingham 1998 has been validated in several other studies, e.g. [13, 14].

The second score was made available in 2002. It only predicts hard CHD outcomes for a time frame of 10 years in men and women aged from 30 to 79 years without prior CHD and, importantly, without prevalent diabetes. Predictor variables are age, quadratic term of age, systolic BP, total and HDL cholesterol, antihypertensive treatment, smoking behavior as well as interaction terms of age with cholesterol and age with smoking. The score has been applied in other population-based cohorts [15, 16].

The third score stems from 2008 [17]. Predicted outcome is CVD for a 10 year time frame in men and women in the age range from 30 to 74 years without prior CHD. Predictor variables are age, systolic BP, total and HDL cholesterol - or, in an alternative version, BMI instead of both lipid values -, antihypertensive treatment, smoking behavior and presence of diabetes. Given the number of outcomes predicted, this score is the most versatile of all three. It has been validated in several other population-based cohorts [18, 19]. Throughout the remainder of this thesis, the notation FRS will denote the 2008 Framingham score. As all Framingham risk scores have been constructed from data from the FHS which included mainly Caucasian participants, the translation of the estimates to other ethnic groups is not straightforward. Also, as already mentioned above, the FHS is one of the oldest population-based studies. This might imply that the transferability of their risk profile to chronologically more current cohorts is questionable.

Systematic Coronary Risk Evaluation (SCORE). This risk score is derived from twelve population-based cohorts throughout Europe [20]. It predicts only CHD mortality, i.e. fatal CHD cases in men and women aged 45 to 64 years. Risk estimates are based on a Weibull Proportional Hazards model where the baseline survival is modeled by a function of age and sex and relative risks are calculated for sex, systolic BP, total cholesterol - or, in an alternative version, ratio of total to HDL cholesterol -, and smoking behavior. SCORE Risk estimates are also available as point sheets for easier utilization by practitioners. The score has been applied in other cohorts, e.g [21, 22] and the use of SCORE for risk stratification is recommended by the European Society of Cardiology [7].

Prospective Cardiovascular Münster Study (PROCAM). The PROCAM study consists

of men and women employed at companies and government authorities in the region of Münster, Germany. The PROCAM risk score, however, has only been derived and validated on male participants of the study. It predicts CHD for a 10 year time frame based on a Cox model with predictor variables age, systolic BP, LDL and HDL cholesterol, triglycerides, smoking behavior, family history of MI and diabetes. PROCAM has been validated in other studies [15, 23].

QRISK2. QRISK2 is the first update of the original QRISK Score [24]. It predicts CHD, stroke, and transient ischaemic attack in men and women aged 35-74 years. The score includes the following risk factors: age, sex, systolic BP, BMI, ratio of total cholesterol to HDL cholesterol, family history of CHD in a first degree relative, Townsend deprivation score, ethnicity (self-reported), smoking behavior, and presence of type 2 diabetes, hypertension treatment, renal disease, atrial fibrillation, and rheumatoid arthritis. The score was derived on approximately 1.5 million patients from 355 medical practices in the UK. The use of QRISK is recommended by the UK National Institute of Health and Care Excellence [25]. Meanwhile there is also QRISK3, which updates QRISK2 and incorporates even more covariates [26].

Pooled Cohort Equations (PCE). This risk score was constructed and recommended by the 2013 Guidelines on the Assessment of Cardiovascular Risk from the American College of Cardiology and the AHA [27]. It predicts 10 year risk of atherosclerotic CVD (death from CHD or stroke and nonfatal MI and stroke) in men and women aged 40 to 79 without prior atherosclerotic CVD. The PCE risk score was derived from five community-based cohorts from the US and provides risk estimates for multiple ethnicities. Predictor variables encompass age, systolic BP, total and HDL cholesterol, antihypertensive treatment, smoking behavior and presence of diabetes.

Efforts to improve the performance of established risk scores, especially FRS, are constantly undertaken, but prove to be difficult [28, 29]. One central point of criticism directed at the FRS is that the cohorts from which these scores originated are decades old. In the meantime, healthcare and treatment regimes have changed and thus the distribution of risk factors in the population might not be comparable to current cohorts. However, to which extent a changing risk factor distribution in the population affects the performance of the FRS has not been quantified so far.
Stratification according to an absolute value of predicted risk can be used to assign treatments, however it does not give insight into potential disease pathways and processes. This is were imaging-based markers enter the stage.

1.3 Current status of imaging-based phenotyping

Compared to traditional CVD risk factors, imaging-based markers are able to provide a deeper insight into anatomical and physiological changes. With imaging data, a detailed visualization of an individual's phenotype is available, which confers important information about disease processess and manifestations. This information can further be used in the context of personalized treatment.

In clinical practice, various imaging modalities such as Computed Tomography (CT), sonography and Magnetic Resonance Imaging (MRI) are routinely used when indicated. To be used prognostically for asymptomatic individuals, however, modalities like CT where individuals are exposed to radiation cannot ethically be employed. Modalities like sonography suffer from low reproducibility and provide prognostic value only in few situations such as specific applications of echocardiography, e.g analyses of cardiac valves. Therefore, for imaging in clinically healthy individuals, MRI is usually the imaging modality of choice. Besides the advantage of non-radiation and high reproducibility, MRI is also characterized by high-resolution and high quality images. Furthermore, whole-body imaging is possible, which enables studying multiple organ systems simultaneously.

Data contained in this thesis is derived from the Cooperative Health Research in the Region of Augsburg (KORA) study, which will be described more thoroughly in the Methods section. Besides the KORA study, several other population-based studies have already included MRI protocols in their standardized examinations, or are planning to do so, to exploit the potential of these data. These studies are briefly outlined in the following.

FHS. The design of the FHS has already been introduced above. Imaging in the FHS focused on brain and cardiac data. Approximately N $\approx$ 2500 individuals from the Framingham Offspring Cohort underwent brain MRI and N $\approx$ 1800 underwent cardiac MRI on a 1.5T machine. Main findings from the FHS-MRI studies include the association of white matter lesions (WML)s to cerebrovascular risk factors [30], establishing WMLs as potential risk factors for stroke and Alzheimer's Disease [31] and the description of sex differences in key cardiac parameters [32].

The Rotterdam Scan Study. The Rotterdam Study is a prospective population-based cohort from the Netherlands comprising $\approx$ 15 000 individuals aged 45 or older enrolled in different cycles between 1990 and 2008. Imaging in the Rotterdam Scan Study focused on brain and carotid arteries; N $\approx$ 6000 underwent brain MRI and $\approx$ 2000 underwent scanning of the carotid arteries on a 1.5T scanner. Relevant results from imaging in this study are e.g. reporting of the high prevalence of cerebral microbleeds [33] and assymetrical distribution of carotid plaque burden [34].

Multi Ethnic Study of Atherosclerosis (MESA). This US study was primarily designed to study the progression of subclinical, asymptomatic CVD in the general population. Imaging in MESA focused on cardiac MRI and has longitudinal measurements available: N = 5004 participants underwent cardiac imaging at the baseline examination between 2000-2002 and N = 3015 participated in a follow up, including MRI, 10 years later. Measurements were taken at six study centers on a 1.5T scanner. Relevant findings from MESA include the establishment of reference values for left ventricular (LV) wall thickness [35], associations of obesity to LV structure [36] and development of LV parameters with age [37].

Study of Health in Pomerania (SHIP). The SHIP-TREND study is a population-based cohort from North-East Germany including N = 4420 participants enrolled between 2008 and 2012. N = 2188 participants underwent whole-body MRI on 1.5T scanners, including measures of adipose tissue, cardiac structure and function and brain data. Important findings from SHIP include reporting of prevalences of hepatic steatosis [38] and the impact of incidental findings on participants [39].

UK Biobank. This study is among the largest ongoing population studies and comprises 500 000 participants from the general UK population, enrolled from 2006-2010. Imaging by MRI focused on brain, heart and abdomen is still ongoing and is planned on 100 000 individuals [40].

German National Cohort. This currently still ongoing study aims to enroll 200 000 individuals from the general population across Germany [41]. Besides standardized interviews and examinations, 30 000 participants are planned to undergo whole-body MRI, including assessments of adipose tissue, brain parameters and cardiac function and morphology. Scans are performed on 3T scanners at five study centers [42].

MRI-based imaging becomes especially relevant in the context of cardiometabolic disease. Besides the possibility to detailedly depict the myocardium, including measures of LV function and structure, also precise assessment of segments of LV wall thickness are feasible. MRI is also the gold standard for quantifying adipose tissue. Different adipose tissue compartments vary substantially in their metabolic activity and their systemic role in metabolism. Adipose tissue is a metabolically active endocrine organ and confers a high amount of information about metabolic risk. Particularly the accrual of ectopic fat, i.e. storage of adipose tissue in and around organs such as liver, kidney and pancreas has been recognized as an important factor in metabolic diseases [43, 44]. Traditional markers of body size are BMI and waist circumference (WC), as they are (relatively) easily obtained. However, these rather crude measures only give an incomplete picture about body fat distribution and cannot accurately report the actual amount of metabolically

active adipose tissue, which is one key strength of quantification by MRI.

1.4 Special role of type 2 diabetes

Among the traditional CVD risk factors, diabetes takes an important position. The debate whether diabetes can be considered a CHD equivalent, has not yet been fully resolved. The concept of diabetes as a CHD equivalent implies that individuals with diabetes have the same risk to experience a CHD event in the future as do individuals without diabetes, who already suffered from a prior CHD event.

A seminal study in this respect was published 20 years ago, finding that the CHD risk of individuals with diabetes was indeed equivalent to those with prior CHD [45]. The AHA has implemented the risk equivalence in their 2002 guidelines for statin therapy (Adult Treatment Panel III, [46]). European guidelines [47] place individuals with diabetes in the highest risk category, without specifically claiming a risk equivalence.

However, published data are not unequivocally in favor of this interpretation. A meta-analysis including cohort and observational studies with a follow-up period of five years or longer, came to the conclusion that diabetes in itself is not a CHD risk equivalent [48]; as the summary odds ratio for individuals with diabetes to develop CHD was 0.56 compared to individuals with prior CHD. Another meta-analysis [49] found that CVD risk in diabetes was strongly depending on sex; the unfavorable effect of diabetes was higher in women than in men.

Although the equivalence of prior CHD and diabetes in CHD risk is questionable, it is undisputed that diabetes predisposes to a higher CVD risk. Concomitant risk factors and diabetes duration are likely contributors [50]. Current data indicate that diabetes-related cardiac damage such as peripheral artery disease modulates the higher CVD risk [51]. Imaging-based markers can therefore help to shed light on changes in cardiac structure and function in individuals with diabetes. Moreover, as diabetes has systemic effects on the organism, it is therefore of interest to holistically study multiple organs together.

Furthermore, as the glycemic spectrum is continuous, there are precursor states of diabetes, termed intermediate hyperglycemia or prediabetes. These terms comprise both (isolated) Impaired Fasting Glucose ((i)-IFG) and (isolated) Impaired Glucose Tolerance ((i)-IGT). The World Health Organization (WHO) defines (i)-IFG as fasting glucose levels between 110 and 125 mg/dL with normal 2h glucose levels and (i)-IGT as 2h glucose levels between 140 and 200 mg/dL with normal fasting glucose levels, with 2h glucose obtained after an Oral Glucose Tolerance Test. Individuals with prediabetes have a high risk to progress to overt diabetes during their lifetime [52].

Prediabetes represents an important phenotype, as (i)-IFG and (i)-IGT are associated to increased risk of CVD and mortality [53]. Possible pathways include fibrinolytic dysfunction of the endothelium and impaired blood flow in the microvasculature, although the mechanisms are not fully elucidated [54]. However, prediabetes is not a homogeneous entity; not everyone with prediabetes will progress to diabetes and not everyone will profit from pharmacological treatment. In the clinical setting, prediabetes often remains undiagnosed, as it is usually asymptomatic. Therefore, particularly in the context of diabetes and prediabetes, imaging-based markers can serve to elucidate and characterize the systemic roles of impaired glucose metabolism by visualizing changes in physiology and anatomy.

1.5 Specific aims of the thesis

The objective of this thesis is to characterize and quantify the role of traditional and novel imaging-based markers in the context of metabolic risk assessment. For that purpose, the focus is on epidemiological outcomes, i.e. how imaging-based markers associate to cardiometabolic risk, rather than the technical derivation of these imaging-based markers. Specifically, the aims of this thesis are

(a) To evaluate the temporal development of traditional cardiovascular risk factors in different population-based cohorts spanning several time frames and characterize the corresponding development of CVD risk scores - these questions will be treated in manuscript I [55] as outlined in the next section.

(b) To identify longitudinal clusters of traditional cardiovascular risk factor trajectories and associate them to imaging-based metabolic phenotypes - these questions will be treated in manuscript II [56] as outlined in the next section.

(c) To assess the relation of imaging-based metabolic phenotypes to diabetes and its precursor states and identify specific diabetes-related imaging-based signatures - these questions will be treated in manuscripts III [57] and IV [58] as outlined in the next section.

2 Contributing manuscripts

2.1 Manuscripts included in the thesis

This cumulative thesis comprises four manuscripts, which will be referred to with Roman numericals I through IV. A simplified overview of manuscripts I through IV is given in Figure 1, followed by a more detailed description. Three of the manuscripts have been prepared within the framework of the KORA-MRI study, where I also contributed to other manuscripts which are relevant in the context of cardiometabolic risks. Those manuscripts are outlined in the next section.

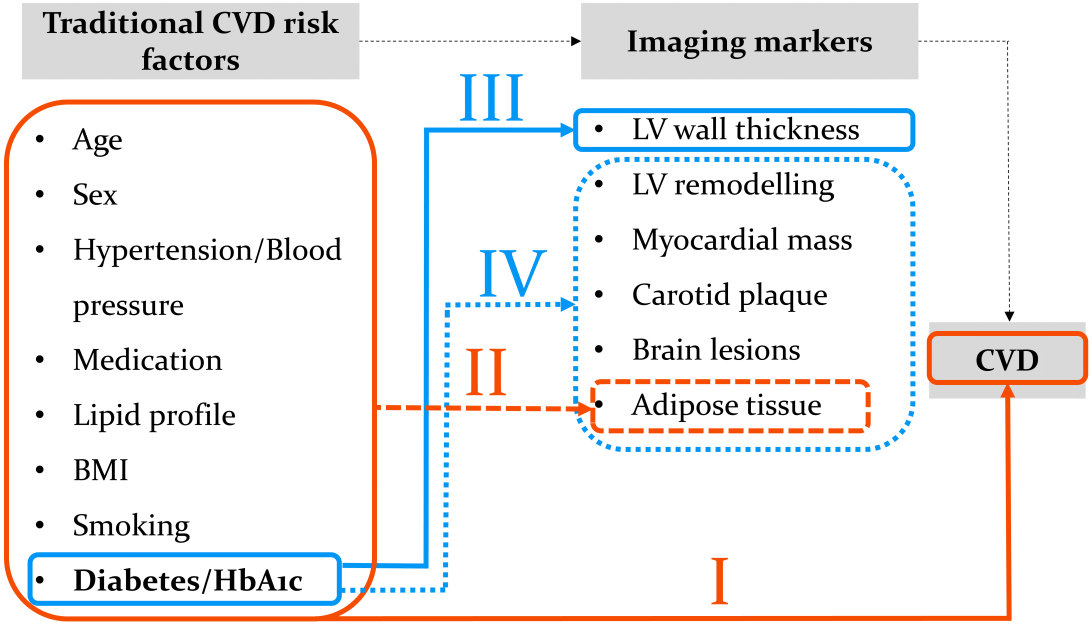

Figure 1: Overview of contributing manuscripts. Thick lines connecting traditional CVD risk factors to imaging markers/CVD denote the associations that are treated within each manuscript. Manuscript I describes the association of traditional risk factors to CVD by analysis of CVD risk scores. Manuscript II describes the association of traditional risk factors to MRI measurements of adipose tissue. Manuscript III describes the association of prediabetes and type 2 diabetes to MRI measurements of LV wall thickness. Manuscript IV describes the association of prediabetes and diabetes to MRI measurements covering several organs. The thin dotted lines connecting Traditional CVD risk factors to Imaging markers to CVD denote the underlying implied association, which is causally probable, but not treated within this thesis.

Manuscript I: Temporal evolvement of CVD risk factors and Risk Scores
In this paper, we analyzed data of n = 7789 individuals from three prospective population-based cohort studies enrolled in 1989/1990, 1994/1995 and 1999/2000. We found significant temporal trends in risk factor distributions which were also reflected in a changing

performance of two commonly used CVD risk scores (FRS and PCE). Nevertheless, the performance of the two risk scores was still adequate and the incorporated risk factors captured a major burden of CVD.
I am first author of the manuscript. I developed the research question to a substantial extent, developed the statistical analysis plan, conducted the statistical analyses, evaluated the results, drafted the paper and revised it according to peer reviewers' comments.
This manuscript is published as "**Temporal trends in cardiovascular risk factors and performance of the Framingham Risk Score and the Pooled Cohort Equations**" in *BMJ Journal of Epidemiology and Community Health* [55].

Manuscript II: Longitudinal Trajectory Clusters and Adipose Tissue
In this paper, we worked with longitudinal data of n = 325 individuals obtained at three time points covering 14 years. We first determined multivariate clusters of the conjoint trajectories of nine traditional CVD risk factors and then associated them to a comprehensive panel of adipose tissue depots obtained by MRI. We found three distinct trajectory clusters which represented graded levels of cumulative risk factor burden and which showed graded associations to all adipose tissue traits.
I am shared first author of the manuscript. I contributed to the research question by directing the focus on outcomes of adipose tissue. I developed the main part of the statistical analysis plan by introducing the longitudinal multivariate k-means clustering method, conducted all statistical analyses, evaluated the results and drafted the paper.
This manuscript will be submitted as "**Association of longitudinal risk profile trajectory clusters with adipose tissue depots measured by magnetic resonance imaging**" [56].

Manuscript III: Diabetes and LV Wall Thickness
In this paper, we analyzed the impact of prediabetes and type 2 diabetes on LV wall thickness, as increased LV wall thickness is a marker for future cardiovascular complications. To identify regional LV remodeling, we used the established LV 16-segments model of the AHA. We found significant associations of prediabetes and diabetes to overall wall thickness, as well as single segment groups as well as interaction effects with blood pressure in certain segments of the LV wall.
I am first author of the manuscript. I developed the research question, designed the statistical analysis plan, conducted the statistical analyses, evaluated the results, drafted the paper and revised it according to peer reviewers' comments.
This manuscript is published as "**Association of glycemic status and segmental left ventricular wall thickness in subjects without prior cardiovascular disease: a cross-sectional study**" in *BMC Cardiovascular Disorders* [57].

Manuscript IV: Multiorgan Involvement in Diabetes
In this paper, we worked with six MRI parameters (Age Related White Matter Changes (ARWMC), intrahepatic fat as measured by proton-density fat fraction (PDFF), visceral adipose tissue (VAT), LV remodeling, carotid plaque, Late Gadolinium Enhancement (LGE)) that were dichotomized into "normal" and "abnormal" values according to predefined clinical cutoffs. We constructed a phenotypic score from these six dichotomized parameters and found that high values of the score were strongly correlated to prediabetes and diabetes status. Furthermore, unsupervised fuzzy clustering of the dichotomized parameters revealed two distinct clusters which were highly associated to prediabetes and diabetes status. Finally, specific combinations containing abnormal values of intrahepatic fat and VAT were specific for prediabetes and diabetes status, as identified by regularized Least Absolute Selection and Shrinkage Operator (LASSO) regression.
I am second author of the manuscript. I designed parts of the statistical analysis plan by introducing LASSO regression and fuzzy clustering, conducted the statistical analyses, created tables and graphics and wrote parts of the manuscript.
This manuscript is published as **"Phenotypic Multiorgan Involvement of Subclinical Disease as Quantified by Magnetic Resonance Imaging in Subjects With Prediabetes, Diabetes, and Normal Glucose Tolerance"** in *Investigative Radiology* [58].
Largely based on work from this paper, we successfully applied for a grant from the German Center of Diabetes Research (DZD), enabling us to continue and extend this the work in a collaboration with the SHIP study from Greifswald, Germany.

2.2 Other manuscripts

The KORA-MRI study is a population-based imaging study and was designed with the specific focus of assessing subclinical disease states in individuals with diabetes and its precursor stages. I was involved in several projects concerned with the assessment of cardiometabolic risk, as itemized below.

Cohort Profile of the KORA-MRI Study [59]. This paper presents the general setup of the KORA-MRI study as well as its main findings. There was a gradually increasing subclinical disease burden from normoglycemic individuals to individuals with prediabetes to diabetes, as measured by key cardiac, neurological and metabolic imaging markers.
I designed the statistical analysis plan, conducted the statistical analyses, created tables and graphics, wrote parts of the manuscript and replied to reviewer comments.

Characteristics of Diverticular Disease [60]. Diverticula are structural alterations in the colonic wall that originate from herniation of the colonic mucosa. Individuals with diverticular disease might be affected by abdominal pain, inflammation and bowel com-

plications. In this paper, prevalence and potential metabolic risk factors of diverticular disease are assessed. The prevalence of diverticular disease was found to be 42% and BMI, cholesterol levels and blood pressure were associated to increased risk of diverticular disease.
I designed the statistical analysis plan, conducted the statistical analyses, created tables and graphics and wrote parts of the manuscript.

Adipose Tissue and Diabetes [61]. This paper demonstrates the association of glycemic status to different adipose tissue compartments (VAT, subcutaneous adipose tissue (SAT)). Results showed a strong correlation of VAT and SAT and a strong association of prediabetes and diabetes to both adipose tissues as well as their ratio. However, an interaction analysis yielded that the marginal effect of both prediabetes and diabetes decreased with rising BMI and WC, indicating that the role of diabetes for cardiometabolic risk recedes behind that of general obesity with rising BMI and WC.
I designed the statistical analysis plan including the focus on interaction effects, analyzed the data, created tables and graphics and wrote parts of the manuscript.

Characteristics of Fatty Muscle [62]. This paper evaluates the amount of fatty infiltration within various skeleto-muscular tissues subject to an individuals glycemic status. Results showed that skeletal muscle in individuals with prediabetes and diabetes had a higher degree of fatty infiltration compared to normoglycemic individuals. However, this was mainly attributable to the higher amount of VAT in these individuals.
I designed the statistical analysis plan, conducted the statistical analyses, created tables and graphics and wrote parts of the manuscript.

Adipose Tissue and Uric Acid [63] This manuscript evaluates cross-sectional associations of uric acid as a breakdown product of purine metabolism to MRI-derived adipose tissue compartments (VAT, SAT, intrahepatic fat). There was a significant association of uric acid to VAT and hepatic fat, but not to SAT, indicating different metabolic properties of the respective adipose tissue depots.
This work is a Master's Thesis that I supervised, written by a student from the MSc Epidemiology Program at the Ludwig-Maximilians-Universität Munich. I developed the initial research question, recruited the student, assisted with the statistical analyses and oversaw the writing process. The manuscript is currently being finalized and will be submitted to *BMC Gastroenterology*.

3 Methods

3.1 Study Population

This thesis builds on the prospective population-based cohort studies of KORA, all sampled in the region of Augsburg, Southern Germany. An overview of the relevant studies is given in Figure 2. The sampling scheme and the examination protocols of the KORA cohorts have been described previously [64]. Participants were sampled in a two-step procedure. First, communities from the city of Augsburg and two adjacent counties were chosen by cluster sampling, followed by a stratified random sampling of participants within each community. As depicted in Figure 2, four cross-sectional surveys (S1-S4) are followed up longitudinally. KORA participants underwent extensive, standardized interviews and physical examinations conducted by trained medical staff. For some surveys, additional measurements, e.g. genomics, electrocardiograms, accelerometry are also available. Whole-body MRI measurements were obtained for a selected sample from the participants in KORA-FF4.

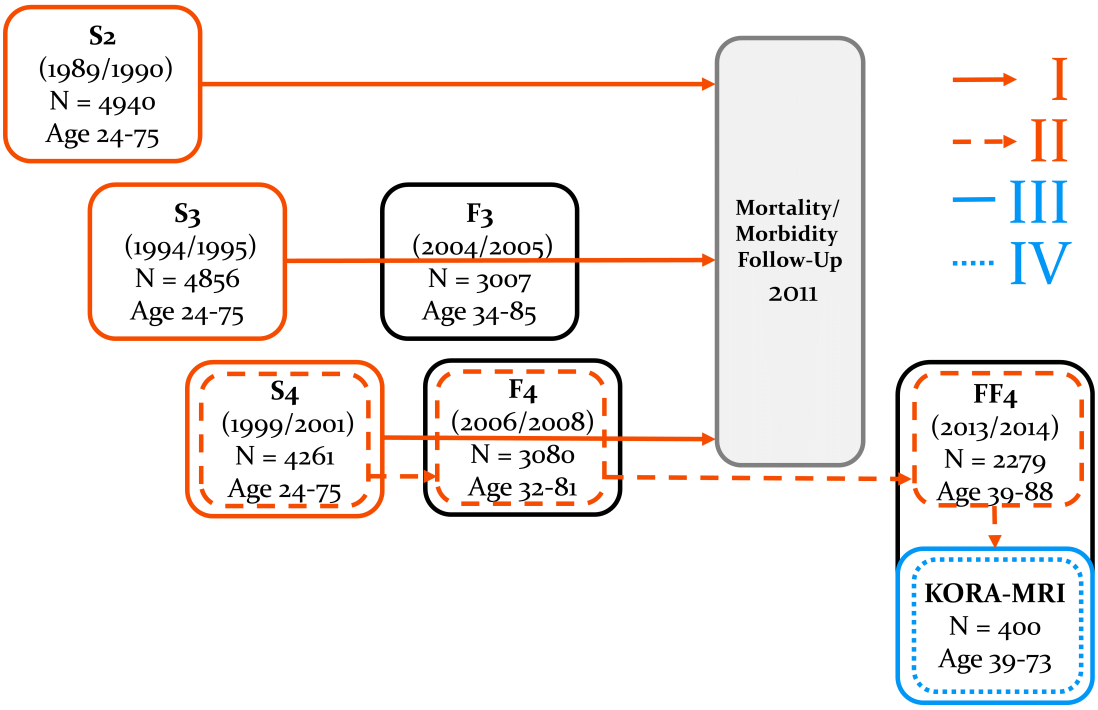

Figure 2: Overview of those KORA studies that were used in manuscripts I through IV.

For each manuscript, additional exclusion criteria were applied to arrive at the final analytical sample. For manuscript I, exclusion criteria were pre-established by the definitions of the analyzed risk scores. For the other manuscripts, exclusion of participants was

mainly due to missing data. Note that as depicted in Figures 1 and 2, the direct association of imaging markers to CVD cannot be evaluated, as the follow-up data for the MRI participants are not available yet.

3.2 MRI methods

The KORA-MRI study comprises 400 participants from FF4 and was specifically designed to study subclinical disease in individuals with pre-diabetes and diabetes. The study setup has been detailedly described [59]. Criteria for enrollment were readiness for participation, validated glycemic status, age between 39-73 years and, importantly, absence of prior CVD (stroke, MI, revascularization). Furthermore, individuals with contraindications to the MRI procedure (non-removable metal parts within the body, pregnancy or breast-feeding, inability to hold breath, allergy to contrast agent or renal insufficiency) were excluded. Participants were classified according to their glycemic status as being normoglycemic, having prediabetes, or having diabetes, following the WHO definitions as described above.

The whole-body MRI exams took place at the University Clinic of the Ludwig-Maximilians-Universität and were conducted at 3 Tesla (Magnetom Skyra; Siemens AG, Healthcare Sector, Erlangen, Germany) with a whole-body radiofrequency coil-matrix system. The resulting MRI images were analyzed by different teams of radiologists with extensive experience in the respective areas. Subsequently, a comprehensive quality control routine was applied, where measures of inter-and intrareader variability were calculated and the data screened for outliers or implausible values. Radiologists interacting with the participants or reading the MRI images were blinded to other clinical covariates. Data handling staff and statisticians were blinded to the actual images.

Cardiac data. Markers of LV function and morphology were obtained semi-automatically by cine-steady-state free precession sequences. Key markers included LV ejection fraction (EF), end-diastolic volume (EDV), end-systolic volume (ESV), myocardial mass, diastolic filling and ejection rates as well as wall thickness and LGE, a marker of myocardial scarring. Wall thickness and LGE measurement were mapped to the AHA 16-segments model [65] with basal segments 1–6; mid-cavity segments 7–12 and apical AHA segments 12–16.

Carotid plaque. Presence of plaque in the left and right Arteria Carotis Communis and Arteria Carotis Interna was evaluated on a T1-weighted, fat-suppressed sequence and was rated according to AHA criteria.

Brain data. On fluid-attenuated inversion recovery images, presence of WML was defined as T2 hyperintense areas $\geq$5 mm in 5 brain areas in the left and right hemisphere,

respectively.

Adipose tissue data. To determine renal sinus fat fraction, total abdominal adipose tissue, VAT, SAT, a volume-interpolated 3D in/opposed-phase VIBE-Dixon sequence was employed and adipose tissues were segmented semi-automatically [61, 66]. SAT was quantified from cardiac apex to femoral head and VAT was quantified from diaphragm to femoral head. Total abdominal adipose tissue was calculated as the sum of SAT and VAT. Intrahepatic fat fraction was evaluated as PDFF on a multi-echo Dixon-VIBE T1-weighted sequence, accounting for confounding T2* decay and spectral complexity of fat [67]. On the same sequence, intrapancreatic fat content was measured as PDFF in caput, corpus and cauda. As the final intrapancreatic fat measure, the arithmetic mean of these three was calculated [68].

3.3 Statistical methods

Statistical methods that were used in manuscripts I to IV can be roughly distinguished in prediction evaluation methods, methods relating to longitudinal data and methods relating to cross sectional data.

Prediction evaluation methods. We analyzed two established, commonly employed risk scores, the FRS and PCE. Both predict the risk of experiencing a CVD event within a 10-year period and are based on Cox proportional hazard regression models. Scores were recalibrated to the study population by pasting risk factor mean values and baseline survival probabilities from each study into the original risk score equations, keeping the original model structure and model coefficients.

Risk scores have to be evaluated regarding two features: Discrimination and calibration. Discrimination is concerned with distinguishing individuals who experience a CVD event from those who do not. Calibration is concerned with estimating the right amount of absolute risk. Discrimination was quantified by Receiver Operating Characteristic (ROC) curves and their respective Area under the Curve (AUC). Differences in AUC were evaluated by an unpaired DeLong test. Additionally, Somer's D statistic was computed, which indicates the rank correlation between predicted risk probabilities and observed event rate.

Calibration was assessed graphically by continuous calibration curves based on LOESS smoothing [69] and quantitatively by Hosmer-Lemeshow tests, calibration slopes and percent discordance between the number of observed and predicted events.

The Population Attributable Fraction (PAF) denotes how much disease burden is attributable to the presence of a specific exposure, i.e. how much disease could be removed

if the specific exposure is not present. This state is by definition counterfactual, as the situation without presence of a specific exposure cannot be measured in reality. We estimated the PAF of a predicted risk score in the high category (e.g. predicted risk score $\geq$ 10%), thereby answering the question how much less CVD would be present if all individuals had predicted risk scores <10%. The PAF was calculated by Levin's formula

$$\text{PAF} = \frac{p \cdot (RR - 1)}{p \cdot (RR - 1) + 1}$$

with p prevalence of a predicted risk score in the high risk category and RR the relative risk: rate of CVD in individuals with predicted risk score in the high risk category divided by the rate of CVD in individuals with predicted score not in the high risk category (e.g. predicted risk score <10%).

Methods relating to longitudinal data. We were interested in eight continuous risk factors measured for each participant at three time points: S4 (baseline), F4 (first follow-up) and FF4 (second follow-up), as graphically outlined in Figure 2. The risk factors of interest were systolic and diastolic BP, BMI, WC, HbA1c, total cholesterol, LDL, HDL cholesterol. The longitudinal course of each risk factor can be modeled by a risk factor trajectory for each individual, designated by the absolute risk factor values and the relative changes from one time point to another. Outcomes of interest were different MRI derived measurements of abdominal and ectopic adipose tissue accrual (total adipose tissue (TAT), VAT, SAT, renal sinus fat fraction, intrahepatic fat and intrapancreatic fat) as markers of cardiometabolic risk, measured at the FF4 examination.

However, the eight risk factors of interest are correlated to varying degrees; thus their conjoint evolution is more informative than the single trajectories. We therefore looked at multivariate trajectories including all eight risk factors at the same time.
To categorize individuals according to their multivariate trajectories, we applied an unsupervised k-means Expectation-Maximization (EM) clustering algorithm [70]. Generally, the clustering algorithm should agglomerate individuals that are similar in their multivariate risk factor trajectories by assigning them to the same cluster and separate individuals that are less similar in their trajectories by assigning them to different clusters. To determine similarity between individuals, an appropriate mathematical measure is needed which can quantify how similar or dissimilar individuals are. The complete clustering procedure is derived in the following:

Data of interest Y for the individual i can be represented as a matrix $Y_i = (y_{i,t,r})$ which denotes the value of traditional risk factor r at time point t for individual i. More concretely, in our case, Y_i takes the form

$$Y_i = \begin{pmatrix} y_{i,\text{S4,SystolicBP}} & y_{i,\text{F4,SystolicBP}} & y_{i,\text{FF4,SystolicBP}} \\ y_{i,\text{S4,DiastolicBP}} & y_{i,\text{F4,DiastolicBP}} & y_{i,\text{FF4,DiastolicBP}} \\ y_{i,\text{S4,BMI}} & y_{i,\text{F4,BMI}} & y_{i,\text{FF4,BMI}} \\ y_{i,\text{S4,WC}} & y_{i,\text{F4,WC}} & y_{i,\text{FF4,WC}} \\ y_{i,\text{S4,HbA1c}} & y_{i,\text{F4,HbA1c}} & y_{i,\text{FF4,HbA1c}} \\ y_{i,\text{S4,Cholesterol}} & y_{i,\text{F4,Cholesterol}} & y_{i,\text{FF4,Cholesterol}} \\ y_{i,\text{S4,LDL}} & y_{i,\text{F4,LDL}} & y_{i,\text{FF4,LDL}} \\ y_{i,\text{S4,HDL}} & y_{i,\text{F4,HDL}} & y_{i,\text{FF4,HDL}} \end{pmatrix}$$

Now a distance measure d' between individual i and individual j is constructed by

$$\begin{aligned} d'(Y_i, Y_j) = ||&d_{.,.,\text{SystolicBP}}(y_{i,.,\text{SystolicBP}}, y_{j,.,\text{SystolicBP}}), \\ &d_{.,.,\text{DiastolicBP}}(y_{i,.,\text{DiastolicBP}}, y_{j,.,\text{DiastolicBP}}), \\ &..., \\ &d_{.,.,\text{HDL}}(y_{i,.,\text{HDL}}, y_{j,.,\text{HDL}})|| \end{aligned}$$

with d denoting the Minkowski distance and $||.||$ denoting the p-norm, both for $p = 2$.

Now each individual is allocated to a cluster by a simple EM algorithm: An initial configuration for the cluster centers is determined and each individual is assigned to the nearest cluster center, with the distance to cluster centers being determined by d' (Maximization step). Then the cluster centers are recomputed on the information given by all individuals assigned to that cluster (Expectation step). This procedure is repeated until convergence, i.e. until no changes in cluster assignment occur in the Maximization step. Note that the clustering algorithm and thus the cluster assignment is independent of the outcomes of interest (adipose tissue).

Methods relating to cross sectional data. In general, associations between exposure variables and outcomes of interest were estimated by linear or logistic regression models, adjusted for potential confounding covariates. Possible interactions between two exposure variables or effect modification of a covariate on an exposure of interest were determined by running regression models containing multiplicative interaction terms and calculating marginal effects.

We used unsupervised fuzzy clustering to determine clusters of dichotomized MRI parameter combinations. Analogously to the multivariate longitudinal clustering described above, the fuzzy clustering aims to group individuals according to their similarity with respect to patterns in the input data. Whereas for the multivariate longitudinal cluster,

input data were longitudinal risk factor measurements, for fuzzy clustering input data were six cross-sectional MRI parameters, covering several organs. As the MRI parameters are dichotomized, the similarity measure had to be constructed appropriately. We used Gower's general dissimilarity coefficient [71] to construct a dissimilarity matrix.

Fuzzy clustering implies that each individual is not simply assigned to a single cluster but assigned a "membership probability": a probability to belong to each of the constructed clusters. To arrive at a single assignment, an appropriate cutoff can be chosen. In the case of two clusters, a cutoff of 50% is sensible, i.e. if an individual has a probability of $\geq 50\%$ to belong to a cluster, this is treated like a fixed assignment to that cluster.

As we analyzed six dichotomized MRI parameters, $2^6 = 64$ combinations of these are possible. Therefore, an adequate variable selection procedure has to be applied to determine those combinations that are most important in their association to the outcome of interest. For variable selection, we employed LASSO regression. LASSO regularizes the absolute size of the estimated coefficients by imposing a penalty parameter λ on them. Given a linear regression model

$$Y = \beta_0 + \sum_{j=1}^{p} \beta_j X_j$$

with N number of observations and p number of predictors, the LASSO estimator in the Langrangian form can be written as

$$\hat{\beta}[\text{lasso}] = \underset{\beta}{\text{argmin}} \left\{ \frac{1}{2} \sum_{i=1}^{N} (y_i - \beta_0 - \sum_{j=1}^{p} x_{ij}\beta_j)^2 + \lambda \sum_{j=1}^{p} |\beta_j| \right\}$$

The estimated coefficients $\hat{\beta}[\text{lasso}]$ are therefore shrunk towards zero, depending on the size of λ. Variables are discarded by shrinking coefficents to be exactly zero; thus a subset of predictors is selected. Note, however, that the estimated coefficients are biased due to the shrinking procedure and that statistical inference (Confidence Interval (CI)s, p-values) is not possible.

4 Main Results

4.1 CVD risk assessment by traditional risk factors

Our analysis comprised n = 7789 individuals from three population-based cohorts, enrolled in 1989/1990, 1994/1995 and 1999/2000 who were followed up for CVD mortality and MI and stroke morbidity for ten years [55]. Comparing the baseline examinations of the three studies, there were significant temporal trends in risk factor distributions. For instance, mean BMI, mean systolic BP, mean total cholesterol and LDL significantly decreased; at the same time, intake of antihypertensive and lipid-lowering medication increased. The rate of observed CVD events remained relatively stable (in men: 12.4%, 10.4%, 10.4%, in women: 4.4%, 5.7%, 5.6%), though fatal CVD events significantly dropped in men.

Both FRS and PCE emerged similarly in their discrimination performance and calibration. Although recalibrated to the respective sample, both FRS and PCE considerably overestimated real CVD risk; and while calibration improved slightly over time, the improvement was not statistically significant. For men, overestimation by the FRS amounted to 46%, 48% and 42% in the three studies, respectively, whereas for women overestimation was 58%, 55% and 53%.

Discrimination performance of the scores evolved differently for men and women. Whereas the discrimination performance, as measured by AUC nominally declined for men (e.g. AUC PCE: 76.4, 76.1, 72.8), it nominally improved for women (e.g. AUC PCE: 75.9, 79.5, 80.5). The difference between AUC for men and women was statistically significant.

The burden of CVD that can be attributed to a high risk score (and thereby can be attributed to the underlying risk factors) is measured by the PAFs. PAFs of a PCE$\geq$10% steadily declined for men (87%, 76%, 66%) and increased for women (49%, 69%, 82%).

The first specific aim of this thesis stated (a) To evaluate the temporal development of traditional cardiovascular risk factors in different population-based cohorts spanning several timeframes and characterize the corresponding development of CVD risk scores.
We have now shown that there are significant shifts in the distribution of traditional CVD risk factors over time. These shifting distributions affect the performance of established risk scores; and importantly, the performance of these risk scores is affected in a sex-specific manner, differently for men and women. However, as shown by the analysis of PAFs, it is evident that the risk scores still capture a major part of CVD risk.

4.2 Metabolic phenotypes and traditional risk factor clusters

Our analysis comprised N = 325 individuals [56]. Using systolic and diastolic BP, BMI, WC, HbA1c, Total cholesterol, LDL and HDL cholesterol measured at three time points, we identified three compact and well-separated longitudinal multivariate trajectory clusters, characterized by different risk factor exposure levels. Individuals agglomerated in a low-risk cluster (Cluster I, n = 114), an intermediate-risk cluster (Cluster II, n = 129) and a high-risk cluster (Cluster III, n = 82). The clusters were characterized by different mean risk factor levels and risk factor changes along time points, as shown in Figure 3.

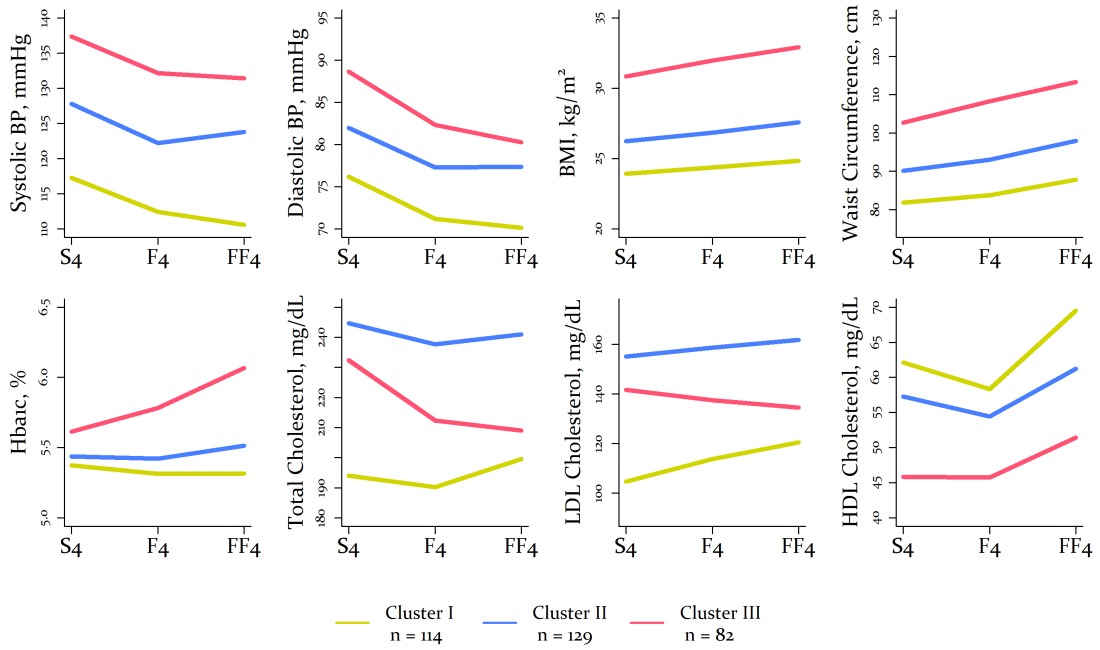

Figure 3: Risk factor trajectories in the three clusters. Adapted from [56]. The clusters were derived in an unsupervised fashion based on longitudinal trajectories of all eight risk factors simultaneously. For each risk factor, the mean risk factor value at every time point is plotted, stratified by cluster. Generally, Cluster I (in green) is characterized by the lowest mean risk factor values and most favorable trajectories for all risk factors and can therefore be considered the "low-risk" cluster. Cluster III (in red) is characterized by the highest mean risk factor values, except for total and LDL cholesterol. Cluster III also shows the highest gains in BMI, WC and HbA1c over time, and can therefore be considered the "high-risk" cluster. Cluster II (in blue) is intermediate between Cluster I and III and is thus considered the "medium-risk" cluster.

Within the trajectory clusters, there was a gradual increase in a broad panel of adipose tissue compartments as measured by MRI. For instance, VAT amounted to (arithmetic mean ± standard deviation) 2.5 liter ± 1.7 liter in Cluster I, 4.6 liter ± 1.9 liter in Cluster II and 7.3 liter ± 2.2 liter in Cluster III. Intrapancreatic fat amounted to (median [first quartile,

third quartile]) 3.7% [2.3%, 5.7%] in Cluster I, 5.9% [4.3%, 9.2%] in Cluster II and 10.7% [5.0%, 16.3%] in Cluster III. Furthermore, trajectory clusters were significantly associated to these adipose tissue compartments after adjustment for potential confounders. For example, the intermediate-risk cluster, Cluster II, was associated with an increase of 1.30 liter in VAT (95%-CI: [0.84; 1.75]) and a 52% increase in intrapancreatic fat (95%-CI: [26; 84]), compared to Cluster I. The high-risk cluster, Cluster III, was associated with an increase of 3.32 liter in VAT (95%-CI: [2.74; 3.90]) and a 120% increase in intrapancreatic fat (95%-CI: [73, 180]) after adjustment for confounders.

Importantly, the variability in adipose tissue that could be explained by the trajectory clusters varied substantially across the respective compartments. The highest amount of variability could be explained for total abdominal adipose tissue with R^2 = 0.89, while the smallest amount of variability was explained for intrahepatic fat with R^2 = 0.27.

The second specific aim of this thesis stated (b) To identify longitudinal clusters of traditional cardiovascular risk factor trajectories and associate them to imaging-based metabolic phenotypes.
We have now shown that individuals can be clustered by their longitudinal trajectories of traditional CVD risk factors; trajectories are characterized by the mean value of a risk factor and the evolvement over time. Furthermore, we have shown that sustained high risk factor levels and unfavorable risk factor trajectories are associated with high levels of adipose tissue.

4.3 Special role of diabetes

We specifically analyzed LV wall thickness and a combination of MRI parameters in their relation to glycemic status [57]. LV wall thickness increased across the glycemic spectrum: mean wall thickness was 8.8 mm ± 1.4 mm in normoglycemic individuals, 9.9 mm ± 1.4 mm in individuals with prediabetes and 10.5 mm ± 1.6 mm in individuals with diabetes. The association of prediabetes and diabetes to wall thickness was independent of potential confounders. For specific segments, also an interaction of glycemic status and systolic BP was discernible: for basal segments, the marginal effect of prediabetes and diabetes decreased with rising blood pressure, whereas for mid-cavity and apical segments, there was an increasing marginal effect of prediabetes and diabetes with rising blood pressure. In the same vein, association of glycemic status was strongest for the mid-cavity segments, while the association of hypertension was strongest for the basal segments.

Clustering of combinations of dichotomized MRI parameters yielded two distinct clusters, which were significantly associated to (pre-)diabetic glycemic status [58]. Importantly, no distinct cluster for prediabetes was identified. Figure 4 shows the distribution

of MRI parameter combinations within the two clusters. The columns denote prevalence of the respective combinations, expressed in % of the whole sample. All MRI markers are dichotomized by clinically relevant cutoffs, compare [58]. Every individual can have exactly one of $2^6 = 64$ possible combinations of these MRI parameters. In our sample, only 33 unique combinations occurred, as depicted by the 33 columns. E.g. the first column shows the prevalence of the combination of abnormal ARWMC with normal PDFF, normal VAT, normal LV remodeling index, normal Carotid Plaque and normal LGE. The second column shows the prevalence of having no abnormal MRI parameter at all; and so forth. The shaded area depicts the proportion of individuals with prediabetes or diabetes that had the respective combination of MRI parameters. Columns colored in orange denote combinations that were assigned to the first cluster, as calculated by fuzzy clustering. Columns colored in turquoise denote the combinations that were assigned to the second cluster. As visible from the shaded areas, combinations that were assigned to the second cluster feature a higher proportion of individuals with prediabetes or diabetes.

Within the clusters, LASSO regression identified specific combinations of MRI parameter combinations that were significantly related to either normal glycemic status or (pre-)diabetes. Individuals with abnormal ARWMC only or the combination of ARWMC and carotid plaque were assigned to the first cluster and these MRI parameter combinations were significantly associated to normoglycemic status. Also individuals without abnormal MRI parameter values were assigned to the first cluster; however having no abnormal MRI parameter value was not associated to normoglycemic status. Individuals with combinations involving abnormal adipose tissue values (VAT and intrahepatic fat) were assigned to the second cluster. Specifically, combinations comprising both abnormal VAT and intrahepatic fat as well as brain changes and/or changes in cardiac structure were significantly associated to (pre-)diabetes.

The third specific aim of this thesis stated (c) To assess the relation of imaging-based metabolic phenotypes to diabetes and its precursor states and identify specific diabetes-related imaging-based signatures.
We have now shown that prediabetes and diabetes are unfavorably associated to cardiac structure, independently of other potential confounders. We have furthermore shown that clusters of abnormal MRI parameters are associated to diabetes status and that combinations including abnormal hepatic fat and abdominal fat in addition to LV remodeling or brain changes are characteristic for diabetes status.

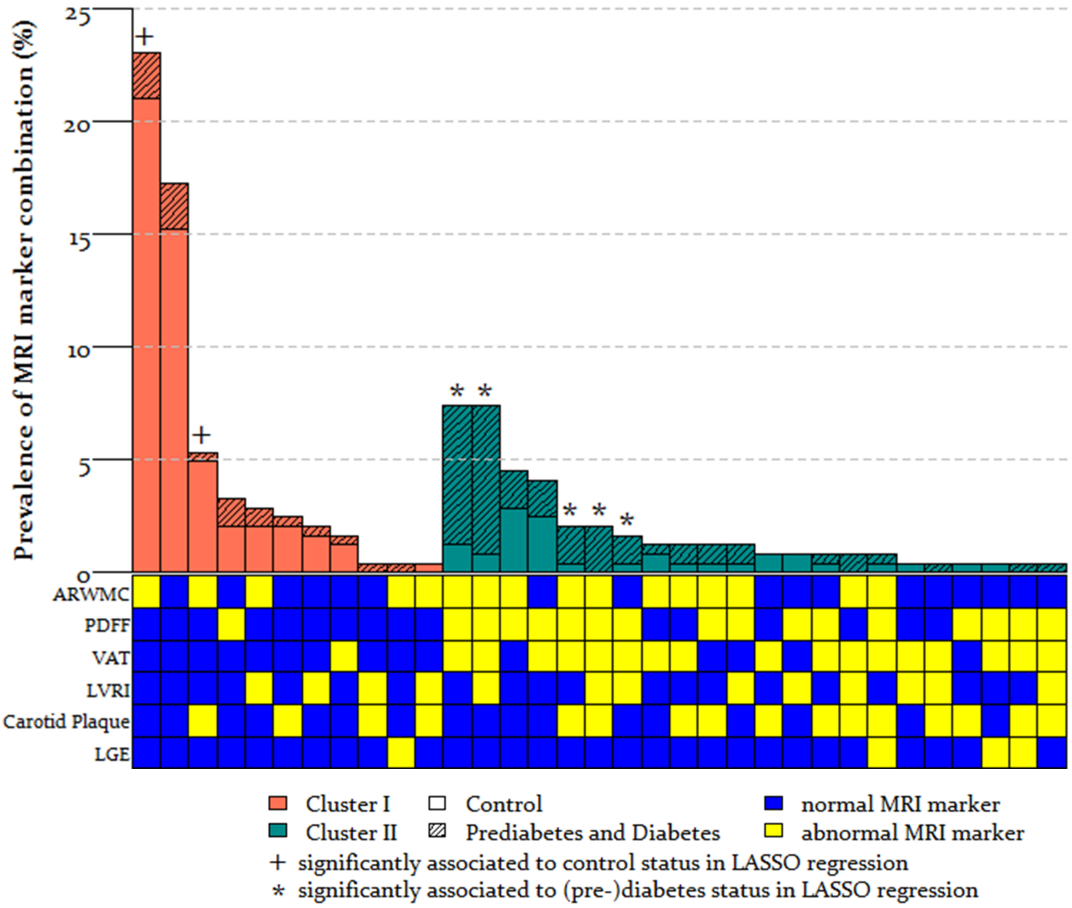

Figure 4: Distribution of normal and abnormal MRI markers for multiple organs. Adapted from [58]. ARWMC: Age-Related White Matter Changes; PDFF: proton-density fat fraction (intrahepatic fat); VAT: visceral adipose tissue; LVRI: left ventricular remodeling index; LGE: late gadolinium enhancement.

5 Discussion

5.1 Performance and development of CVD risk scores

Currently, a plethora of CVD prediction models are available, albeit only a few are commonly used [11]. We have shown how two commonly applied risk scores, the FRS and PCE behave with regard to temporal shifts in risk factor distributions. Although we found a decrease in AUC for men and an increase for women, in all studies and for both sexes, both risk scores showed adequate discrimination with AUCs > 70. Additionally, our analysis of PAFs revealed that these risk scores still capture the relevant part of CVD risk.

The fact that risk prediction models score differently for men and women has already been reported. Generally, women develop CVD later in the life course and have a lower CVD lifetime risk compared to men [72] although these estimates might be underestimating actual risk, as women have a higher life expectancy than men. The associations of specific risk factors, most prominently glycemic status and smoking, are different in women and men [73, 74]. Statistically, higher hazard ratios of the underlying risk factors can contribute to a better performance of the risk models.

With regard to calibration performance, we corroborate findings from other studies that reported substantial overestimation of risk, especially by the PCE [75, 76]. This might be an inherent characteristic of the design of the PCE [77] or due to underreporting of CVD events. A very recent study conducted in the US cohort of the Women's Health Initiative [78] reported that calibration of the PCE improved after additionally including CVD events collected by the insurance provider.

Taken together, our results support the notion that, although established CVD risk scores have been derived from older population-based cohorts, they still perform adequately, if they are properly adjusted to the population at hand. However, for future refinement of CVD risk prediction models, sex-specific risk factor trends will have to be more strongly taken into account.

5.2 Contributions to risk assessment by imaging-based phenotyping

Results from this thesis have demonstrated that MRI derived markers contribute to cardiometabolic risk assessment. By recognizing the manifestation of early, subclinical disorders, these markers provide a better understanding for disease phenotypes which would potentially allow for a timely intervention to prevent disease progression.

We brought together traditional CVD risk factors and metabolic MRI measurements by analyzing longitudinal trajectories of traditional risk factors and relating them to a panel

of adipose tissue compartments as measured by MRI. We highlighted that the amount of variability in adipose tissue that can be explained by these risk factors is substantially varying, indicating different potential pathways in the formation of these adipose tissue compartments and how they impact an individual's metabolism. In line with other findings, our results also indicate that anthropometric measurements, such as BMI and WC are strongly correlated to VAT and SAT, although the correlation is not complete.

Ectopic adipose tissue depots like intrahepatic fat, renal sinus fat and intrapancreatic fat can only be measured by imaging-based modalities, if the measurement should be non-invasive. They cannot be accurately mapped to anthropometric measures such as BMI and WC and there are no other biomarkers (e.g. blood-based) that can properly, reliably and reproducibly describe the amount of adipose tissue [79, 80].

Nevertheless, these ectopic adipose tissue compartments convey considerable information about metabolic risk. The liver is a key player in systemic metabolism and substantially involved in triglyceride synthesis and storage. Increased intrahepatic fat is associated to CVD by its contribution to chronic inflammation, elevated free fatty acids and insulin resistance [81]. Results from the KORA-MRI study also revealed substantial associations with hypertension [67]. Particularly the combination of elevated hepatic fat and diabetes is a major public health concern [82].

The connection of intrapancreatic fat and renal sinus fat to CVD have been less vigorously established. Renal sinus fat induces increased pressure on the vasculature within the kidneys and can therefore lead to structural damage and impaired renal function [83, 84]. Intrapancreatic fat has been discussed to modulate insulin metabolism by constraining beta-cell function [85]. Interestingly, this specific ectopic fat compartment seems to be susceptible to nutrition changes [86].

By the use of imaging-based markers we could quantify the role of traditional risk factors in the development of abdominal and ectopic adipose tissue compartments and provide relevant data on the relation of unfavorable longitudinal trajectories to these phenotypes.

Especially for determining metabolic consequences of prediabetes, the precursor state of diabetes, MRI emerges to be a powerful modality, as prediabetes is usually asymptomatic and not clinically diagnosed. Notwithstanding, consequences of prediabetes are already metabolically manifest and are visible on MRI.
Findings from the KORA-MRI study show that prediabetes and diabetes are strongly associated to unfavorable cardiometabolic phenotypes, e.g. to increased fat infiltration within the muscle [62], increased adipose tissue [68, 61], impaired cardiac function [59, 87, 88]

and alterations in cardiac structure [89].

By analyzing LV wall thickness according to the AHA 16-segments model, we have shown that prediabetes and diabetes are associated to increased wall thickness, independent of traditional CVD risk factors. This is in line with findings from Atherosclerosis Risk in Communities (ARIC) and FHS who found increasing relative LV wall thickness across glycemic categories [90, 91]. However, no measurements of segmental wall thickness were available in theses samples. Other studies reported increased wall thickness in individuals with diabetes, but found no independent effect apart from other traditional CVD risk factors [92, 93]. The exact pathophysiological mechanisms how impaired glucose metabolism works on LV remodeling are still unknown. In individuals with diabetes, LV torsion and strain have been shown to associate with a lower perfusion reserve induced by a decreased myocardial blood flow [94]. Moreover, advanced fibrosis due to accrual of collagen and advanced glycation end products leads to LV stiffness and subsequent remodeling [95, 96]. As increased LV wall thickness is associated with an increased risk for CVD [97], it is of paramount importance to identify modifiable risk factors. By our analysis, we could further illuminate the role of prediabetes in cardiac remodeling.

We have furthermore derived specific combinations of abnormal MRI parameters that are indicative of diabetes status by employing unsupervised clustering methods. In our analysis, the simultaneous incorporation of different organs allowed for studying systemic impacts of diabetes. As an important result, individuals with prediabetes were assigned to the same cluster as those with full-fledged diabetes. This indicates that unfavorable diabetes-related alterations in organic structure and function are already present in prediabetes. Moreover, our findings emphasize the important role of adipose tissue and intrahepatic fat in glucose metabolism [98, 99]. In contrast, brain changes such as ARWMC were not indicative of diabetes status in our study. Particularly in elderly populations, the prevalence of WMLs is high and increasing with age, presumably due to damage in the small vasculature, which can also be diabetes-induced [100, 101]. Recent research suggests that the presence of WML is too crude a measure to distinguish between individuals with and without diabetes; however more refined MRI measures of WML achieve this distinction [102].

Taken together, imaging data sizeably contribute to an intricate characterization of an individual's phenotype, allowing for a more accurate cardiometabolic risk assessment.

5.3 Challenges and limitations

The focus of this thesis is on epidemiological questions, i.e. associations of imaging-based markers to cardiometabolic phenotypes and risk, as opposed to questions regarding the

technical derivation of these markers. Nevertheless, some challenges of imaging-based data acquisition in epidemiological studies shall briefly be mentioned.

In contrast to the clinical setting, where imaging modalities are only employed when indicated, and thus result in manageable numbers of images to process, in well-powered epidemiological studies, the number of enrolled subjects goes up to several thousand. Manual evaluation of these numbers of images is impractical, therefore automated algorithms have to be developed to achieve standardized and reproducible information extraction, e.g. for the automated quantification of adipose tissue [103]. Additionally, by applying advanced statistical and bioinformatical methods, the data contained in these images can be processed as mineable data instead of solely visually inspected. The emerging field of "'radiomics" has already embarked upon this task and is already supplying statistical methods [104].

Moreover, although particularly MRI is a highly reproducible modality, imaging can be conducted through a variety of protocols. To attain comparability within a single, e.g. multi-centered study or comparability across different imaging studies, protocols and methods have to be rigorously standardized to achieve sufficient harmonization.

A major concern in population-based imaging studies is the handling of incidental findings, i.e. pathological findings that were not previously diagnosed and that the participant was unaware of. These findings impose certain ethical problems: On the one hand, undifferentiated information about every finding might trigger additional follow-up for the participant, including potentially invasive tests and procedures which can lead to discomfort, reduced quality of life or put the participant at risk. On the other hand, withholding medically important information from the participant is ethically not feasible. To determine a trade-off between these two sides, the severity of the finding and its medical importance, as well as the participant's preference about if or how they wish to be informed, should be taken into account. To this aim, population-based imaging studies have installed standardized procedures how incidental findings should be handled [42, 105].

5.4 Conclusion

Whereas risk scores based on traditional markers still capture a major part of CVD risk burden, imaging-based phenotyping has a substantive potential to early recognize prepathological cardiometabolic states. These data are ideally utilized together with other metabolic markers, such as glycemic status, from well-characterized studies to embark on their full potential. In the context of individualized medicine, relating imaging data to traditional CVD risk factor data yields a powerful combination.

References

[1] World Health Organization, *Fact Sheet: The top 10 causes of death*. http://www.who.int/en/news-room/fact-sheets/detail/the-top-10-causes-of-death, May 2018. Accessed: 2018-11-26.

[2] M. Ng, T. Fleming, M. Robinson, B. Thomson, N. Graetz, C. Margono, E. C. Mullany, S. Biryukov, C. Abbafati, S. F. Abera, J. P. Abraham, N. M. E. Abu-Rmeileh, T. Achoki, F. S. AlBuhairan, Z. A. Alemu, R. Alfonso, M. K. Ali, R. Ali, N. A. Guzman, W. Ammar, P. Anwari, A. Banerjee, S. Barquera, S. Basu, D. A. Bennett, Z. Bhutta, J. Blore, N. Cabral, I. C. Nonato, J.-C. Chang, R. Chowdhury, K. J. Courville, M. H. Criqui, D. K. Cundiff, K. C. Dabhadkar, L. Dandona, A. Davis, A. Dayama, S. D. Dharmaratne, E. L. Ding, A. M. Durrani, A. Esteghamati, F. Farzadfar, D. F. J. Fay, V. L. Feigin, A. Flaxman, M. H. Forouzanfar, A. Goto, M. A. Green, R. Gupta, N. Hafezi-Nejad, G. J. Hankey, H. C. Harewood, R. Havmoeller, S. Hay, L. Hernandez, A. Husseini, B. T. Idrisov, N. Ikeda, F. Islami, E. Jahangir, S. K. Jassal, S. H. Jee, M. Jeffreys, J. B. Jonas, E. K. Kabagambe, S. E. A. H. Khalifa, A. P. Kengne, Y. S. Khader, Y.-H. Khang, D. Kim, R. W. Kimokoti, J. M. Kinge, Y. Kokubo, S. Kosen, G. Kwan, T. Lai, M. Leinsalu, Y. Li, X. Liang, S. Liu, G. Logroscino, P. A. Lotufo, Y. Lu, J. Ma, N. K. Mainoo, G. A. Mensah, T. R. Merriman, A. H. Mokdad, J. Moschandreas, M. Naghavi, A. Naheed, D. Nand, K. M. V. Narayan, E. L. Nelson, M. L. Neuhouser, M. I. Nisar, T. Ohkubo, S. O. Oti, A. Pedroza, D. Prabhakaran, N. Roy, U. Sampson, H. Seo, S. G. Sepanlou, K. Shibuya, R. Shiri, I. Shiue, G. M. Singh, J. A. Singh, V. Skirbekk, N. J. C. Stapelberg, L. Sturua, B. L. Sykes, M. Tobias, B. X. Tran, L. Trasande, H. Toyoshima, S. van de Vijver, T. J. Vasankari, J. L. Veerman, G. Velasquez-Melendez, V. V. Vlassov, S. E. Vollset, T. Vos, C. Wang, X. Wang, E. Weiderpass, A. Werdecker, J. L. Wright, Y. C. Yang, H. Yatsuya, J. Yoon, S.-J. Yoon, Y. Zhao, M. Zhou, S. Zhu, A. D. Lopez, C. J. L. Murray, and E. Gakidou, *Global, regional, and national prevalence of overweight and obesity in children and adults during 1980–2013: A systematic analysis for the Global Burden of Disease Study 2013*, The Lancet, 384 (2014), pp. 766–781.

[3] K. Ogurtsova, J. D. da Rocha Fernandes, Y. Huang, U. Linnenkamp, L. Guariguata, N. H. Cho, D. Cavan, J. E. Shaw, and L. E. Makaroff, *IDF Diabetes Atlas: Global estimates for the prevalence of diabetes for 2015 and 2040*, Diabetes Research and Clinical Practice, 128 (2017), pp. 40–50.

[4] C. J. L. Murray, *The State of US Health, 1990-2010*, JAMA, 310 (2013), p. 591.

[5] M. Inouye, G. Abraham, C. P. Nelson, A. M. Wood, M. J. Sweeting, F. Dudbridge, F. Y. Lai, S. Kaptoge, M. Brozynska, T. Wang, S. Ye, T. R. Webb, M. K. Rutter, I. Tzoulaki, R. S. Patel, R. J. F. Loos, B. Keavney, H. Hemingway, J. Thompson, H. Watkins, P. Deloukas, E. D. Angelantonio, A. S. Butterworth, J. Danesh, and N. J. Samani, *Genomic Risk Prediction of Coronary Artery Disease in 480,000 Adults*, Journal of the American College of Cardiology, 72 (2018), pp. 1883–1893.

[6] W. B. Kannel, T. R. Dawber, A. Kagan, N. Revotskie, and J. Stokes, *Factors of risk in the development of coronary heart disease–six year follow-up experience. The Framingham Study.*, Annals of Internal Medicine, 55 (1961), pp. 33–50.

[7] M. F. Piepoli, A. W. Hoes, S. Agewall, C. Albus, C. Brotons, A. L. Catapano, M.-T. Cooney, U. Corrà, B. Cosyns, C. Deaton, I. Graham, M. S. Hall, F. D. R. Hobbs, M.-L. Løchen, H. Löllgen, P. Marques-Vidal, J. Perk, E. Prescott, J. Redon, D. J. Richter, N. Sattar, Y. Smulders, M. Tiberi, H. B. van der Worp, I. van Dis, and W. M. M. Verschuren, *2016 European Guidelines on cardiovascular disease prevention in clinical practice*, European Heart Journal, 37 (2016), pp. 2315–2381.

[8] R. H. Eckel, J. M. Jakicic, J. D. Ard, J. M. de Jesus, N. H. Miller, V. S. Hubbard, I.-M. Lee, A. H. Lichtenstein, C. M. Loria, B. E. Millen, C. A. Nonas, F. M. Sacks, S. C. Smith, L. P. Svetkey, T. A. Wadden, and S. Z. Yanovski, *2013 AHA/ACC guideline on lifestyle management to reduce cardiovascular risk*, Journal of the American College of Cardiology, 63 (2014), pp. 2960–2984.

[9] S. Si, J. R. Moss, T. R. Sullivan, S. S. Newton, and N. P. Stocks, *Effectiveness of general practice-based health checks: A systematic review and meta-analysis*, British Journal of General Practice, 64 (2013), pp. e47–e53.

[10] T. Lauritzen, A. Sandbaek, and K. Borch-Johnsen, *General health checks may work*, BMJ, 349 (2014), pp. g4697–g4697.

[11] J. A. Damen, L. Hooft, E. Schuit, T. P. Debray, G. S. Collins, I. Tzoulaki, C. M. Lassale, G. C. Siontis, V. Chiocchia, C. Roberts, M. M. Schlussel, S. Gerry, J. A. Black, P. Heus, Y. T. van der Schouw, L. M. Peelen, and K. G. Moons, *Prediction models for cardiovascular disease risk in the general population: Systematic review*, BMJ, 353 (2016), p. i2416.

[12] P. W. Wilson, R. B. D'Agostino, D. Levy, A. M. Belanger, H. Silbershatz, and W. B. Kannel, *Prediction of coronary heart disease using risk factor categories*, Circulation, 97 (1998), pp. 1837–1847.

[13] R. B. D'Agostino, S. Grundy, L. M. Sullivan, and P. Wilson, *Validation of the Framingham Coronary Heart Disease Prediction Scores*, JAMA, 286 (2001), p. 180.

[14] J. S. Rana, M. Cote, J.-P. Despres, M. S. Sandhu, P. J. Talmud, E. Ninio, N. J. Wareham, J. J. P. Kastelein, A. H. Zwinderman, K.-T. Khaw, and S. M. Boekholdt, *Inflammatory biomarkers and the prediction of coronary events among people at intermediate risk: the EPIC-Norfolk prospective population study*, Heart, 95 (2009), pp. 1682–1687.

[15] J. A. Cooper, G. J. Miller, and S. E. Humphries, *A comparison of the PROCAM and Framingham point-scoring systems for estimation of individual risk of coronary heart disease in the Second Northwick Park Heart Study*, Atherosclerosis, 181 (2005), pp. 93–100.

[16] T. P. Murphy, R. Dhangana, M. J. Pencina, A. M. Zafar, and R. B. D'Agostino, *Performance of current guidelines for coronary heart disease prevention: Optimal use of the Framingham-based risk assessment*, Atherosclerosis, 216 (2011), pp. 452–457.

[17] S. D'Agostino, R. B., R. S. Vasan, M. J. Pencina, P. A. Wolf, M. Cobain, J. M. Massaro, and W. B. Kannel, *General cardiovascular risk profile for use in primary care: The Framingham Heart Study*, Circulation, 117 (2008), pp. 743–53.

[18] E. Zomer, A. Owen, D. J. Magliano, D. Liew, and C. Reid, *Validation of two Framingham cardiovascular risk prediction algorithms in an Australian population: the 'old' versus the 'new' Framingham equation*, European Journal of Cardiovascular Prevention & Rehabilitation, 18 (2010), pp. 115–120.

[19] M. Hamer, Y. Chida, and E. Stamatakis, *Utility of C-reactive protein for cardiovascular risk stratification across three age groups in subjects without existing cardiovascular diseases*, The American Journal of Cardiology, 104 (2009), pp. 538–542.

[20] R. M. Conroy, K. Pyörälä, A. P. Fitzgerald, S. Sans, A. Menotti, G. De Backer, D. De Bacquer, P. Ducimetiere, P. Jousilahti, and U. Keil, *Estimation of ten-year risk of fatal cardiovascular disease in europe: the SCORE project*, European Heart Journal, 24 (2003), pp. 987–1003.

[21] R. Bhopal, C. Fischbacher, E. Vartiainen, N. Unwin, M. White, and G. Alberti, *Predicted and observed cardiovascular disease in South Asians: application of FINRISK, Framingham and SCORE models to Newcastle Heart Project data*, Journal of Public Health, 27 (2005), pp. 93–100.

[22] A. H. H. Merry, J. M. A. Boer, L. J. Schouten, T. Ambergen, E. W. Steyerberg, E. J. M. Feskens, W. M. M. Verschuren, A. P. M. Gorgels, and P. A. van den Brandt, *Risk prediction of incident coronary heart disease in the Netherlands: re-estimation and improvement of the SCORE risk function*, European Journal of Preventive Cardiology, 19 (2011), pp. 840–848.

[23] K. Dunder, L. Lind, B. Zethelius, L. Berglund, and H. Lithell, *Evaluation of a scoring scheme, including proinsulin and the apolipoprotein B/apolipoprotein A1 ratio, for the risk of acute coronary events in middle-aged men: Uppsala Longitudinal Study of Adult Men (ULSAM)*, American Heart Journal, 148 (2004), pp. 596–601.

[24] J. Hippisley-Cox, C. Coupland, Y. Vinogradova, J. Robson, M. May, and P. Brindle, *Derivation and validation of QRISK, a new cardiovascular disease risk score for the united kingdom: prospective open cohort study*, BMJ, 335 (2007), p. 136.

[25] National Institute for Health and Care Excellence, *Public health guideline: Cardiovascular disease prevention*. http://www.nice.org.uk/guidance/ph25, 2010. Accessed: 2018-11-26.

[26] J. Hippisley-Cox, C. Coupland, and P. Brindle, *Development and validation of QRISK3 risk prediction algorithms to estimate future risk of cardiovascular disease: prospective cohort study*, BMJ, (2017), p. j2099.

[27] D. C. Goff Jr, D. M. Lloyd-Jones, G. Bennett, S. Coady, R. B. D'Agostino Sr, R. Gibbons, P. Greenland, D. T. Lackland, D. Levy, and C. J. O'Donnell, *2013 ACC/AHA guideline on the assessment of cardiovascular risk: a report of the American College of Cardiology/American Heart Association Task Force on Practice Guidelines*, Journal of the American College of Cardiology, 63 (2014), pp. 2935–2959.

[28] I. Tzoulaki, G. Liberopoulos, and J. P. Ioannidis, *Assessment of claims of improved prediction beyond the Framingham Risk Score*, JAMA, 302 (2009), p. 2345.

[29] G. C. M. Siontis, I. Tzoulaki, K. C. Siontis, and J. P. A. Ioannidis, *Comparisons of established risk prediction models for cardiovascular disease: Systematic review*, BMJ, 344 (2012), pp. e3318–e3318.

[30] T. Jeerakathil, P. A. Wolf, A. Beiser, J. Massaro, S. Seshadri, R. B. D'Agostino, and C. DeCarli, *Stroke Risk Profile predicts White Matter Hyperintensity Volume*, Stroke, 35 (2004), pp. 1857–1861.

[31] G. Weinstein, A. S. Beiser, C. DeCarli, R. Au, P. A. Wolf, and S. Seshadri, *Brain Imaging and Cognitive Predictors of Stroke and Alzheimer Disease in the Framing-*

ham Heart Study, Stroke, 44 (2013), pp. 2787–2794.

[32] C. J. Salton, M. L. Chuang, C. J. O'Donnell, M. J. Kupka, M. G. Larson, K. V. Kissinger, R. R. Edelman, D. Levy, and W. J. Manning, *Gender differences and normal left ventricular anatomy in an adult population free of hypertension: A cardiovascular magnetic resonance study of the Framingham Heart Study Offspring cohort*, Journal of the American College of Cardiology, 39 (2002), pp. 1055–1060.

[33] M. M. F. Poels, M. W. Vernooij, M. A. Ikram, A. Hofman, G. P. Krestin, A. van der Lugt, and M. M. B. Breteler, *Prevalence and Risk Factors of Cerebral Microbleeds: An Update of the Rotterdam Scan Study*, Stroke, 41 (2010), pp. S103–S106.

[34] M. Selwaness, Q. van den Bouwhuijsen, R. S. van Onkelen, A. Hofman, O. H. Franco, A. van der Lugt, J. J. Wentzel, and M. Vernooij, *Atherosclerotic plaque in the left carotid artery is more vulnerable than in the right*, Stroke, 45 (2014), pp. 3226–3230.

[35] N. Kawel, E. B. Turkbey, J. J. Carr, J. Eng, A. S. Gomes, W. G. Hundley, C. Johnson, S. C. Masri, M. R. Prince, R. J. van der Geest, J. A. C. Lima, and D. A. Bluemke, *Normal left ventricular myocardial thickness for middle-aged and older subjects with Steady-State Free Precession Cardiac Magnetic Resonance: The Multi-Ethnic Study of Atherosclerosis*, Circulation: Cardiovascular Imaging, 5 (2012), pp. 500–508.

[36] E. B. Turkbey, R. L. McClelland, R. A. Kronmal, G. L. Burke, D. E. Bild, R. P. Tracy, A. E. Arai, J. A. Lima, and D. A. Bluemke, *The impact of obesity on the left ventricle: the Multi-Ethnic Study of Atherosclerosis (MESA)*, JACC Cardiovascular Imaging, 3 (2010), pp. 266–74.

[37] J. Eng, R. L. McClelland, A. S. Gomes, W. G. Hundley, S. Cheng, C. O. Wu, J. J. Carr, S. Shea, D. A. Bluemke, and J. A. C. Lima, *Adverse left ventricular remodeling and age assessed with Cardiac MR Imaging: The Multi-Ethnic Study of Atherosclerosis*, Radiology, 278 (2016), pp. 714–722.

[38] J.-P. Kühn, P. Meffert, C. Heske, M.-L. Kromrey, C. O. Schmidt, B. Mensel, H. Völzke, M. M. Lerch, D. Hernando, J. Mayerle, and S. B. Reeder, *Prevalence of fatty liver disease and hepatic iron overload in a Northeastern German population by using quantitative MR Imaging*, Radiology, 284 (2017), pp. 706–716.

[39] C. O. Schmidt, E. Sierocinski, K. Hegenscheid, S. E. Baumeister, H. J. Grabe, and H. Völzke, *Impact of whole-body MRI in a general population study*, European Journal of Epidemiology, 31 (2015), pp. 31–39.

[40] S. E. Petersen, P. M. Matthews, F. Bamberg, D. A. Bluemke, J. M. Francis, M. G. Friedrich, P. Leeson, E. Nagel, S. Plein, F. E. Rademakers, A. A. Young, S. Garratt, T. Peakman, J. Sellors, R. Collins, and S. Neubauer, *Imaging in population science: Cardiovascular Magnetic Resonance in 100,000 participants of UK Biobank - rationale, challenges and approaches*, Journal of Cardiovascular Magnetic Resonance, 15 (2013), p. 46.

[41] German National Cohort Consortium, *The German National Cohort: aims, study design and organization*, European Journal of Epidemiology, 29 (2014), pp. 371–382.

[42] F. Bamberg, H.-U. Kauczor, S. Weckbach, C. L. Schlett, M. Forsting, S. C. Ladd, K. H. Greiser, M.-A. Weber, J. Schulz-Menger, T. Niendorf, T. Pischon, S. Caspers, K. Amunts, K. Berger, R. Bülow, N. Hosten, K. Hegenscheid, T. Kröncke, J. Linseisen, M. Günther, J. G. Hirsch, A. Köhn, T. Hendel, H.-E. Wichmann, B. Schmidt, K.-H. Jöckel, W. Hoffmann, R. Kaaks, M. F. Reiser, and H. Völzke, *Whole-Body MR Imaging in the German National Cohort: Rationale, design, and technical background*, Radiology, 277 (2015), pp. 206–220.

[43] G. I. Shulman, *Ectopic fat in insulin resistance, dyslipidemia, and cardiometabolic disease*, New England Journal of Medicine, 371 (2014), pp. 1131–1141.

[44] S. Lim and J. B. Meigs, *Links between ectopic fat and vascular disease in humans*, Arteriosclerosis, Thrombosis, and Vascular Biology, 34 (2014), pp. 1820–1826.

[45] S. M. Haffner, S. Lehto, T. Rönnemaa, K. Pyörälä, and M. Laakso, *Mortality from Coronary Heart Disease in subjects with Type 2 Diabetes and in nondiabetic subjects with and without prior Myocardial Infarction*, New England Journal of Medicine, 339 (1998), pp. 229–234.

[46] S. M. Grundy, D. Becker, L. T. Clark, R. S. Cooper, M. A. Denke, J. Howard, D. B. Hunninghake, D. R. Illingworth, R. V. Luepker, P. McBride, J. M. McKenney, R. C. Pasternak, N. J. Stone, and L. Van Horn, *Detection, evaluation, and treatment of high blood cholesterol in adults (Adult Treatment Panel III)*, Circulation, 106 (2002), pp. 3143–3421.

[47] A. L. Catapano, I. Graham, G. D. Backer, O. Wiklund, M. J. Chapman, H. Drexel, A. W. Hoes, C. S. Jennings, U. Landmesser, T. R. Pedersen, Ž. Reiner,

G. Riccardi, M.-R. Taskinen, L. Tokgozoglu, W. M. M. Verschuren, C. Vlachopoulos, D. A. Wood, and J. L. Zamorano, *2016 ESC/EAS Guidelines for the Management of Dyslipidaemias*, Atherosclerosis, 253 (2016), pp. 281–344.

[48] U. Bulugahapitiya, S. Siyambalapitiya, J. Sithole, and I. Idris, *Is diabetes a coronary risk equivalent? Systematic review and meta-analysis*, Diabetic Medicine, 26 (2009), pp. 142–148.

[49] C. Lee, L. Joseph, A. Colosimo, and K. Dasgupta, *Mortality in diabetes compared with previous cardiovascular disease: A gender-specific meta-analysis*, Diabetes & Metabolism, 38 (2012), pp. 420–427.

[50] F. B. Hu, M. J. Stampfer, C. G. Solomon, S. Liu, W. C. Willett, F. E. Speizer, D. M. Nathan, and J. E. Manson, *The impact of diabetes mellitus on mortality from all causes and coronary heart disease in women: 20 years of follow-up.*, Archives of Internal Medicine, 161 (2001), pp. 1717–1723.

[51] J. D. Newman, C. B. Rockman, M. Kosiborod, Y. Guo, H. Zhong, H. S. Weintraub, A. Z. Schwartzbard, M. A. Adelman, and J. S. Berger, *Diabetes mellitus is a coronary heart disease risk equivalent for peripheral vascular disease*, American Heart Journal, 184 (2017), pp. 114–120.

[52] A. G. Tabák, C. Herder, W. Rathmann, E. J. Brunner, and M. Kivimäki, *Prediabetes: a high-risk state for diabetes development*, The Lancet, 379 (2012), pp. 2279–2290.

[53] Y. Huang, X. Cai, W. Mai, M. Li, and Y. Hu, *Association between prediabetes and risk of cardiovascular disease and all cause mortality: Systematic review and meta-analysis*, BMJ, (2016), p. i5953.

[54] D. H. Wasserman, T. J. Wang, and N. J. Brown, *The Vasculature in Prediabetes*, Circulation Research, 122 (2018), pp. 1135–1150.

[55] S. Rospleszcz, B. Thorand, T. de las Heras Gala, C. Meisinger, R. Holle, W. Koenig, U. Mansmann, and A. Peters, *Temporal trends in cardiovascular risk factors and performance of the Framingham Risk Score and the Pooled Cohort Equations*, Journal of Epidemiology and Community Health, (2018), pp. jech–2018–211102.

[56] S. Rospleszcz*, R. Lorbeer*, C. Storz, C. L. Schlett, C. Meisinger, B. Thorand, W. Rathmann, F. Bamberg, W. Lieb+, and A. Peters+, *Association of longitudi-*

nal risk profile trajectory clusters with adipose tissue depots measured by magnetic resonance imaging, PLOS ONE, (To be submitted.).

[57] S. Rospleszcz, A. Schafnitzel, W. Koenig, R. Lorbeer, S. Auweter, C. Huth, W. Rathmann, M. Heier, B. Linkohr, C. Meisinger, H. Hetterich, F. Bamberg, and A. Peters, *Association of glycemic status and segmental left ventricular wall thickness in subjects without prior cardiovascular disease: a cross-sectional study*, BMC Cardiovascular Disorders, 18 (2018), p. 162.

[58] C. Storz, S. Rospleszcz, R. Lorbeer, H. Hetterich, S. D. Auweter, W. Sommer, J. Machann, S. Gatidis, W. Rathmann, M. Heier, B. Linkohr, C. Meisinger, M. Reiser, U. Hoffmann, A. Peters, C. L. Schlett, and F. Bamberg, *Phenotypic Multiorgan Involvement of Subclinical Disease as Quantified by Magnetic Resonance Imaging in Subjects with Prediabetes, Diabetes, and Normal Glucose Tolerance*, Investigative Radiology, 53 (2018), pp. 357–364.

[59] F. Bamberg, H. Hetterich, S. Rospleszcz, R. Lorbeer, S. D. Auweter, C. L. Schlett, A. Schafnitzel, C. Bayerl, A. Schindler, T. Saam, K. Müller-Peltzer, W. Sommer, T. Zitzelsberger, J. Machann, M. Ingrisch, S. Selder, W. Rathmann, M. Heier, B. Linkohr, C. Meisinger, C. Weber, B. Ertl-Wagner, S. Massberg, M. Reiser, and A. Peters, *Subclinical Disease in Subjects with Prediabetes, Diabetes and Normal Controls from the General Population: the KORA MRI-Study*, Diabetes, 66 (2017), pp. 158–169.

[60] C. Storz, T. Rothenbacher, S. Rospleszcz, J. Linseisen, H. Messmann, C. N. D. Cecco, J. Machann, R. Lorbeer, L. S. Kiefer, E. Wintermeyer, S. D. Rado, K. Nikolaou, S. Elser, W. Rathmann, M. F. Reiser, A. Peters, C. L. Schlett, and F. Bamberg, *Characteristics and associated risk factors of diverticular disease assessed by magnetic resonance imaging in subjects from a Western general population*, European Radiology, (2018), pp. 1–10.

[61] C. Storz, S. D. Heber, S. Rospleszcz, J. Machann, S. Sellner, K. Nikolaou, R. Lorbeer, S. Gatidis, S. Elser, A. Peters, C. L. Schlett, and F. Bamberg, *The role of visceral and subcutaneous adipose tissue measurements and their ratio by Magnetic Resonance Imaging in subjects with prediabetes, diabetes and healthy controls from a general population without cardiovascular disease*, The British Journal of Radiology, 91 (2018), p. 20170808.

[62] L. S. Kiefer, J. Fabian, S. Rospleszcz, R. Lorbeer, J. Machann, C. Storz, M. S. Kraus, C. L. Schlett, F. Roemer, E. Wintermeyer, W. Rathmann, K. Nikolaou, A. Peters, and F. Bamberg, *Assessment of the degree of abdominal myosteatosis*

by magnetic resonance imaging in subjects with diabetes, prediabetes and healthy controls from the general population, European Journal of Radiology, 105 (2018), pp. 261–268.

[63] D. Dermyshi, S. Rospleszcz, F. Bamberg, and A. Peters, *Association of serum uric acid to visceral, subcutaneous and hepatic fat tissue: A cross-sectional magnetic resonance imaging study*, BMC Gastroenterology, (To be submitted).

[64] R. Holle, M. Happich, H. Löwel, and H. E. Wichmann, *KORA –A research platform for population based health research*, Gesundheitswesen (Bundesverband der Arzte des Öffentlichen Gesundheitsdienstes (Germany)), 67 (2005), pp. S19–25.

[65] M. D. Cerqueira, N. J. Weissman, V. Dilsizian, A. K. Jacobs, S. Kaul, W. K. Laskey, D. J. Pennell, J. A. Rumberger, T. Ryan, and M. S. Verani, *Standardized myocardial segmentation and nomenclature for tomographic imaging of the heart a statement for healthcare professionals from the cardiac imaging committee of the Council on Clinical Cardiology of the American Heart Association*, Circulation, 105 (2002), pp. 539–542.

[66] R. Lorbeer, S. Rospleszcz, C. L. Schlett, S. D. Heber, J. Machann, B. Thorand, C. Meisinger, M. Heier, A. Peters, and F. Bamberg, *Correlation of MRI-derived adipose tissue measurements and anthropometric markers with prevalent hypertension in the community*, Journal of Hypertension, 36 (2018), pp. 1555–1562.

[67] R. Lorbeer, C. Bayerl, S. Auweter, S. Rospleszcz, W. Lieb, C. Meisinger, M. Heier, A. Peters, F. Bamberg, and H. Hetterich, *Association between MRI-derived hepatic fat fraction and blood pressure in participants without history of cardiovascular disease*, Journal of Hypertension, 35 (2017), pp. 737–744.

[68] S. D. Heber, H. Hetterich, R. Lorbeer, C. Bayerl, J. Machann, S. Auweter, C. Storz, C. L. Schlett, K. Nikolaou, and M. Reiser, *Pancreatic fat content by magnetic resonance imaging in subjects with prediabetes, diabetes, and controls from a general population without cardiovascular disease*, PLOS ONE, 12 (2017), p. e0177154.

[69] B. Van Calster, D. Nieboer, Y. Vergouwe, B. De Cock, M. J. Pencina, and E. W. Steyerberg, *A calibration hierarchy for risk models was defined: from utopia to empirical data*, Journal of Clinical Epidemiology, 74 (2016), pp. 167–76.

[70] C. Genolini and B. Falissard, *Kml: k-means for longitudinal data*, Computational Statistics, 25 (2009), pp. 317–328.

[71] J. C. Gower, *A general coefficient of similarity and some of its properties*, Biometrics, 27 (1971), p. 857.

[72] J. D. Berry, A. Dyer, X. Cai, D. B. Garside, H. Ning, A. Thomas, P. Greenland, L. V. Horn, R. P. Tracy, and D. M. Lloyd-Jones, *Lifetime risks of cardiovascular disease*, New England Journal of Medicine, 366 (2012), pp. 321–329.

[73] R. R. Huxley and M. Woodward, *Cigarette smoking as a risk factor for coronary heart disease in women compared with men: A systematic review and meta-analysis of prospective cohort studies*, The Lancet, 378 (2011), pp. 1297–1305.

[74] S. A. E. Peters, R. R. Huxley, and M. Woodward, *Diabetes as risk factor for incident coronary heart disease in women compared with men: A systematic review and meta-analysis of 64 cohorts including 858,507 individuals and 28,203 coronary events*, Diabetologia, 57 (2014), pp. 1542–1551.

[75] A. P. DeFilippis, R. Young, C. J. Carrubba, J. W. McEvoy, M. J. Budoff, R. S. Blumenthal, R. A. Kronmal, R. L. McClelland, K. Nasir, and M. J. Blaha, *An analysis of calibration and discrimination among multiple cardiovascular risk scores in a modern multiethnic cohort*, Annals of Internal Medicine, 162 (2015), pp. 266–75.

[76] M. Kavousi, M. G. Leening, D. Nanchen, and et al., *Comparison of application of the ACC/AHA Guidelines, Adult Treatment Panel III Guidelines, and European Society of Cardiology Guidelines for cardiovascular disease prevention in a European cohort*, JAMA, 311 (2014), pp. 1416–1423.

[77] N. R. Cook and P. M. Ridker, *Calibration of the Pooled Cohort equations for atherosclerotic cardiovascular disease: an update*, Annals of Internal Medicine, 165 (2016), pp. 786–794.

[78] S. Mora, N. K. Wenger, N. R. Cook, J. Liu, B. V. Howard, M. C. Limacher, S. Liu, K. L. Margolis, L. W. Martin, N. P. Paynter, P. M. Ridker, J. G. Robinson, J. E. Rossouw, M. M. Safford, and J. E. Manson, *Evaluation of the Pooled Cohort Risk Equations for cardiovascular risk prediction in a multiethnic cohort from the Women's Health Initiative*, JAMA Internal Medicine, 178 (2018), p. 1231.

[79] E. Fabbrini, C. Conte, and F. Magkos, *Methods for assessing intrahepatic fat content and steatosis*, Current Opinion in Clinical Nutrition and Metabolic Care, 12 (2009), pp. 474–481.

[80] I. Lingvay, V. Esser, J. L. Legendre, A. L. Price, K. M. Wertz, B. Adams-Huet, S. Zhang, R. H. Unger, and L. S. Szczepaniak, *Noninvasive quantification of pan-*

creatic fat in humans, The Journal of Clinical Endocrinology & Metabolism, 94 (2009), pp. 4070–4076.

[81] G. Targher, C. P. Day, and E. Bonora, *Risk of Cardiovascular Disease in patients with nonalcoholic fatty liver disease*, New England Journal of Medicine, 363 (2010), pp. 1341–1350.

[82] A. J. Buckley, E. L. Thomas, N. Lessan, F. M. Trovato, G. M. Trovato, and S. D. Taylor-Robinson, *Non-alcoholic fatty liver disease: Relationship with cardiovascular risk markers and clinical endpoints*, Diabetes Research and Clinical Practice, 144 (2018), pp. 144–152.

[83] N. Stefan, F. Artunc, N. Heyne, J. Machann, E. D. Schleicher, and H.-U. Häring, *Obesity and renal disease: not all fat is created equal and not all obesity is harmful to the kidneys*, Nephrology Dialysis Transplantation, 31 (2016), pp. 726–730.

[84] H. Zelicha, D. Schwarzfuchs, I. Shelef, Y. Gepner, G. Tsaban, L. Tene, A. Yaskolka Meir, A. Bilitzky, O. Komy, N. Cohen, N. Bril, M. Rein, D. Serfaty, S. Kenigsbuch, Y. Chassidim, B. Sarusi, J. Thiery, U. Ceglarek, M. Stumvoll, M. Blüher, Y. S. Haviv, M. J. Stampfer, A. Rudich, and I. Shai, *Changes of renal sinus fat and renal parenchymal fat during an 18-month randomized weight loss trial*, Clinical Nutrition, 37 (2017), pp. 1145–1153.

[85] M. Heni, J. Machann, H. Staiger, N. F. Schwenzer, A. Peter, F. Schick, C. D. Claussen, N. Stefan, H.-U. Häring, and A. Fritsche, *Pancreatic fat is negatively associated with insulin secretion in individuals with impaired fasting glucose and/or impaired glucose tolerance: a nuclear magnetic resonance study*, Diabetes/Metabolism Research and Reviews, 26 (2010), pp. 200–205.

[86] L. Tene, I. Shelef, D. Schwarzfuchs, Y. Gepner, A. Yaskolka Meir, G. Tsaban, H. Zelicha, A. Bilitzky, O. Komy, N. Cohen, N. Bril, M. Rein, D. Serfaty, S. Kenigsbuch, Y. Chassidim, B. Sarusy, U. Ceglarek, M. Stumvoll, M. Blüher, J. Thiery, M. J. Stampfer, A. Rudich, and I. Shai, *The effect of long-term weight-loss intervention strategies on the dynamics of pancreatic fat and morphology: An MRI RCT study*, Clinical Nutrition ESPEN, 24 (2018), pp. 82–89.

[87] C. L. Schlett, R. Lorbeer, C. Arndt, S. Auweter, J. Machann, H. Hetterich, B. Linkohr, W. Rathmann, A. Peters, and F. Bamberg, *Association between abdominal adiposity and subclinical measures of left-ventricular remodeling in diabetics, prediabetics and normal controls without history of cardiovascular disease as*

measured by magnetic resonance imaging: results from the KORA-FF4 Study, Cardiovascular Diabetology, 17 (2018), p. 88.

[88] H. Patscheider, R. Lorbeer, S. Auweter, A. Schafnitzel, C. Bayerl, A. Curta, W. Rathmann, M. Heier, C. Meisinger, A. Peters, F. Bamberg, and H. Hetterich, *Subclinical changes in MRI-determined right ventricular volumes and function in subjects with prediabetes and diabetes*, European Radiology, 28 (2018), pp. 3105–3113.

[89] C. Storz, H. Hetterich, R. Lorbeer, S. D. Heber, A. Schafnitzel, H. Patscheider, S. Auweter, T. Zitzelsberger, W. Rathmann, K. Nikolaou, M. Reiser, C. L. Schlett, F. von Knobelsdorff-Brenkenhoff, A. Peters, J. Schulz-Menger, and F. Bamberg, *Myocardial tissue characterization by contrast-enhanced cardiac magnetic resonance imaging in subjects with prediabetes, diabetes, and normal controls with preserved ejection fraction from the general population*, European Heart Journal: Cardiovascular Imaging, 19 (2017), pp. 701–708.

[90] H. Skali, A. Shah, D. K. Gupta, S. Cheng, B. Claggett, J. Liu, N. Bello, D. Aguilar, O. Vardeny, and K. Matsushita, *Cardiac structure and function across the glycemic spectrum in elderly men and women free of prevalent heart disease: The Atherosclerosis Risk In the Community Study*, Circulation: Heart Failure, 8 (2015), pp. 448–454.

[91] R. S. Velagaleti, P. Gona, M. L. Chuang, C. J. Salton, C. S. Fox, S. J. Blease, S. B. Yeon, W. J. Manning, and C. J. O'Donnell, *Relations of insulin resistance and glycemic abnormalities to cardiovascular magnetic resonance measures of cardiac structure and function: the Framingham Heart Study*, Circulation: Cardiovascular Imaging, 3 (2010), pp. 257–63.

[92] A. G. Bertoni, D. C. Goff, R. B. D'Agostino, K. Liu, W. G. Hundley, J. A. Lima, J. F. Polak, M. F. Saad, M. Szklo, and R. P. Tracy, *Diabetic cardiomyopathy and subclinical cardiovascular disease: The Multi-Ethnic Study of Atherosclerosis (MESA)*, Diabetes Care, 29 (2006), pp. 588–594.

[93] R. M. A. Henry, O. Kamp, P. J. Kostense, A. M. W. Spijkerman, J. M. Dekker, R. van Eijck, G. Nijpels, R. J. Heine, L. M. Bouter, and C. D. A. Stehouwer, *Left ventricular mass increases with deteriorating glucose tolerance, especially in women: Independence of increased arterial stiffness or decreased flow-mediated dilation: The Hoorn Study*, Diabetes Care, 27 (2004), pp. 522–529.

[94] A. M. Larghat, P. P. Swoboda, J. D. Biglands, M. T. Kearney, J. P. Greenwood, and S. Plein, *The microvascular effects of insulin resistance and diabetes on cardiac structure, function, and perfusion: a cardiovascular magnetic resonance study*, European Heart Journal: Cardiovascular Imaging, 15 (2014), pp. 1368–1376.

[95] J. Asbun and F. J. Villarreal, *The pathogenesis of myocardial fibrosis in the setting of diabetic cardiomyopathy*, Journal of the American College of Cardiology, 47 (2006), pp. 693–700.

[96] L. Van Heerebeek, N. Hamdani, M. L. Handoko, I. Falcao-Pires, R. J. Musters, K. Kupreishvili, A. J. Ijsselmuiden, C. G. Schalkwijk, J. G. Bronzwaer, and M. Diamant, *Diastolic stiffness of the failing diabetic heart*, Circulation, 117 (2008), pp. 43–51.

[97] C. W. Tsao, P. N. Gona, C. J. Salton, M. L. Chuang, D. Levy, W. J. Manning, and C. J. O'Donnell, *Left ventricular structure and risk of cardiovascular events: A Framingham Heart Study cardiac magnetic resonance study*, Journal of the American Heart Association, 4 (2015), p. e002188.

[98] N. Stefan, A. Fritsche, F. Schick, and H.-U. Häring, *Phenotypes of prediabetes and stratification of cardiometabolic risk*, The Lancet Diabetes & Endocrinology, 4 (2016), pp. 789–798.

[99] K. Kantartzis, J. Machann, F. Schick, A. Fritsche, H.-U. Häring, and N. Stefan, *The impact of liver fat vs visceral fat in determining categories of prediabetes*, Diabetologia, 53 (2010), pp. 882–889.

[100] F. E. de Leeuw, J. C. de Groot, E. Achten, M. Oudkerk, L. M. Ramos, R. Heijboer, A. Hofman, J. Jolles, J. van Gijn, and M. M. Breteler, *Prevalence of cerebral white matter lesions in elderly people: a population based magnetic resonance imaging study. The Rotterdam Scan Study.*, Journal of Neurology, Neurosurgery, and Psychiatry, 70 (2001), pp. 9–14.

[101] V. Novak, D. Last, D. C. Alsop, A. M. Abduljalil, K. Hu, L. Lepicovsky, J. Cavallerano, and L. A. Lipsitz, *Cerebral blood flow velocity and periventricular White Matter Hyperintensities in type 2 diabetes*, Diabetes Care, 29 (2006), pp. 1529–1534.

[102] J. de Bresser, H. J. Kuijf, K. Zaanen, M. A. Viergever, J. Hendrikse, and G. J. Biessels, *White matter hyperintensity shape and location feature analysis on brain: proof of principle study in patients with diabetes*, Scientific Reports, 8 (2018), p. 1893.

[103] C. Würslin, J. Machann, H. Rempp, C. Claussen, B. Yang, and F. Schick, *Topography mapping of whole body adipose tissue using a fully automated and standardized procedure*, Journal of Magnetic Resonance Imaging, 31 (2010), pp. 430–439.

[104] R. J. Gillies, P. E. Kinahan, and H. Hricak, *Radiomics: Images are more than pictures, they are data*, Radiology, 278 (2016), pp. 563–577.

[105] K. Hegenscheid, R. Seipel, C. O. Schmidt, H. Völzke, J. P. Kühn, R. Biffar, H. K. Kroemer, N. Hosten, and R. Puls, *Potentially relevant incidental findings on research whole-body MRI in the general adult population: frequencies and management*, European Radiology, 23 (2013), pp. 816–26.

Appendix

Manuscript I

Title: Temporal trends in cardiovascular risk factors and performance of the Framingham Risk Score and the Pooled Cohort Equations

Authors: Susanne Rospleszcz,
Barbara Thorand,
Tonia de las Heras Gala,
Christa Meisinger,
Rolf Holle,
Wolfgang Koenig,
Ulrich Mansmann,
Annette Peters

Journal: Journal of Epidemiology and Community Health
Status: Published
doi: 10.1136/jech-2018-211102

Research report

Temporal trends in cardiovascular risk factors and performance of the Framingham Risk Score and the Pooled Cohort Equations

Susanne Rospleszcz,[1] Barbara Thorand,[1] Tonia de las Heras Gala,[1] Christa Meisinger,[1,2] Rolf Holle,[3] Wolfgang Koenig,[4,5,6] Ulrich Mansmann,[7] Annette Peters[1,6,8]

► Additional material is published online only. To view please visit the journal online (http://dx.doi.org/10.1136/jech-2018-211102).

For numbered affiliations see end of article.

Correspondence to
Susanne Rospleszcz, Institute of Epidemiology, Helmholtz Zentrum München, German Research Center for Environmental Health, Neuherberg 85764, Germany; susanne.rospleszcz@helmholtz-muenchen.de

Received 28 May 2018
Revised 1 August 2018
Accepted 31 August 2018

To cite: Rospleszcz S, Thorand B, de las Heras Gala T, *et al*. *J Epidemiol Community Health* Epub ahead of print: [*please include* Day Month Year]. doi:10.1136/jech-2018-211102

ABSTRACT

Background The Framingham Risk Score (FRS) and the Pooled Cohort Equations (PCE) are established tools for the prediction of cardiovascular disease (CVD) risk. In the Western world, decreases in incidence rates of CVD were observed over the last 30 years. Thus, we hypothesise that there are also temporal trends in the risk prediction performance of the FRS and PCE from 1990 to 2000.

Methods We used data from n=7789 men and women aged 40–74 years from three prospective population-based cohort studies enrolled in Southern Germany in 1989/1990, 1994/1995 and 1999/2000. 10-year CVD risk was calculated by recalibrated equations of the FRS or PCE. Calibration was evaluated by percentage of overestimation and Hosmer-Lemeshow tests. Discrimination performance was assessed by receiver operating characteristic (ROC) curves and corresponding area under the curve (AUC).

Results Across the three studies, we found significant temporal trends in risk factor distributions and predicted risks by both risk scores (men: 18.0%, 15.4%, 14.9%; women: 8.7%, 11.2%, 10.8%). Furthermore, also the discrimination performance evolved differently for men (AUC PCE: 76.4, 76.1, 72.8) and women (AUC PCE: 75.9, 79.5, 80.5). Both risk scores overestimated actual CVD risk.

Conclusion There are temporal trends in the performance of the FRS and PCE. Although the overall performance remains adequate, sex-specific trends have to be taken into account for further refinement of risk prediction models.

BACKGROUND

Cardiovascular disease (CVD) is a leading cause of mortality and morbidity worldwide.[1]

To reduce the burden of CVD, prevention strategies such as lifestyle counselling and treatment with medication are called for and have to be tailored to the population at risk. For effective prevention, people at a high risk of CVD who would benefit most from these strategies have to be identified. This is often done by predicting the risk of developing CVD based on an individual's risk factor levels, such as age, blood pressure or serum cholesterol levels. Risk prediction models are crucial tools for establishing general treatment guidelines. However, they are also used by clinicians to decide on the best therapy for an individual patient.

A vast number of CVD risk prediction models are available nowadays, and their number is constantly growing.[2] Often the development of a new model is motivated by the claim that, as existing models have been calculated from older data, they fail to capture the changing distribution of risk factors in the population. Indeed, the distribution of traditional risk factors and metabolic profiles in Western populations changed during the last decades. Specifically, mean systolic blood pressure has decreased, probably due to increased awareness and more aggressive treatment.[3] The prevalence of smoking has decreased with considerable variation according to region and education status[4] and total cholesterol levels have declined with age-specific and sex-specific variations.[5] At the same time, the prevalence of obesity has risen substantially for both men and women.[6]

Additionally, total cardiovascular mortality has been declining in the USA and Europe.[7] However, it remains unclear how this shifting risk factor distribution and reduction of overall risk translates into changes in the performance of risk prediction models. We therefore aimed to assess temporal trends in traditional cardiovascular risk factors and how their changing distribution relates to a change in risk prediction performance. To this aim, we analyse 10-year risks of CVD predicted by the Framingham Risk Score (FRS)[8] and the Pooled Cohort Equations (PCE).[9]

We hypothesise that changes in risk factor distributions are reflected in a changing performance of the CVD risk scores.

METHODS

Study sample

We used data from three population-based cohorts that were established in the Region of Augsburg, Germany (KORA: 'Kooperative Gesundheitsforschung in der Region Augsburg'). Time of data collection was 1989–1990 for cohort S2, 1994–1995 for cohort S3 and 1999–2000 for cohort S4. Sampling methods and cohort profiles have been described elsewhere.[10 11] All cohorts were followed up for mortality and for myocardial infarction (MI) and stroke incidence until 2011. For each cohort, we used 10 years of follow-up to calculate the risk scores. Participants were excluded according to criteria for FRS and PCE as presented in online supplementary figure 1: in particular we only analysed subjects aged 40–74 years.

Outcome assessment

Death from CVD was defined as International Classification of Diseases, ninth revision codes 390–459

and 798. Death certificates were obtained to determine the cause of death.

Non-fatal MI and stroke incidence was assessed by questionnaire and validated by reviewing the medical documentation of the participant's physician. MI was additionally validated with the information from the MONICA/KORA Myocardial Infarction Registry.[12]

Covariable assessment

Blood pressure and serum cholesterol measurements for the S2 and S3 studies were carried out according to the MONICA Manual as described elsewhere.[10] For the S4 study, blood pressure was measured after a 15-min rest using a validated automatic device (OMRON HEM 705-CP). Serum total and high-density lipoprotein cholesterol (HDL-C) were measured by enzymatic methods (CHOD-PAP; Boehringer, Mannheim).[11 13]

Diabetes was defined as self-reported diabetes or use of anti-diabetic medication. Antihypertensive treatment was defined according to the most recent guidelines of the German Hypertension Society.[14] Smoking and intake of lipid-lowering agents was determined via questionnaire.

Statistical methods

Predicted 10-year risks were calculated according to the published formulae for FRS and PCE[8 9] with recalibration. Both FRS and PCE are based on Cox proportional hazard regression models and predict the risk of experiencing a cardiovascular event over a 10-year period. The published formulae provide the regression model coefficients and use risk factor mean values and baseline survival probabilities from the original populations to derive a risk score estimate. For our analysis, recalibration consisted of inserting risk factor mean values and baseline survival probabilities from each study into the original risk score equations, while maintaining the original model coefficients. Thereby, the original model structure, including sex stratification, non-linear model terms and interaction terms are retained and within this original framework, the recalibration only reflects the specific properties of the sample at hand. We tested for linear trends in baseline characteristics and predicted 10-year risks with linear and logistic regression using orthogonal contrasts.[15]

Calibration of the risk scores was assessed visually by calibration plots and quantitatively by Hosmer-Lemeshow χ^2tests, calibration slopes and % discordance between the number of observed and predicted events.[16] Clinically relevant thresholds of 5, 7.5, 10% and 20% were used, as well as continuous calibration curves based on LOESS smoothing.[17]

Discrimination performance was assessed by receiver operating characteristic (ROC) curves and their respective area under the curve (AUC), which is equivalent to the c-statistic.[18] Differences in AUCs over time were evaluated by an unpaired DeLong test. Additionally, we report Somer's D statistic, which indicates the rank correlation between predicted risk probabilities and observed event rate. For relevant thresholds, sensitivity was calculated and differences were assessed by meta-regression assuming fixed effects.[19] Population-attributable fractions (PAFs) of risk scores ≥20% or ≥10% as opposed to risk scores <20% and <10%, respectively, were calculated by Levin's formula with CIs obtained by percentile bootstrapping. We use the term 'attributable' without implying causality.

RESULTS

Trends in risk factor distributions

Table 1 shows the baseline characteristics of the participants of all three studies.

Mean age was similar across all studies for both men and women. There was a significant trend for increasing body mass index (BMI) for both men and women.

Mean systolic blood pressure decreased for both men and women, but more pronounced in women. The proportion of men receiving antihypertensive treatment increased significantly.

There was no significant linear trend in mean HDL-C levels. Mean total cholesterol levels and mean low-density lipoprotein cholesterol (LDL-C) levels declined significantly for both sexes. The proportion of both men and women receiving lipid-lowering treatment increased significantly.

Table 1 Baseline characteristics of participants in Kooperative Gesundheitsforschung in der Region Augsburg S2 (1989–1990), S3 (1994–1995) and S4 (1999–2000)

	Men					Women				
	S2	S3	S4	Linear trend		S2	S3	S4	Linear trend	
	n=1432	n=1332	n=1139	Estimate	P values	n=1360	n=1322	n=1204	Estimate	P values
Age, years	55.8 (9.7)	56.6 (9.6)	56.0 (9.5)	0.10	0.70	55.7 (9.4)	55.4 (9.7)	55.4 (9.6)	−0.24	0.36
BMI, kg/m^2	27.6 (3.6)	27.8 (3.5)	28.0 (3.9)	0.30	<0.05	27.0 (4.7)	27.4 (4.9)	27.5 (4.9)	0.34	<0.05
Systolic BP, mm Hg	138.1 (18.4)	138.7 (18.8)	136.8 (18.4)	−0.87	0.09	133.6 (20.2)	134.0 (20.6)	127.0 (19.5)	−4.66	<0.05
Diastolic BP, mm Hg	83.2 (11.2)	83.9 (11.3)	84.7 (10.7)	1.04	<0.05	79.9 (10.8)	80.3 (10.9)	79.4 (10.2)	−0.35	0.25
Total cholesterol, mg/dL	245.0 (44.5)	238.8 (42.6)	236.1 (41.1)	−6.29	<0.05	245.9 (46.5)	237.4 (42.4)	235.8 (41.1)	−7.19	<0.05
HDL-C, mg/dL	51.6 (15.2)	48.5 (14.1)	51.5 (14.2)	−0.03	0.95	63.8 (15.9)	59.9 (16.8)	64.5 (17.2)	0.53	0.26
LDL-C, mg/dL	155.3 (40.5)	149.8 (40.3)	148.4 (38.9)	−4.90	<0.05	152.6 (44.4)	145.6 (41.6)	141.8 (40.1)	−7.62	<0.05
Type 2 diabetes	83 (5.8%)	67 (5.0%)	74 (6.5%)	0.09	0.46	59 (4.3%)	43 (3.3%)	58 (4.8%)	0.08	0.56
Antihypertensive treatment	229 (16.0%)	232 (17.4%)	218 (19.1%)	0.15	<0.05	268 (19.7%)	266 (20.1%)	266 (22.1%)	0.10	0.14
Lipid-lowering treatment	50 (3.5%)	43 (3.2%)	73 (6.4%)	0.45	<0.05	41 (3.0%)	56 (4.2%)	82 (6.8%)	0.60	<0.05
Smoking	400 (27.9%)	331 (24.8%)	274 (24.1%)	−0.14	<0.05	219 (16.1%)	230 (17.4%)	209 (17.4%)	0.06	0.39
CVD event	177 (12.4%)	139 (10.4%)	119 (10.4%)	−0.13	0.13	60 (4.4%)	76 (5.7%)	67 (5.6%)	0.17	0.18
Fatal CVD event	106 (7.4%)	62 (4.7%)	46 (4.0%)	−0.45	<0.05	36 (2.6%)	31 (2.3%)	28 (2.3%)	−0.01	0.61

Continuous variables are presented as arithmetic mean (SD). Categorical variables are presented as counts (%). CVD event is defined as death from CVD, non-fatal MI and stroke.
BMI, body mass index; BP, blood pressure; CVD, cardiovascular disease; HDL-C, high-density lipoprotein cholesterol; LDL-C, low-density lipoprotein cholesterol; MI, myocardial infarction.

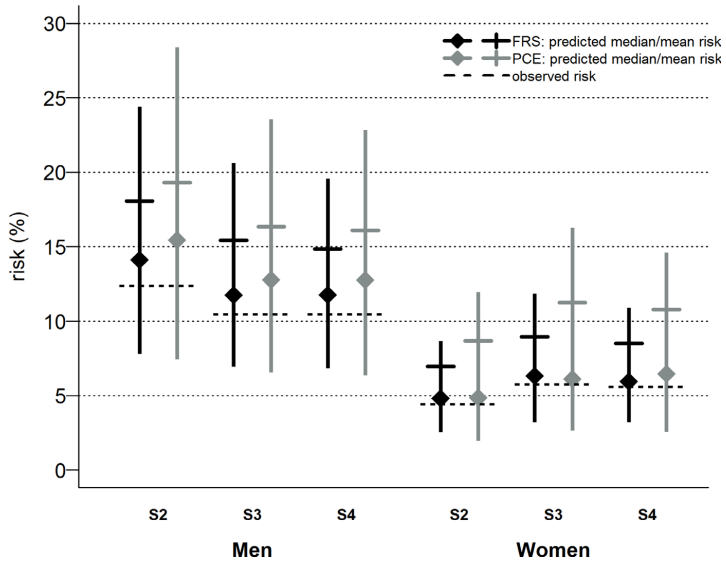

Figure 1 Predicted risks by Framingham Risk Score (FRS) and Pooled Cohort Equations (PCE). On the y-axis: risk of cardiovascular disease event in %. On the x-axis: FRS (black) and PCE (grey) for the three studies, for men (dashed lines) and women (solid lines), respectively. Displayed are the median (filled diamond) and mean (cross) predicted risks with interquartile range as calculated by the recalibrated equations of the FRS and PCE. Actually observed risk is indicated by a dashed line.

The prevalence of diabetes slightly increased non-linearly for both men and women. Prevalence of smoking significantly decreased in men and increased slightly in women.

There was no significant trend in CVD event rates, though they slightly declined for men and increased for women. However, fatal CVD event rates were significantly declining for men.

Trends in predicted risks of the FRS and PCE

Figure 1 shows mean and median predicted risk for both risk scores and the actually observed event rate. Mean predicted risks by both FRS and PCE declined significantly for men (estimate of linear trend: both −2.3, $p<0.001$), but increased for women (estimate of linear trend FRS 1.1, PCE 1.5, $p<0.001$).

Trends in calibration of the FRS and PCE

Both the FRS and PCE substantially overestimated actual CVD risk. Discordance for the FRS was 46%, 48% and 42% for men in the three studies, respectively, whereas for women discordance was 58%, 55% and 53%. Discordance for the PCE was 56%, 57% and 54% for men and 96%, 96% and 94% for women. Smooth calibration plots are displayed in figure 2, and further details are presented in online supplementary figure 2 and table 1. Overall, the FRS showed better calibration for men and women and calibration slightly improved for both the FRS and PCE in the three studies. Calibration slopes for the FRS were 1.07, 1.13 and 0.97 for men and 0.99, 1.14 and 1.00 for women, whereas calibration slopes for the PCE were 1.01, 1.11 and 0.87 for men and 0.81, 0.93 and 0.90 for women.

Trends in discrimination performance of the FRS and PCE

As shown in figure 3, for men, the discrimination performance of both the FRS and PCE declined from the S2 to the S4 study; however, the difference in AUC was not statistically significant ($p=0.232$ and 0.223, respectively). In contrast, for women the discrimination performance increased for both the FRS and PCE; however, the difference in AUC was not significant ($P=0.749$ and 0.220, respectively). In the S4 study, the difference in AUC between men and women was statistically significant for the PCE ($p=0.02$), but not for the FRS ($p=0.12$).

In the same vein, Somer's D rank correlation for the FRS decreased from 0.53 in S2 and S3 to 0.46 in S4 in men and increased from 0.54 to 0.55 and 0.57 in women. Corresponding values for the PCE were 0.53, 0.52 and 0.46 for men and 0.52, 0.59 and 0.61 for women, respectively.

The sensitivity at clinically relevant thresholds decreased for men and increased for women; again for both risk scores in a similar pattern as presented in table 2.

Trends in PAFs

The evolvement of PAFs is displayed in figure 4. For men, the PAF of a risk score ≥20% or ≥10% declined from the S2 to the S4 study for both risk scores. For women, the PAF of a risk score ≥10% increased over the three studies, whereas the PAFs of a risk score ≥20% were more divergent: The PAF of an FRS ≥20% was comparable in the S2 and S4 study, but the PAF of a PCE ≥20% increased in the same time frame.

DISCUSSION

In this study, we evaluated temporal trends in the distribution of traditional cardiovascular risk factors in a German population and in the performance of two commonly employed CVD risk scores, the FRS and the PCE. We found (i) significant trends in risk factor distributions with declining levels of systolic blood pressure and lipid values and increasing BMI for both men and women, (ii) significant trends in predicted risks for both FRS and PCE, and (iii) sex-specific differences in the temporal development of the risk scores' performance with nominally decreasing performance for men and increasing performance for women.

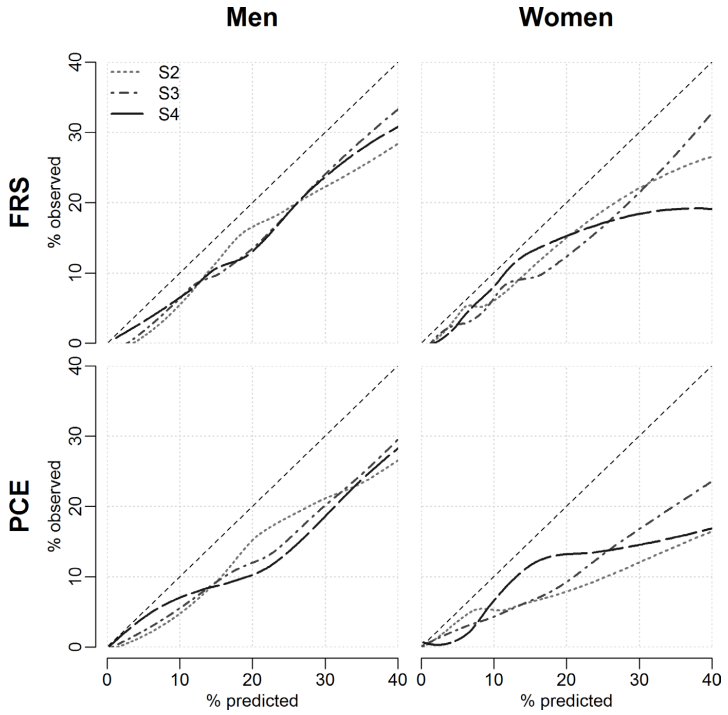

Figure 2 Smooth calibration of the Framingham Risk Score (FRS) and Pooled Cohort Equations (PCE) in the three studies. On the x-axis: predicted probability of cardiovascular disease (CVD) event by the respective risk score, calculated by LOESS smoothing. On the y-axis: rate of observed CVD events. Light grey, dotted line: S2 study; medium grey, dashed-and-dotted line: S3 study, dark grey, dashed line: S4 study. This figure was created by an adapted version of the the R function val.prob.ci.2 from Van Calster *et al*.[17]

Overall, the FRS and the PCE evolved over time in a similar pattern. We observed fundamental overestimation of actual CVD risk, especially for the PCE. This has already been reported by other studies[20–22] and seems to indicate an inherent feature of the design of the PCE.[23] We could show that calibration slightly increased over time; however, not to a substantial extent. This development was comparable for men and women.

Trends in predicted risks can give important hints about future CVD development in a population. Ford[15] analysed predicted CVD risks by the FRS in six consecutive 2-year cycles of the National Health and Nutrition Examination Survey and found decreasing predicted risks in white subjects; however, the decrease was not significant and men and women were combined. No data on actual CVD events were available.

In our analysis, the change in absolute numbers of predicted risk resulted into sex-specific changes in prediction performance of the risk scores. We observed a decline in AUC for men and an increase for women. However, in all studies and for both men and women, the discrimination performance of both risk scores as measured by AUC was >70.

It has been noted that risk prediction models perform differently for men and women.[24] Women develop CVD later in life and the strength of associations of some risk factors, especially smoking and diabetes, are different.[25 26] In our sample, although CVD risk was lower for women, both risk scores performed better than for men. These findings were also reported from other studies[27] and are probably due to higher hazard ratios of the single underlying risk factors.

Our analysis of the PAF showed that high-risk categories (≥10%, ≥20%) of both risk scores capture a major part of CVD burden. For women, the PAF increased over time, supporting our other findings of a developing better discrimination performance of the risk models for women. Further research is needed to disentangle the effects of the single risk factors that contribute to the risk scores. Cheng *et al*, who analysed data from the ARIC cohort, found that due to a shifting risk factor distribution the PAF of most traditional risk factors was declining for both men and women with profound sex differences.[28]

Our results support the idea that established models derived from older population- based data still perform sufficiently well in risk prediction, if appropriately adapted to the population at hand.[2 29]

We used standardised measurement techniques on independent cohorts with the same study design and sampling scheme with the same length of follow-up. These cohorts stem from the same geographical area and therefore comprise the same genetic background. This design has the advantage—compared with using the same cohort at different time points—that we can rule out ageing effects, survivor bias and longitudinal dependencies of risk factor profiles in subjects.

Our study has several limitations. Most importantly, we might have had insufficient power to discover some differences due to the low event rate, especially in women. Replication of our findings in a population with higher CVD event rates is therefore needed. The possibility of residual confounding cannot be ruled out. Additionally, we cannot exclude that different response

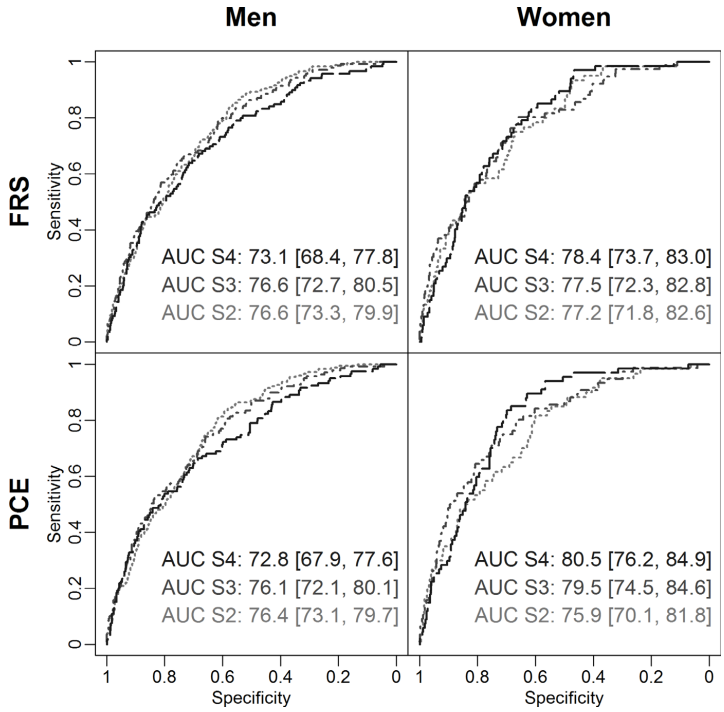

Figure 3 Receiver operating characteristic (ROC) curves and area under the curve (AUC) for Framingham Risk Score (FRS) and Pooled Cohort Equations (PCE) in the three studies. Displayed are the ROC curves and corresponding AUC when the respective risk score is used as the only predictor for a CVD event. Light grey, dotted: S2 study; medium grey, dashed-and-dotted: S3 study; dark grey, dashed: S4 study.

rates in the three cohorts affected the distribution of the participants' risk factors. However, potential incomplete ascertainment of CVD events does not seem to have profound influence on the risk scores' performance.[30] Furthermore, we refrained from reporting other common measures of model assessment, such as the Net Reclassification Index, as this measure is mainly used to compare an extended model to a baseline model to quantify the potential improvement in risk performance, or positive predictive values (PPVs), as these are highly dependent on the rate of CVD events, which differ between our three cohorts, thus rendering a comparison of PPVs invalid.

Many other CVD risk scores exist besides the FRS and PCE. For European populations, SCORE[31] is often used; however, this score only predicts CVD mortality. Using only fatal CVD events would have further diminished our already low event rate (compare table 1); therefore, we did not analyse the performance of SCORE in this study. Other commonly used risk scores such as PROCAM,[32] Reynolds Risk Score[33 34] and QRISK2[35] require

Table 2 Performance of the Framingham Risk Score (FRS) and Pooled Cohort Equations (PCE) at clinically relevant thresholds in Kooperative Gesundheitsforschung in der Region Augsburg S2, S3 and S4

		FRS						PCE					
		7.5%		10%		20%		7.5%		10%		20%	
Threshold		Estimate	95% CI	Estimate	95% CI	Estimate	95% CI	Estimate	95% CI	Estimate	95% CI	Estimate	95% CI
Men													
Sensitivity	S2	98.3	95.1 to 99.6	94.4	89.9 to 97.3	66.1	58.6 to 73.0	97.2	93.5 to 99.1	94.4	89.9 to 97.3	75.7	68.7 to 81.8
	S3	96.4	91.8 to 98.8	89.2	82.8 to 93.8	59.7	51.1 to 67.9	95.7	90.8 to 98.4	89.9	83.7 to 94.4	65.5	56.9 to 73.3
	S4	93.3	87.2 to 97.1	83.2	75.2 to 89.4	52.1	42.8 to 61.3	91.6	85.1 to 95.9	86.6	79.1 to 92.1	60.5	51.1 to 69.3
	P values	0.079		0.008		0.054		0.085		0.068		0.015	
Women													
Sensitivity	S2	61.7	48.2, 73.9	55.0	41.6 to, 67.9	20.0	10.8 to 32.3	71.7	58.6 to 82.5	61.7	48.2 to 73.9	35.0	23.1 to 48.4
	S3	80.3	69.5, 88.5	71.1	59.5 to 80.9	36.8	26.1 to 48.7	84.2	74.0 to 91.6	80.3	69.5 to 88.5	57.9	46.0 to 69.1
	S4	80.6	69.1, 89.2	67.2	54.6 to 78.2	25.4	15.5 to 37.5	91.0	81.5 to 96.6	85.1	74.3 to 92.6	47.8	35.4 to 60.3
	P values	0.019		0.135		0.079		0.014		0.005		0.03	

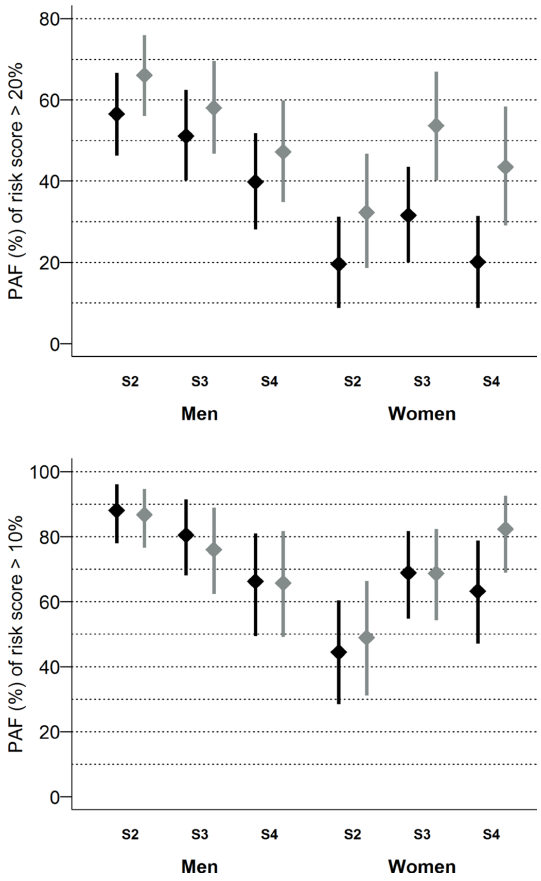

Figure 4 Trends in population-attributable fractions (PAFs). On the y-axis: PAF of a predicted risk of ≥ 20% (above) or ≥ 10% (below) as compared to a predicted risk <20% (above) or <10% (below) in % with respective 95% CIs. On the x-axis: all three studies, men and women, Framingham Risk Score (black), Pooled Cohort Equations (grey).

additional variables, such as family history of CVD, C-reactive protein or measures of deprivation, which were not readily available in all of our cohorts.

In conclusion, risk models have to be modified to the population at hand to maximise their clinical utility. Particular attention has to be paid to refining sex-specific risk predictions. Our results show that the performance of both the FRS and the PCE is susceptible to changes in the underlying risk factor distributions and event rates; however, the overall performance of the risk scores is still adequate and the underlying risk factors capture a major part of the burden of CVD.

What is already known on this subject

- Risk scores based on the Framingham Equations and the Pooled Cohort Equations are commonly used tool to predict cardiovascular disease (CVD) risk.
- These scores rely on traditional cardiovascular risk factors such as age, blood pressure and lipid profile.
- The distribution of these risk factors has shifted in the last decades in Western populations and CVD incidence has decreased.

What this study adds

- We used three independent studies to analyse the impact of a shifting risk factor distribution on the performance of both risk scores.
- We found temporal trends in the amount of predicted risk as well as in the discrimination performance.
- We found a sex-specific temporal evolvement, with improving discrimination performance in women and decreasing performance in men.
- These sex-specific differences should be more strongly taken into account for the future refinement and development of prediction models.

Author affiliations
[1]Institute of Epidemiology, Helmholtz Zentrum München, German Research Center for Environmental Health, Neuherberg, Germany
[2]Chair of Epidemiology, Ludwig-Maximilians-Universität München, UNIKA-T, Augsburg, Germany
[3]Institute of Health Economics and Health Care Management, Helmholtz Zentrum München, German Research Center for Environmental Health, Neuherberg, Germany
[4]Department of Internal Medicine II – Cardiology, University of Ulm Medical Center, Ulm, Germany
[5]Deutsches Herzzentrum München, Technische Universität München, München, Germany
[6]German Centre for Cardiovascular Research (DZHK e.V.), Munich, Germany
[7]Department of Medical Information Sciences, Biometry, and Epidemiology, Ludwig-Maximilians- Universität München, Munich, Germany
[8]Chair of Epidemiology, Ludwig-Maximilians-Universität München, Munich, Germany

Contributors SR derived the study questions, conducted the statistical analyses and interpretation of results and drafted the manuscript. BT, TdlHG, CM, RH and WK participated substantially in the data acquisition and quality control of the cohort data used for the study, reviewed the manuscript and revised it for important intellectual content. UM contributed substantially to the statistical analyses of the manuscript, reviewed the manuscript and revised it for important intellectual content. AP contributed substantially to the design of the study questions, participated substantially in the data acquisition and quality control of the cohort data used for the study, reviewed the manuscript and revised it for important intellectual content. All authors have approved the final manuscript.

Funding The KORA study was initiated and financed by the Helmholtz Zentrum München – German Research Center for Environmental Health, which is funded by the German Federal Ministry of Education and Research (BMBF) and by the State of Bavaria.

Competing interests None declared.

Patient consent Not required.

Ethics approval The KORA studies were approved by the ethics committee of the Bavarian Chamber of Physicians, Munich. The investigations were carried out in accordance with the Declaration of Helsinki.

Provenance and peer review Not commissioned; externally peer reviewed.

Data sharing statement The informed consent given by KORA study participants does not cover data posting in public databases. However, data are available upon request from KORA-gen (http://epi.helmholtz-muenchen.de/kora-gen/) by means of a project agreement. Requests should be sent to kora.passt@helmholtz-muenchen.de and are subject to approval by the KORA Board.

REFERENCES

1 World Health Organization. *Global status report on noncommunicable diseases 2014*: World Health Organization, 2014.
2 Damen JA, Hooft L, Schuit E, *et al*. Prediction models for cardiovascular disease risk in the general population: systematic review. *BMJ* 2016;353:i2416.

3 NCD Risk Factor Collaboration (NCD-RisC). Worldwide trends in blood pressure from 1975 to 2015: a pooled analysis of 1479 population-based measurement studies with 19·1 million participants. *Lancet* 2017;389:37–55.
4 Ng M, Freeman MK, Fleming TD, *et al*. Smoking prevalence and cigarette consumption in 187 countries, 1980-2012. *JAMA* 2014;311:183–92.
5 Capewell S, Ford ES. Why have total cholesterol levels declined in most developed countries? *BMC Public Health* 2011;11:11(1):1.
6 Collaboration NRF. Trends in adult body-mass index in 200 countries from 1975 to 2014: a pooled analysis of 1698 population-based measurement studies with 19·2 million participants. *The Lancet* 2016;387:1377–96.
7 Levi F, Chatenoud L, Bertuccio P, *et al*. Mortality from cardiovascular and cerebrovascular diseases in Europe and other areas of the world: an update. *Eur J Cardiovasc Prev Rehabil* 2009;16:333–50.
8 D'Agostino RB, Vasan RS, Pencina MJ, *et al*. General cardiovascular risk profile for use in primary care: the Framingham Heart Study. *Circulation* 2008;117:743–53.
9 Goff DC, Lloyd-Jones DM, Bennett G, *et al*. 2013 ACC/AHA guideline on the assessment of cardiovascular risk: a report of the American College of Cardiology/American Heart Association Task Force on Practice Guidelines. *J Am Coll Cardiol* 2014;63(Pt B):2935–59.
10 Hense H, Filipiak B, Döring A, *et al*. Ten-year trends of cardiovascular risk factors in the MONICA Augsburg Region in Southern Germany. Results from 1984/1985, 1989/1990, and 1994/1995 surveys. *CVD Prevention* 1998;1:318–27.
11 Rathmann W, Haastert B, Icks A, *et al*. High prevalence of undiagnosed diabetes mellitus in Southern Germany: target populations for efficient screening. The KORA survey 2000. *Diabetologia* 2003;46:182–9.
12 Löwel H, Lewis M, Hörmann A, *et al*. Case finding, data quality aspects and comparability of myocardial infarction registers: results of a south German register study. *J Clin Epidemiol* 1991;44:249–60.
13 Müller S, Martin S, Koenig W, *et al*. Impaired glucose tolerance is associated with increased serum concentrations of interleukin 6 and co-regulated acute-phase proteins but not TNF-alpha or its receptors. *Diabetologia* 2002;45:805–12.
14 Deutsche Hochdruckliga. *Empfehlungen zur Hochdruckbehandlung*. 20th edn. Heidelberg, 2010.
15 Ford ES. Trends in predicted 10-year risk of coronary heart disease and cardiovascular disease among U.S. adults from 1999 to 2010. *J Am Coll Cardiol* 2013;61:2249–52.
16 Steyerberg EW, Vickers AJ, Cook NR, *et al*. Assessing the performance of prediction models: a framework for traditional and novel measures. *Epidemiology* 2010;21:128–38.
17 Van Calster B, Nieboer D, Vergouwe Y, *et al*. A calibration hierarchy for risk models was defined: from utopia to empirical data. *J Clin Epidemiol* 2016;74:167–76.
18 Austin PC, Steyerberg EW. Interpreting the concordance statistic of a logistic regression model: relation to the variance and odds ratio of a continuous explanatory variable. *BMC Med Res Methodol* 2012;12:82.
19 Doebler P, Holling H, 2015. Meta-analysis of diagnostic accuracy with mada. https://cran rproject org/web/packages/mada/vignettes/mada pdf
20 DeFilippis AP, Young R, Carrubba CJ, *et al*. An analysis of calibration and discrimination among multiple cardiovascular risk scores in a modern multiethnic cohort. *Ann Intern Med* 2015;162:266–75.
21 Kavousi M, Leening MJ, Nanchen D, *et al*. Comparison of application of the ACC/AHA guidelines, Adult Treatment Panel III guidelines, and European Society of Cardiology guidelines for cardiovascular disease prevention in a European cohort. *JAMA* 2014;311:1416–23.
22 de Las Heras Gala T, Geisel MH, Peters A, *et al*. Recalibration of the ACC/AHA Risk Score in Two Population-Based German Cohorts. *PLoS One* 2016;11:e0164688.
23 Cook NR, Ridker PM. Calibration of the pooled cohort equations for atherosclerotic cardiovascular disease: an update. *Ann Intern Med* 2016;165:786–94.
24 Paynter NP, Everett BM, Cook NR. Cardiovascular disease risk prediction in women: is there a role for novel biomarkers? *Clin Chem* 2014;60:88–97.
25 Huxley RR, Woodward M. Cigarette smoking as a risk factor for coronary heart disease in women compared with men: a systematic review and meta-analysis of prospective cohort studies. *Lancet* 2011;378:1297–305.
26 Peters SA, Huxley RR, Woodward M. Diabetes as risk factor for incident coronary heart disease in women compared with men: a systematic review and meta-analysis of 64 cohorts including 858,507 individuals and 28,203 coronary events. *Diabetologia* 2014;57:1542–51.
27 McGeechan K, Macaskill P, Irwig L, *et al*. An assessment of the relationship between clinical utility and predictive ability measures and the impact of mean risk in the population. *BMC Med Res Methodol* 2014;14:86.
28 Cheng S, Claggett B, Correia AW, *et al*. Temporal trends in the population attributable risk for cardiovascular disease: the Atherosclerosis Risk in Communities Study. *Circulation* 2014;130:820–8.
29 Moons KG, Kengne AP, Grobbee DE, *et al*. Risk prediction models: II. External validation, model updating, and impact assessment. *Heart* 2012;98:691–8.
30 Cook NR, Ridker PM. Further insight into the cardiovascular risk calculator: the roles of statins, revascularizations, and underascertainment in the Women's Health Study. *JAMA Intern Med* 2014;174:1964–71.
31 Conroy RM, Pyörälä K, Fitzgerald AP, *et al*. Estimation of ten-year risk of fatal cardiovascular disease in Europe: the SCORE project. *Eur Heart J* 2003;24:987–1003.
32 Assmann G, Cullen P, Schulte H. Simple scoring scheme for calculating the risk of acute coronary events based on the 10-year follow-up of the prospective cardiovascular Münster (PROCAM) study. *Circulation* 2002;105:310–5.
33 Ridker PM, Buring JE, Rifai N, *et al*. Development and validation of improved algorithms for the assessment of global cardiovascular risk in women: the Reynolds Risk Score. *JAMA* 2007;297:611–9.
34 Ridker PM, Paynter NP, Rifai N, *et al*. C-reactive protein and parental history improve global cardiovascular risk prediction: the Reynolds Risk Score for men. *Circulation* 2008;118:2243–51.
35 Hippisley-Cox J, Coupland C, Vinogradova Y, *et al*. Predicting cardiovascular risk in England and Wales: prospective derivation and validation of QRISK2. *BMJ* 2008;336:1475–82.

Supplementary Figure 1: Flowchart of participants for the three cohort studies

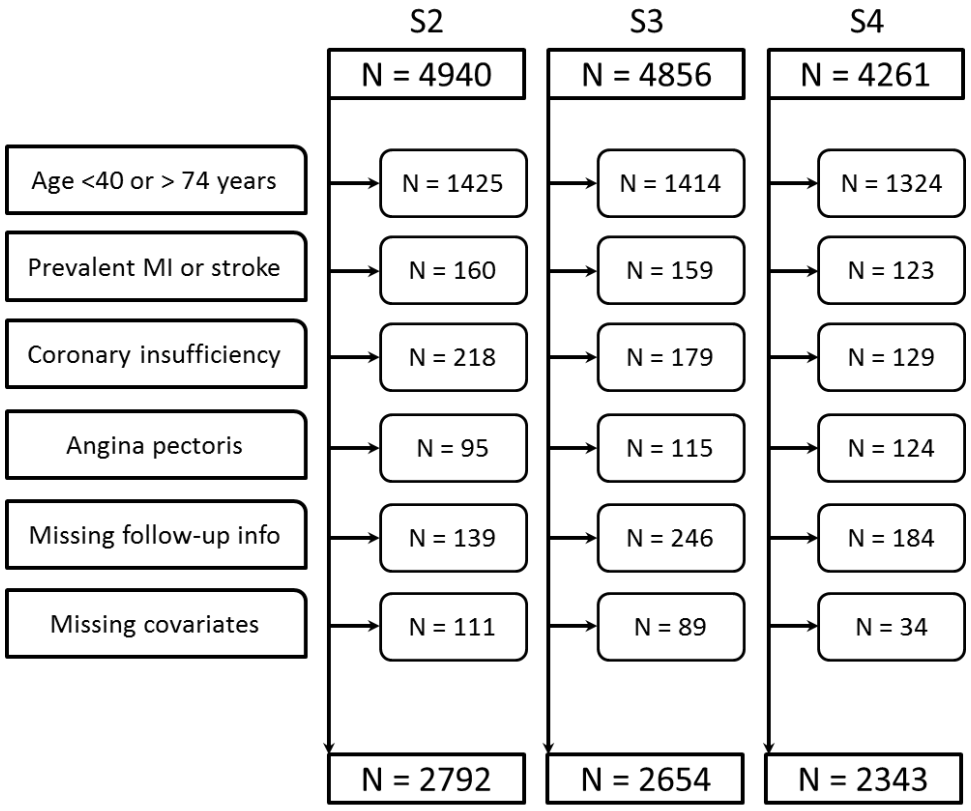

Supplementary Figure 2: Calibration of the FRS and PCE in the three studies, based on risk thresholds

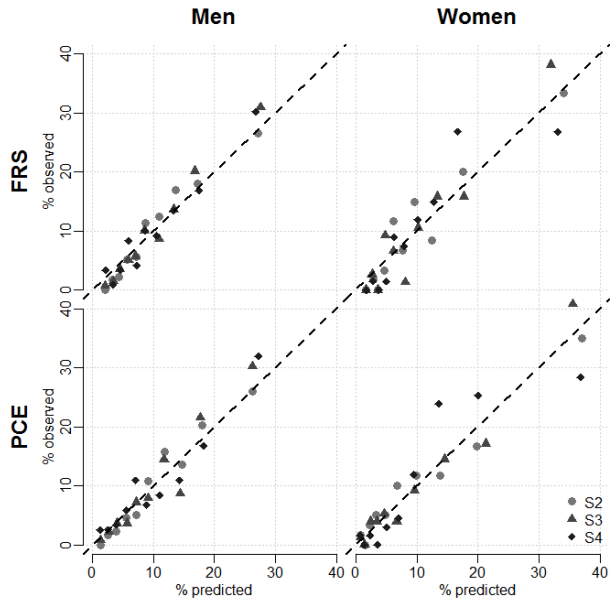

On the x-axis: mean predicted probability of CVD event by interval. Intervals are defined by risk score thresholds of 5%, 7.5%, 10% and 20%. On the y-axis: proportion of observed events, by interval. Light grey, filled circle: S2 study; medium grey, filled triangle: S3 study, dark grey, filled diamond: S4 study

Supplementary Table 1 : Calibration measures of the two risk scores. a) Men b) Women

a) MEN		Risk Score	Subjects, n	Observed Events, n	Predicted Events, n	Discordance , %	Hosmer-Lemeshow χ2	Hosmer-Lemeshow *P*
FRS	S2	[0, 5)	153	0	5.8	Inf	5.8	0.215
	S3	[0, 5)	183	1	6.6	560	4.76	0.313
	S4	[0, 5)	171	5	6.3	27	0.28	0.991
	S2	[5, 7.5)	188	3	11.7	291	6.5	0.165
	S3	[5, 7.5)	179	4	11	175	4.46	0.347
	S4	[5, 7.5)	155	3	9.6	221	4.56	0.335
	S2	[7.5, 10)	146	7	12.8	83	2.62	0.623
	S3	[7.5, 10)	173	10	15.3	53	1.81	0.770
	S4	[7.5, 10)	142	12	12.5	4	0.02	1.000
	S2	[10, 20)	448	50	64.4	29	3.24	0.519
	S3	[10, 20)	445	41	63.5	55	7.96	0.093
	S4	[10, 20)	391	37	54.9	48	5.84	0.211
	S2	[20, 100]	497	117	163.7	40	13.32	0.010
	S3	[20, 100]	352	83	109	31	6.2	0.185
	S4	[20, 100]	280	62	85.9	39	6.66	0.155
	S2	**[0, 100]**	**1432**	**177**	**258.5**	**46**	**25.67**	**0.000**
	S3	**[0, 100]**	**1332**	**139**	**205.3**	**48**	**21.44**	**0.000**
	S4	**[0, 100]**	**1139**	**119**	**169.2**	**42**	**14.91**	**0.000**
PCE	S2	[0, 5)	231	1	7.3	633	5.46	0.243
	S3	[0, 5)	237	3	7.3	143	2.52	0.641
	S4	[0, 5)	212	6	6.3	5	0.01	1.000
	S2	[5, 7.5)	131	4	8.1	102	2.07	0.722
	S3	[5, 7.5)	138	3	8.5	183	3.54	0.472
	S4	[5, 7.5)	125	4	7.6	91	1.73	0.785
	S2	[7.5, 10)	114	5	9.8	96	2.33	0.675
	S3	[7.5, 10)	139	8	12.2	53	1.45	0.836
	S4	[7.5, 10)	111	6	9.7	62	1.43	0.839
	S2	[10, 20)	384	33	55.9	69	9.35	0.053
	S3	[10, 20)	373	34	53.4	57	7.06	0.133
	S4	[10, 20)	346	31	49.6	60	6.98	0.137
	S2	[20, 100]	572	134	195.2	46	19.19	0.001
	S3	[20, 100]	445	91	136.2	50	15.02	0.005
	S4	[20, 100]	345	72	110.2	53	13.22	0.010
	S2	**[0, 100]**	**1432**	**177**	**276.3**	**56**	**35.67**	**0.000**
	S3	**[0, 100]**	**1332**	**139**	**217.6**	**57**	**28.41**	**0.000**
	S4	**[0, 100]**	**1139**	**119**	**183.4**	**54**	**22.62**	**0.000**

b) WOMEN	Risk Score, %	Subjects, n	Observed Events, n	Predicted Events, n	Discordance, %	Hosmer-Lemeshow χ2	Hosmer-Lemeshow *P*
FRS	S2	[0, 5)	705	10	19	90	4.27	0.370
	S3	[0, 5)	544	10	15.6	56	2.01	0.734
	S4	[0, 5)	510	2	14.9	646	11.2	0.024
	S2	[5, 7.5)	249	13	15.2	17	0.32	0.989
	S3	[5, 7.5)	200	5	12.3	146	4.32	0.365
	S4	[5, 7.5)	213	11	13.2	20	0.36	0.985
	S2	[7.5, 10)	130	4	11.2	181	4.66	0.324
	S3	[7.5, 10)	163	7	14.1	101	3.54	0.472
	S4	[7.5, 10)	135	9	11.8	31	0.65	0.957
	S2	[10, 20)	205	21	27.9	33	1.72	0.788
	S3	[10, 20)	299	26	41.8	61	5.98	0.200
	S4	[10, 20)	248	28	33	18	0.76	0.943
	S2	[20, 100]	71	12	21.2	76	3.97	0.411
	S3	[20, 100]	116	28	34.4	23	1.18	0.881
	S4	[20, 100]	98	17	29.6	74	5.35	0.253
	S2	**[0, 100]**	**1360**	**60**	**94.5**	**58**	**12.61**	**0.000**
	S3	**[0, 100]**	**1322**	**76**	**118.1**	**55**	**15.03**	**0.000**
	S4	**[0, 100]**	**1204**	**67**	**102.5**	**53**	**12.29**	**0.000**
PCE	S2	[0, 5)	690	9	15.4	71	2.63	0.622
	S3	[0, 5)	585	9	14.3	59	1.97	0.740
	S4	[0, 5)	507	2	11.6	478	7.91	0.095
	S2	[5, 7.5)	142	8	8.7	9	0.05	1.000
	S3	[5, 7.5)	141	3	8.6	187	3.67	0.453
	S4	[5, 7.5)	153	4	9.4	136	3.13	0.536
	S2	[7.5, 10)	122	6	10.6	77	2.03	0.730
	S3	[7.5, 10)	98	3	8.4	181	3.49	0.479
	S4	[7.5, 10)	120	4	10.5	162	3.99	0.407
	S2	[10, 20)	251	16	35.5	122	10.7	0.030
	S3	[10, 20)	233	17	32.9	94	7.7	0.103
	S4	[10, 20)	221	25	31.6	26	1.37	0.849
	S2	[20, 100]	155	21	47.6	127	14.86	0.005
	S3	[20, 100]	265	44	84.4	92	19.35	0.001
	S4	[20, 100]	203	32	66.7	108	18.06	0.001
	S2	**[0, 100]**	**1360**	**60**	**117.8**	**96**	**28.33**	**0.000**
	S3	**[0, 100]**	**1322**	**76**	**148.7**	**96**	**35.54**	**0.000**
	S4	**[0, 100]**	**1204**	**67**	**129.8**	**94**	**30.35**	**0.000**

Manuscript II

Title: Association of longitudinal risk profile trajectory clusters with adipose tissue depots measured by magnetic resonance imaging

Authors: Susanne Rospleszcz*, Roberto Lorbeer*, Corinna Storz, Christopher L. Schlett, Christa Meisinger, Barbara Thorand, Wolfgang Rathmann, Fabian Bamberg, Wolfgang Lieb†, Annette Peters†

Journal: To be submitted.

Status: To be submitted.

* : these authors contributed equally

† : these authors contributed equally

Association of longitudinal risk profile trajectory clusters with adipose tissue depots measured by magnetic resonance imaging

Running title: Trajectory clusters and adipose tissue

Susanne Rospleszcz*[1], Roberto Lorbeer*[2,9], Corinna Storz[3], Christopher L. Schlett[4], Christa Meisinger[1,5], Barbara Thorand[1], Wolfgang Rathmann[6,7], Fabian Bamberg[2,3], Wolfgang Lieb‡[8], Annette Peters‡[1,9,10]

* These authors contributed equally

‡ These authors contributed equally

[1]Institute of Epidemiology, Helmholtz Zentrum München, German Research Center for Environmental Health, Neuherberg, Germany
[2]Department of Radiology, Ludwig-Maximilians-University Hospital, Munich, Germany
[3]Department of Diagnostic and Interventional Radiology University of Tuebingen, Germany
[4]Department of Diagnostic and Interventional Radiology, University Hospital Heidelberg
[5]Chair of Epidemiology, Ludwig-Maximilians-University München, UNIKA-T Augsburg, Augsburg, Germany
[6]German Center for Diabetes Research (DZD), München-Neuherberg, Germany
[7]Institute for Biometrics and Epidemiology, German Diabetes Center, Duesseldorf, Germany
[8]Institute of Epidemiology and Biobank PopGen, Kiel University, Kiel, Germany
[9]German Centre for Cardiovascular Research (DZHK e.V.), Munich, Germany
[10]Chair of Epidemiology, Ludwig-Maximilians-University München, Munich, Germany

Keywords

Abdominal fat, ectopic fat, cardiovascular risk factors, Magnetic Resonance Imaging

FUNDING INFORMATION

The KORA study was initiated and financed by the Helmholtz Zentrum München – German Research Center for Environmental Health, which is funded by the German Federal Ministry of Education and Research (BMBF) and by the State of Bavaria. Furthermore, KORA research was supported within the Munich Center of Health Sciences (MC-Health), Ludwig-Maximilians-Universität, as part of LMUinnovativ. The KORA-MRI sub-study received funding by the German Research Foundation (DFG, Deutsche Forschungsgemeinschaft, BA 4233/4-1, http://www.dfg.de). The KORA-MRI sub-study was supported by an unrestricted grant from Siemens Healthcare (https://www.healthcare.siemens.de). The funders had no role in study design, data collection and analysis, decision to publish, or preparation of the manuscript.

DATA SHARING

The informed consent given by KORA study participants does not cover data posting in public databases. However, data are available upon request from KORA-gen (http://epi.helmholtz-muenchen.de/kora-gen/) by means of a project agreement. Requests should be sent to kora.passt@helmholtz-muenchen.de and are subject to approval by the KORA Board.

AUTHOR CONTRIBUTIONS

SR, RL and WL conceived the research question. SR and RL performed the statistical analyses, evaluated the results and drafted the paper. CS, CLS and FB collected the MRI data and analyzed the images. SR, RL, CS, CLS, CM, BT, WR, FB, WL and AP contributed substantially to data preparation and quality assurance. FB, WL and AP participated in the conception and design of the study. CS, CLS, CM, BT, WR, FB, WL and AP revised the paper for important intellectual content. All authors have read and approved the final manuscript.

CONFLICT OF INTEREST

The authors declared no conflict of interest.

Corresponding author:

Susanne Rospleszcz, Institute of Epidemiology, Helmholtz Zentrum München, German Research Center for Environmental Health, Ingolstaedter Landstrasse 1, 85764 Neuherberg, Germany

Phone: 0049-89-3187-4234

E-mail: susanne.rospleszcz@helmholtz-muenchen.de

Study Importance Questions

What is already known about this subject?

- Some, but not all, abdominal and ectopic fat depots are associated to cardiovascular disease risk.
- Abdominal and ectopic fat are metabolically highly active tissues and connected to traditional cardiovascular risk factors in a complex interplay.

What does this study add?

- We quantify the explanatory value of traditional cardiometabolic risk factors to a comprehensive panel of MRI-derived adipose tissue traits.
- We identify three different longitudinal risk profile trajectory clusters which represent different risk factor burdens.
- We provide strong evidence that sustained high risk factor levels and unfavorable risk factor trajectories are associated with high levels of ectopic adipose tissue.

ABSTRACT

Objective: To identify associations of longitudinal trajectories of traditional cardiometabolic risk factors with abdominal and ectopic adipose tissue depots.

Methods: We measured total abdominal, visceral, and subcutaneous adipose tissue in liter and intrahepatic, intrapancreatic and renal sinus fat as fat fractionsby magnetic resonance imaging (MRI) in 325 individuals without cardiovascular disease at the 3rd examination cycle of a population-based cohort. We examined multivariate longitudinal risk profile trajectory clusters based on measurements from the 3rd, 2nd (seven years prior) and 1st (14 years prior) examination cycle.

Results: Risk factor profiles (blood pressure, lipid profile, anthropometric measurements, HbA1c), obtained at the 3rd examination cycle, provided substantially varying explanatory value for adipose tissue traits within a range of R^2=0.26 to R^2=0.87 (lowest for pancreatic fat fraction, highest for subcutaneous adipose tissue). Longitudinally, we identified three distinct clusters of trajectories which displayed a graded association with all adipose tissue traits after adjustment for potential confounders (e.g. visceral adipose tissue: $\beta_{ClusterII}$=1.30l, 95%-CI:[0.84l;1.75l], $\beta_{ClusterIII}$=3.32l[2.74l;3.90l]; intrahepatic: $Estimate_{ClusterII}$=1.54[1.27,1.86], $Estimate_{ClusterIII}$=2.48[1.93,3.16]. Trajectory clusters provided additional explanatory value, beyond single point measurements.

Conclusion: The association with cardiometabolic risk factors varies between different ectopic adipose tissues. Sustained high risk factor levels and unfavorable trajectories are associated to high levels of adipose tissue.

INTRODUCTION

Obesity confers an increased risk for several disease conditions, including clinical cardiovascular disease (CVD) events and mortality as well as type 2 diabetes. Recent research has strengthened evidence for a causal role of obesity in CVD mortality (1, 2).

Apart from visceral and subcutaneous abdominal obesity, ectopic fat depots, i.e. the accumulation of adipose tissue in and around organs might have local as well as systemic effects and, thereby, modulate overall CVD risk.

Easily applicable measures such as body mass index (BMI) and waist circumference (WC) are often used as measures of adiposity. However, both BMI and WC do not reflect well the distribution of fat in the body, nor can they adequately quantify the amount of metabolically active adipose tissue. Although the anthropometric markers BMI and WC are correlated to adipose tissue, the correlation is not complete, and these markers cannot explain the full variation in adipose tissue content (3).For a more precise quantification of the amount and distribution of adipose tissue, non-invasive imaging is increasingly utilized, including magnetic resonance imaging (MRI).

Prior studies have indeed shown that accurate quantification of adipose tissue provides additional value in the prediction of cardiovascular outcomes, beyond anthropometric measures. For example, in the Dallas Heart study, MRI-derived visceral adipose tissue (VAT) was associated with incident CVD and type 2 diabetes, independent of BMI (4, 5). Similarly, in the Multi-Ethnic Study of Atherosclerosis, VAT, as assessed by computed tomography, predicted CVD beyond BMI and traditional risk factors (6).

In contrast, subcutaneous adipose tissue (SAT) seems not to be associated with CVD or to even exhibit a protective effect(6, 7). On a parallel note, excess hepatic fat is associated with impaired glucose tolerance (8, 9) and hypertension (10). Furthermore, a recent study from the UK biobank reported that individuals with coronary heart disease or type 2 diabetes are characterized by a complex interplay of different MRI measured fat compartments (11).

Several risk factors contribute to the development of adipose tissue, including lifestyle choices like nutrition and physical activity and genetic variation (12). Furthermore, etiologically linked traditional cardiometabolic risk factors such as age, hypertension and lipid traits are connected to VAT, (13, 14, 15), SAT (16, 17), hepatic fat (18), pancreatic fat (19) and renal fat (20, 21). The relation of the development of the above-mentioned traditional cardiometabolic factors over the adult life course on different adipose tissues is not well descried thus far.

Longitudinal trajectories of risk profiles convey more information than single time point measurements; as these trajectories reflect more adequately the joint contribution and evolvement of multiple risk factors over time.

In the present manuscript, we aimed to analyze the association of traditional CVD risk factors to total adipose tissue (TAT), VAT, SAT, renal sinus fat fraction (RSFF), intrahepatic fat, measured as hepatic fat fraction (HFF) and intrapancreatic fat, measured as pancreatic fat fraction (PFF) derived by MRI. Specifically, we aim to i) determine risk factor trajectories over three time points, covering 14 years of follow-up, ii) assess whether earlier or more recent risk profiles display stronger association with MRI-determined adipose tissue traits iii) identify distinct clusters of longitudinal risk profile trajectories, iv) quantify the association of these clusters to adipose tissue traits.

METHODS

Study sample

We used longitudinal data from the KORA (Cooperative Health Research in the Region of Augsburg) S4/F4/FF4 studies, a population-based sample from Bavaria, Germany. The sampling scheme and the examination protocols of the KORA cohorts have been described previously (22, 23). Briefly, participants were sampled in a two-step procedure. First, communities from the city of Augsburg and two adjacent counties were chosen by cluster sampling, followed by a stratified random sampling of participants within each community. The baseline examination of this population-based sample (S4 survey) was conducted in 1999-2001 and included 4261 participants; the 2nd examination cycle (F4) took place in 2006-2008 with 3080 participants and the 3rd examination cycle (FF4) was conducted in 2013-2014, including 2279 participants. At the 3rd examination cycle, a whole-body MRI was obtained in a subsample of 400 participants without prior CVD (8). The MRI sample followed a case-control study design and was enriched with prediabetes and type 2 diabetes cases.

For the present analyses, a total of 75 of the 400 KORA-MRI study participants had to be excluded. Specifically, 20 individuals had to be excluded because they did not participate in the 2nd examination cycle (F4 study) and 55 individuals had to be excluded because of missing values in any of the MRI parameters of interest (HFF: n = 11, VAT: n = 8, SAT: n = 6, PFF: n = 5, RSFF: n = 25). Reasons for missing values in the MRI parameters comprised insufficient image quality, imaging artifacts and technical errors and were unrelated to each subject's clinical covariates.

Covariate assessment

At all three examination cycles, participants underwent a physical examination, including a blood draw and a standardized face-to-face interview by trained examiners.

Height and weight were determined by Seca's measuring systems (Seca GmbH & Co, KG, Hamburg, Germany) with either calibrated steelyards or digital scales. Height was quantified to the closest 0.1 cm and weight to the closest 0.1 kg. BMI was calculated as weight in kg divided by squared height in m.

WC was measured with an inelastic tape at the level midway between the lower rib margin and the iliac crest. Hip circumference was measured at the level of maximal gluteal protrusion.

Blood pressure was measured on the right upper arm by OMRON type HEM-705CP oscillometric devices. After at least 5 minutes of rest, three measurements were taken at intervals of three minutes. The mean of the second and third blood pressure measurement was used for the present analyses. Hypertension was defined as systolic/diastolic blood pressure above 140/90 mmHg or intake of antihypertensive medication, given that the participant was aware of being hypertensive. Antihypertensive medication was defined according to German national guidelines (24).

Laboratory measurements have been described previously (25). Briefly, for the assessment of total cholesterol, LDL cholesterol and HDL cholesterol, enzymatic, photometric assays were used at the 1st examination (S4 study) and enzymatic, colorimetric Flex assays were used at the 2nd (F4) and 3rd examination cycle (FF4). HbA1c was measured by a turbidimetric inhibition immunoassay at the 1st examination and by cation-exchange high performance liquid chromatographic, photometric assays at the 2nd and 3rd examination cycle.

Diabetes status, cigarette consumption, physical activity, alcohol intake and medication intake were self-reported. Participants were labeled as being physically active if they reported engaging in sports activities regularly for ≥1 hour per week or as physically inactive if they reported engaging in sports activities irregularly and less than 1 hour per week. At the 3rd examination cycle (FF4 study), glycemic status was additionally validated by an oral glucose tolerance test and categorized into normoglycemic control, prediabetes or diabetes according to the WHO guidelines (26).

We defined the combination of systolic blood pressure, diastolic blood pressure, BMI, WC, total cholesterol, HDL, LDL and HbA1c at the time point of the 1st examination cycle as "remote", at the time point of the 2nd examination cycle as "recent" and at the time point of the 3rd examination cycle as "current" risk profile, respectively.

MRI outcome assessment

The whole-body MRI protocol as well as the measurements of single adipose tissue compartments have been detailed previously (8). In brief, all MRI scans were performed on a 3 Tesla Magnetom Skyra (Siemens Healthineers, Erlangen, Germany). All images were read by independent radiologists blinded to the participants' clinical covariates and standard quality measures of inter-and intrareader variability were evaluated.

For quantification of adipose tissue compartments, volume-interpolated 3D in/opposed-phase VIBE-Dixon sequence was performed and adipose tissues were segmented semi-automatically (27, 28). SAT was quantified from cardiac apex to femoral head and VAT was quantified from

diaphragm to femoral head; TAT was defined as the sum of SAT and VAT, all indicated in liter. Figure 1 exemplifies the segmentation and quantification of VAT and SAT.

For the determination ofHFF in %, a multi-echo Dixon-VIBE T1-weighted sequence was used, accounting for confounding T2* decay and spectral complexity of fat (10). HFF was calculated as the mean fat fraction of right liver lobe (measured in segment VIII according to Couinaud classification) and left liver lobe (measured in segment II).

PFF was measured by the 3D multi-echo Dixon-VIBE sequence by drawing regions of interest into the pancreatic head, body and tail, and was measured as proton-density fat fraction in % (29).

Additionally, based on the volume-interpolated 3D in/opposed-phase T1 weighted VIBE-Dixon sequence, an inhouse MATLAB algorithm was used for semi-automatic segmentation of total renal volume, renal cortex, medulla and sinus (30). RSFF was then determined by overlaying the segmentation with the respective Water-Only and Fat-Only Dixon images, as exemplarily shown in **Figure 2**.

Statistical analysis

Continuous covariates are summarized by arithmetic means and standard deviation (SD) and categorical variables are presented as counts and percentagesand compared by repeated measures ANOVA and Cochran's Q-Test, respectively. MRI-derived adipose tissue outcome variables at the 3rd examination cycle are displayed as mean and SD or median with interquartile range. For regression modeling, HFF and PFF were log-transformed. The associations of remote,

recent and current risk profiles with the different MRI derived adipose tissue outcome variable (TAT, SAT, VAT, RSFF, log (HFF), log (PFF)) were evaluated by linear regression models for each time point. The models included all risk profile variables as well as age, sex, antihypertensive medication, lipid-lowering medication and smoking behavior measured at that time point. The Goodness-Of-Fit statistic R^2 served as a measure of how much variance in the outcome is explained by the respective statistical model.

Longitudinal risk factor trajectories were computed by non-parametric k-means clustering using Euclidean distance (31). The clusters were calculated for a combination of all risk factors, resulting in a strictly multivariate cluster. Associations of the trajectory clusters with the MRI-derived adipose tissue outcomes were evaluated by linear regression adjusted for potential confounding variables, measured at the 3rd examination cycle. Furthermore, regression models were additionally adjusted for i) the risk factor values, measured at the 1st examination cycle and ii) the risk factor values, measured at the 3rd examination cycle. Given the design of the KORA MRI study with its focus on participants with diabetes and prediabetes, we additionally adjusted all models for validated diabetes status (control, prediabetes, diabetes), assessed at the 3rd examination cycle to avoid potential bias by the presence of undetected diabetes.

Additionally, all analyses were repeated with BMI and WC excluded from the risk profile variables and included as outcomes. Furthermore, we constructed an ordinal logistic regression model using the trajectory clusters as outcomes and the MRI parameters, BMI and WC as risk factors. The ordinal logistic regression model estimates an Odds Ratio (OR) for each risk factor: The odds of being in Cluster II or higher (compared to Cluster I) associated with an increase of the risk factor in one unit.

Two sided p-values <0.05 were considered to indicate statistical significance. All computations were performed with Stata 14.1 (Stata Corporation, College Station, Texas, USA) and R 3.4.1 (R Core Team, Vienna, Austria).

RESULTS

Trends in risk factor profiles

The cardiometabolic risk factor profiles at each examination cycle are presented in **Table 1**. A description of the different MRI-derived adipose tissue traits that served as outcome variables is provided in **Table 2**. The sample comprised 59.4% men;mean age at baseline was 42.2 years. Over the course of 14 years, mean systolic and diastolic blood pressure declined significantly, while the percentage of individuals treated with antihypertensive medication increased significantly. Body weight, WC and BMI increased (**Table 1**). We also observed decreasing total cholesterol. Alcohol consumption remained stable whereas more participants quit smoking and became physically active. Prevalence of self-reported diabetes and mean HbA1c increased significantly.

Associations of current, recent and remote risk factor profile with adipose tissue traits

The associations of individual risk factor measurements at the three time points (1^{st} , 2^{nd} and 3^{rd} examination cycle) with the respective adipose tissue traits are displayed in **Supplementary Figures S1a-f and S2a-g**. Overall, WC was most strongly associated at all time points for almost

all adipose tissue traits. When excluding WC from the risk factor set, HDL showed the strongest association. **Figure 3** shows the ability of current, recent and remote risk profiles to explain the variance in the different adipose tissue traits. When including all eight risk factors in the profile, for TAT, VAT, SAT and HFF, the current risk profile, concurrent to the MRI measurements, showed decidedly the strongest association to the outcome. At the same time, for these adipose tissue traits the model explained a high amount of variance of the outcome (all R^2>0.5, respectively). For RSFF and PFF, the amount of variance explained by the set of traditional risk factors was substantially less than for TAT, VAT, and SAT, and the performance of the recent and current risk profiles was comparable.

When excluding BMI and WC from the risk factor profile, the amount of variance explained was considerably lower for all adipose tissue traits (compare Figure 3). The highest R^2 values were obtained for VAT, WC and HFF (all R^2>0.4), whereas the values for SAT and BMI were substantially decreased.

Characterization of longitudinal risk profile trajectory clusters

We identified three distinct clusters of risk profile trajectories over a time period of 14 years, as described in **Figure 4** and **Supplementary Table S2.**. In essence, these clusters differ in the mean risk factor levels at the baseline and in the trend of the risk factor development over time. Specifically, Cluster I comprises 114 subjects (35 % of the overall sample) with the youngest age, and the lowest mean levels of systolic and diastolic blood pressure, WC, BMI, HbA1c, total and LDL cholesterol at baseline. In addition, Cluster I is characterized by the lowest increase of WC

and BMI and the highest increase of lipid parameters over time. Cluster II comprises 129 subjects (40% of the overall sample). Mean age, mean blood pressure values, mean BMI and WC, HBA1c and HDL reside between Cluster I and Cluster III. However, total cholesterol and LDL values are higher in this cluster than in the other two clusters.

Cluster III, comprising 82 subjects (25% of the overall sample), has the highest mean age and highest levels of blood pressure, BMI, and WC as well as the lowest levels of HDL. Furthermore, BMI, WC and HbA1c increased over time with the highest % change of all clusters (see **Supplementary Table S3**).

When excluding WC and BMI from the risk factor set, the resulting clusters comprised 122, 107 and 96 individuals, respectively. Cluster I had lowest blood pressure, lowest HBa1c and highest HDL at all time points. There was a gradual relation in blood pressure, HbA1c and HDL, between the clusters, where Cluster I had the most favorable profile and Cluster III the most unfavorable. Cluster III also had the highest total cholesterol and LDL values (compare Supplementary Figure 3)

Association of longitudinal risk profile trajectory clusters to adipose tissue traits

Figure 5 shows the boxplots of the MRI-derived adipose tissue traits according to the three risk factor clusters. A gradual increase in adipose tissue content for all traits is discernible from Cluster I to III (e.g TAT:$mean_{ClusterI}$=8.6±3.4l, $mean_{ClusterII}$=12.3±3.5l, $mean_{ClusterIII}$=18.4±4.6l), with the differences being statistically significant (all $p<0.001$, compare **Supplementary Table S2**).

When excluding BMI and WC from the risk factor set, the gradual relation between the clusters was less clear-cut (compare Supplementary Figure S4). Adipose tissue levels in Cluster I were lower compared to the other two clusters, but levels between Cluster II and II were comparable (e.g TAT:$mean_{ClusterI}$=10.0±4.8l, $mean_{ClusterII}$=13.9±4.4l, $mean_{ClusterIII}$=14.3±5.6l). BMI was similar between cluster II and III (28.8 ± 4.2 kg/m^2 and 29.4 ± 4.6 kg/m^2, respectively), whereas WC was significantly different (101.3±11.4cm vs 105.3±13.1cm, p=0.02).

As presented as Model 1 in **Table 3**, in a multivariable model adjusting for age, sex, medication intake (antihypertensive and lipid-lowering medication), smoking and diabetes, the trajectory clusters (coded as a categorical variable with Cluster I serving as referent) were significantly associated to all adipose tissue outcomes. For example, Cluster II was associated with an increase of 1.30 l in VAT (95%-CI:[0.84; 1.75]) and a 2.60l increase in SAT (95%-CI:[1.87; 3.34]) whereas Cluster III was associated with an increase of 3.32l in VAT (95%-CI:[2.74; 3.90]) and a 6.16l increase in SAT (95%-CI:[5.23, 7.10]). In the same vein, Cluster II was associated with a 52% increase in PFF (95%-CI:[26; 84]) and Cluster III was associated with a 120% increase in PFF (95%-CI:[73, 180]).

When excluding BMI and WC from the risk factor set, associations were attenuated and less gradual, e.g. Cluster II was associated with an increase of 1.09 l in VAT (95%-CI:[0.53; 1.66]) and a 1.57l increase in SAT (95%-CI:[0.62; 2.53]) whereas Cluster III was associated with an increase of 1.09l in VAT (95%-CI:[0.48; 1.70]) and a 1.71l increase in SAT (95%-CI:[0.68, 2.74]).

As presented as Model 2 in **Table 3,** after adjustment for the remote risk profile (obtained at the 1st examination cycle), associations were attenuated but remained highly statistically significantly

associated with the various adiposity traits, except for RSFF.. As shown as Model 3 in **Table 3,** when adjusting for the current risk profile (3rd examination cycle, concurrent to the MRI examination) trajectory clusters were still significantly associated with TAT, VAT and PFF. R^2 measures for TAT, VAT, RSFF, HFF and PFF were higher compared to the model using the current risk profile alone (compare **Supplementary Table S5**).

An ordinal logistic regression with the trajectory clusters as outcomes revealed an OR of 1.10 for TAT (95%CI:[1.05, 1.16]), 1.21[1.08, 1.36] for VAT, 1.13[1.06, 1.22] for SAT, 1.03[1.00, 1.06] for RSFF, 1.05[1.02, 1.09] for HFF, 1.05[1.02, 1.09] for PFF, 1.10[1.04, 1.16] for BMI and 1.05[1.03, 1.07] for WC. This indicates that MRI derived VAT confers the most information about risk factor profiles.

DISCUSSION

To our knowledge, this is the first study to analyze longitudinal trajectories of multiple cardiometabolic risk factors by identifying clusters of these risk factors, and to evaluate the association of these longitudinal risk profile trajectory clusters with a broad panel of MRI-derived abdominal and ectopic adipose tissue traits.

Identification of trajectory clusters

We identified three clusters, which reflect low, medium and high cumulative risk factor exposure. The identified trajectories are based on the mean risk factor values and the change in mean risk factor levels from the 1st to the 2nd and 3rd examination cycle. Cluster III is characterized both by high risk factor values at baseline over time and by the largest gains (%change over time) in BMI, WC, and HbA1c.

Association of longitudinal risk factor trajectories with MRI adipose tissue traits

There are notable differences in the amount of variation of the MRI adipose tissue traits that were explained by the individual risk factor profiles and the trajectory clusters, with a large amount of variation being explained by the models for TAT, VAT and SAT. For RSFF and PFF only a smaller amount of variation could be explained by traditional CVD risk factors in our sample (**Figure 1**).

Total abdominal, visceral and subcutaneous fat

VAT contributes to CVD risk e.g. by elevated lipolytic activity, increased low-grade inflammation, and raised production of cytokines and other chemical messenger compounds (32). Our observations of an association between longitudinal risk factor profiles and these adipose tissue traits are in line with results from the Framingham study. There, changes in VAT and to a lesser extent in SAT were significantly associated with changes in metabolic and cardiovascular risk factors while adipose tissue traits where modeled as exposure and risk factors as the outcome (33, 34). In our analyses, however, the respective MRI derived adipose tissue traits served as outcome variables and we observed how longitudinal changes in risk factors correlate with these traits. We also confirm that anthropometric measurements are strongly correlated to VAT and SAT (35).

Hepatic fat fraction

The liver is a central metabolic organ and plays a critical role e.g. in triglyceride storage and synthesis. Elevated hepatic fat is related to CVD by its involvement in the development of insulin resistance, increased free fatty acids and chronic inflammation (36). In the CARDIA study, unfavorable BMI trajectories over the life course (25 years) were associated with an increased risk of developing non-alcoholic fatty liver disease (37). In line with this report, in our sample, traditional CVD risk factors and their trajectories over 14 years explained more than half of the variance in hepatic fat. We also found that longitudinal trajectory clusters provided additional value beyond the current risk profile (at examination cycle 3 when also the MRI measures were

obtained) for the prediction of hepatic fat, although the association was attenuated. As we made similar observations with respect to VAT, this could corroborate findings from Yaskolka Meir et al that MRI derived hepatic fat is partly modulated by VAT (38).

Pancreatic fat fraction

The role of pancreatic fat in CVD development has not been fully established (39). It is hypothesized that accumulation of pancreatic fat may affect beta-cell function and thus modulate insulin metabolism. Results regarding the association of pancreatic fat to impaired glucose metabolism and type 2 diabetes are inconclusive (29, 40). Other studies showed that pancreatic fat content is associated with serum triglyceride and nutritional fat intake (41) and susceptible to exercise and nutrition changes (42). In our study, the CVD risk profile could only explain approximately a quarter of the variance in pancreatic fat. However, the longitudinal trajectories provided substantial additional informative value. This could be due to the fact that these trajectory clusters might also reflect information on unmeasured features that contribute to pancreatic fat.

Renal sinus fat fraction

Adipose tissue in the renal sinus can lead to increased pressure on the renal vasculature and thereby to structural damage in the kidney (43). Associations of renal sinus fat to blood pressure and renal function have been proposed (21, 44). In our analysis, we found that approximately a third of the variance in renal sinus fat could be explained by traditional CVD risk factors. Longitudinal trajectories provided no distinct additional explanatory value beyond single point measures of these risk factors. This supports recent findings from Gepner et al. who reported

that weight loss affected all MRI measured ectopic fat depots; however, in their study, renal sinus fat was not modified by specific interventions such as diet and physical activity. Only reduced VAT and hepatic fat (in response to lifestyle interventions) were independently associated with a more favorable lipid profile (45).

Strengths and limitations

Limitations of our study include the relatively small sample size which prevents sex-stratified analyses and the limited number of CVD risk factors analyzed. Several other risk factors, such as triglycerides, glucose levels, inflammation markers or liver enzymes have been hypothesized to be associated with ectopic fat depots. However, in our study, these factors were not available for all individuals at all time points and could therefore not be included in the present analysis. Another important issue is the role of medication for risk factor assessment. Although we adjusted for lipid-lowering and antihypertensive treatment in our regression models, further disentanglement of the role of medication is warranted. Furthermore, MRI measurements were only available at the 3rd examination cycle; thus we cannot assess longitudinal changes in MRI parameters.

A major strength of our analyses is the longitudinal study design with repeated standardized assessment of several established CVD risk factors over a long time period, which enables us to describe and analyze the temporal development of risk profiles. We used unbiased machine learning algorithms to characterize the participants based on their cardiometabolic risk factor profiles and to group them in clusters based on different longitudinal trajectories of several

cardiometabolic risk factors. Furthermore, MRI is considered to be the gold standard for the quantification of adipose tissue.

CONCLUSIONS

Our results characterize the differential contribution of traditional risk factors to the variation in abdominal and ectopic adipose tissue depots. We provide strong evidence that sustained high risk factor levels and unfavorable risk factor trajectories are associated with high levels of ectopic adipose tissue. The trajectories are remarkably stable and emphasize the need for long-term interventions regarding traditional cardiovascular risk factors.

REFERENCES

1. Dale CE, Fatemifar G, Palmer TM, White J, Prieto-Merino D, Zabaneh D*, et al.* Causal Associations of Adiposity and Body Fat Distribution With Coronary Heart Disease, Stroke Subtypes, and Type 2 Diabetes Mellitus. Clinical Perspective: A Mendelian Randomization Analysis. *Circulation* 2017;**135:** 2373-2388.

2. Hägg S, Fall T, Ploner A, Mägi R, Fischer K, Draisma HH*, et al.* Adiposity as a cause of cardiovascular disease: a Mendelian randomization study. *International journal of epidemiology* 2015;**44:** 578-586.

3. Camhi SM, Bray GA, Bouchard C, Greenway FL, Johnson WD, Newton RL*, et al.* The Relationship of Waist Circumference and BMI to Visceral, Subcutaneous, and Total Body Fat: Sex and Race Differences. *Obesity* 2011;**19:** 402-408.

4. Neeland IJ, Turer AT, Ayers CR, Berry JD, Rohatgi A, Das SR*, et al.* Body fat distribution and incident cardiovascular disease in obese adults. *Journal of the American College of Cardiology* 2015;**65:** 2150-2151.

5. Neeland IJ, Turer AT, Ayers CR, Powell-Wiley TM, Vega GL, Farzaneh-Far R*, et al.* Dysfunctional adiposity and the risk of prediabetes and type 2 diabetes in obese adults. *Jama* 2012;**308:** 1150-1159.

6. Mongraw-Chaffin M, Allison MA, Burke GL, Criqui MH, Matsushita K, Ouyang P*, et al.* CT-Derived Body Fat Distribution and Incident Cardiovascular Disease: The Multi-Ethnic Study of Atherosclerosis. *The Journal of Clinical Endocrinology & Metabolism* 2017;**102:** 4173-4183.

7. Lee SW, Son JY, Kim JM, Hwang S-s, Han JS, Heo NJ. Body fat distribution is more predictive of all-cause mortality than overall adiposity. *Diabetes, Obesity and Metabolism* 2018;**20:** 141-147.

8. Bamberg F, Hetterich H, Rospleszcz S, Lorbeer R, Auweter SD, Schlett CL*, et al.* Subclinical disease burden as assessed by whole-body MRI in subjects with prediabetes, subjects with diabetes, and normal control subjects from the general population: the KORA-MRI Study. *Diabetes* 2017;**66:** 158-169.

9. Borel A, Nazare J, Smith J, Aschner P, Barter P, Van Gaal L*, et al.* Visceral, subcutaneous abdominal adiposity and liver fat content distribution in normal glucose tolerance, impaired fasting glucose and/or impaired glucose tolerance. *International Journal of Obesity* 2015;**39:** 495.

10. Lorbeer R, Bayerl C, Auweter S, Rospleszcz S, Lieb W, Meisinger C*, et al.* Association between MRI-derived hepatic fat fraction and blood pressure in participants without history of cardiovascular disease. *J Hypertens* 2017;**35:** 737-744.

11. Linge J, Borga M, West J, Tuthill T, Miller MR, Dumitriu A*, et al.* Body Composition Profiling in the UK Biobank Imaging Study. *Obesity* 2018.

12. Han TS, Lean MEJ. A clinical perspective of obesity, metabolic syndrome and cardiovascular disease. *JRSM Cardiovascular Disease* 2016;**5:** 2048004016633371.

13. Fox CS, Massaro JM, Hoffmann U, Pou KM, Maurovich-Horvat P, Liu C-Y*, et al.* Abdominal Visceral and Subcutaneous Adipose Tissue Compartments: Association With Metabolic Risk Factors in the Framingham Heart Study. *Circulation* 2007;**116:** 39-48.

14. Liu J, Fox CS, Hickson D, Bidulescu A, Carr JJ, Taylor HA. Fatty Liver, Abdominal Visceral Fat, and Cardiometabolic Risk Factors: The Jackson Heart Study. *Arteriosclerosis, thrombosis, and vascular biology* 2011;**31:** 2715-2722.

15. Liu J, Fox CS, Hickson DA, May WD, Hairston KG, Carr JJ*, et al.* Impact of Abdominal Visceral and Subcutaneous Adipose Tissue on Cardiometabolic Risk Factors: The Jackson Heart Study. *The Journal of Clinical Endocrinology & Metabolism* 2010;**95:** 5419-5426.

16. Newton Jr RL, Bouchard C, Bray G, Greenway F, Johnson WD, Ravussin E*, et al.* Abdominal adiposity depots are correlates of adverse cardiometabolic risk factors in Caucasian and African-American adults. *Nutrition & Diabetes* 2011;**1:** e2.

17. Oka R, Miura K, Sakurai M, Nakamura K, Yagi K, Miyamoto S*, et al.* Impacts of Visceral Adipose Tissue and Subcutaneous Adipose Tissue on Metabolic Risk Factors in Middle-aged Japanese. *Obesity* 2010;**18:** 153-160.

18. Speliotes EK, Massaro JM, Hoffmann U, Vasan RS, Meigs JB, Sahani DV*, et al.* Fatty liver is associated with dyslipidemia and dysglycemia independent of visceral fat: The Framingham heart study. *Hepatology* 2010;**51:** 1979-1987.

19. Wang C-Y, Ou H-Y, Chen M-F, Chang T-C, Chang C-J. Enigmatic Ectopic Fat: Prevalence of Nonalcoholic Fatty Pancreas Disease and Its Associated Factors in a Chinese Population. *Journal of the American Heart Association* 2014;**3**.

20. Chughtai HL, Morgan TM, Rocco M, Stacey B, Brinkley TE, Ding J*, et al.* Renal Sinus Fat and Poor Blood Pressure Control in Middle-Aged and Elderly Individuals at Risk for Cardiovascular Events. *Hypertension* 2010;**56:** 901-906.

21. Foster MC, Hwang S-J, Porter SA, Massaro JM, Hoffmann U, Fox CS. Fatty Kidney, Hypertension, and Chronic Kidney Disease: The Framingham Heart Study. *Hypertension* 2011;**58:** 784-790.

22. Holle R, Happich M, Löwel H, Wichmann H. KORA--a research platform for population based health research. *Gesundheitswesen (Bundesverband der Arzte des Offentlichen Gesundheitsdienstes (Germany))* 2005;**67:** S19-25.

23. Rathmann W, Haastert B, Icks A, Lowel H, Meisinger C, Holle R*, et al.* High prevalence of undiagnosed diabetes mellitus in Southern Germany: target populations for efficient screening. The KORA survey 2000. *Diabetologia* 2003;**46:** 182-189.

24. Deutsche Hochdruckliga. Empfehlungen zur Hochdruckbehandlung. Heidelberg, 2010.

25. Laxy M, Knoll G, Schunk M, Meisinger C, Huth C, Holle R. Quality of Diabetes Care in Germany Improved from 2000 to 2007 to 2014, but Improvements Diminished since 2007. Evidence from the Population-Based KORA Studies. *PLoS One* 2016;**11:** e0164704.

26. World Health Organization (WHO). Definition, diagnosis and classification of diabetes mellitus and its complications. Report of a WHO Consultation, Department of Noncommunicable Disease Surveillance, Geneva, 1999.

27. Storz C, Heber SD, Rospleszcz S, Machann J, Sellner S, Nikolaou K*, et al.* The role of visceral and subcutaneous adipose tissue measurements and their ratio by magnetic resonance imaging in subjects with prediabetes, diabetes and healthy controls from a general population without cardiovascular disease. *The British Journal of Radiology* 2018;**0:** 20170808.

28. Lorbeer R, Rospleszcz S, Schlett CL, Heber SD, Machann J, Thorand B*, et al.* Correlation of MRI-derived adipose tissue measurements and anthropometric markers with prevalent hypertension in the community. *Journal of hypertension* 2018;**36:** 1555-1562.

29. Heber SD, Hetterich H, Lorbeer R, Bayerl C, Machann J, Auweter S*, et al.* Pancreatic fat content by magnetic resonance imaging in subjects with prediabetes, diabetes, and controls from a general population without cardiovascular disease. *PloS one* 2017;**12:** e0177154.

30. Will S, Martirosian P, Würslin C, Schick F. Automated segmentation and volumetric analysis of renal cortex, medulla, and pelvis based on non-contrast-enhanced T1-and T2-weighted MR images. *Magnetic Resonance Materials in Physics, Biology and Medicine* 2014;**27:** 445-454.

31. Genolini C, Falissard B. KmL: k-means for longitudinal data. *Computational Statistics* 2009;**25:** 317-328.

32. Cornier M-A, Després J-P, Davis N, Grossniklaus DA, Klein S, Lamarche B*, et al.* Assessing Adiposity. *A Scientific Statement From the American Heart Association* 2011;**124:** 1996-2019.

33. Lee JJ, Pedley A, Hoffmann U, Massaro JM, Fox CS. Association of Changes in Abdominal Fat Quantity and Quality With Incident Cardiovascular Disease Risk Factors. *Journal of the American College of Cardiology* 2016;**68:** 1509-1521.

34. Abraham TM, Pedley A, Massaro JM, Hoffman U, Fox CS. Association Between Visceral and Subcutaneous Adipose Depots and Incident Cardiovascular Disease Risk Factors. *Circulation* 2015.

35. Rothney MP, Catapano AL, Xia J, Wacker WK, Tidone C, Grigore L*, et al.* Abdominal visceral fat measurement using dual-energy X-ray: Association with cardiometabolic risk factors. *Obesity* 2013;**21:** 1798-1802.

36. Targher G, Day CP, Bonora E. Risk of Cardiovascular Disease in Patients with Nonalcoholic Fatty Liver Disease. *New England Journal of Medicine* 2010;**363:** 1341-1350.

37. Vanwagner LB, Khan SS, Ning H, Siddique J, Lewis CE, Carr JJ*, et al.* Body mass index trajectories in young adulthood predict non-alcoholic fatty liver disease in middle age: The CARDIA cohort study. *Liver International* 2017.

38. Yaskolka Meir A, Tene L, Cohen N, Shelef I, Schwarzfuchs D, Gepner Y*, et al.* Intrahepatic fat, abdominal adipose tissues, and metabolic state: magnetic resonance imaging study. *Diabetes/Metabolism Research and Reviews* 2017.

39. Singh RG, Yoon HD, Wu LM, Lu J, Plank LD, Petrov MS. Ectopic fat accumulation in the pancreas and its clinical relevance: A systematic review, meta-analysis, and meta-regression. *Metabolism* 2017;**69:** 1-13.

40. Heni M, Machann J, Staiger H, Schwenzer NF, Peter A, Schick F*, et al.* Pancreatic fat is negatively associated with insulin secretion in individuals with impaired fasting glucose and/or impaired glucose tolerance: a nuclear magnetic resonance study. *Diabetes/Metabolism Research and Reviews* 2010;**26:** 200-205.

41. Rossi Andrea P, Fantin F, Zamboni Giulia A, Mazzali G, Rinaldi Caterina A, Giglio M*, et al.* Predictors of Ectopic Fat Accumulation in Liver and Pancreas in Obese Men and Women. *Obesity* 2012;**19:** 1747-1754.

42. Tene L, Shelef I, Schwarzfuchs D, Gepner Y, Yaskolka Meir A, Tsaban G*, et al.* The effect of long-term weight-loss intervention strategies on the dynamics of pancreatic-fat and morphology: An MRI RCT study. *Clinical Nutrition ESPEN* 2018.

43. Stefan N, Artunc F, Heyne N, Machann J, Schleicher ED, Häring H-U. Obesity and renal disease: not all fat is created equal and not all obesity is harmful to the kidneys. *Nephrology Dialysis Transplantation* 2016;**31:** 726-730.

44. Zelicha H, Schwarzfuchs D, Shelef I, Gepner Y, Tsaban G, Tene L*, et al.* Changes of renal sinus fat and renal parenchymal fat during an 18-month randomized weight loss trial. *Clinical Nutrition* 2017.

45. Gepner Y, Shelef I, Schwarzfuchs D, Zelicha H, Tene L, Yaskolka Meir A*, et al.* Effect of Distinct Lifestyle Interventions on Mobilization of Fat Storage Pools: The CENTRAL MRI Randomized Controlled Trial. *Circulation* 2017.

FIGURE LEGENDS

Figure 1: MRI-based assessment of VAT (red) and SAT (yellow) adipose tissue in a 46-year-old male (VAT 6.57 l), displayed in coronar (A), sagittal (B) and axial (C) slices.

Figure 2: Exemplary image of MRI-based RSFF assessment. Displayed is the overlay of renal sinus segmentation with Water-Only (A) and Fat-Only (B) Dixon images.

Figure 3: Goodness-of-Fit of current (3rd examination cycle), recent (2nd examination cycle) and remote (1st examination cycle) risk factor profiles to individual adipose tissue depots, as measured by explained variance (adjusted R^2). The risk factor profiles included: A, left: age, sex, smoking, intake of hypertensive or lipid-lowering medication, systolic blood pressure, diastolic blood pressure, BMI, WC, Total Cholesterol, HDL, LDL and HbA1c, B, right: as A, but without BMI and without WC. TAT: Total adipose tissue, VAT: Visceral adipose tissue, SAT: Subcutaneous adipose tissue, RSFF: Renal sinus fat fraction, HFF: Hepatic fat fraction, PFF: Pancreatic fat fraction

Figure 4: Mean risk factor levels at the 3rd examination cycle (contemporary to the MRI adipose tissue measurement), at the 2nd examination cycle (recent) and at the 1st examination cycle (remote) in the three longitudinal risk profile trajectory clusters.

Figure 5: Box plots, reflecting key measures of the distribution of the respective adipose tissue traits in the three longitudinal risk profile trajectory clusters. TAT: Total adipose tissue, VAT: Visceral adipose tissue, SAT: Subcutaneous adipose tissue, RSFF: Renal sinus fat fraction, HFF: Hepatic fat fraction, PFF: Pancreatic fat fraction

TABLES

Table 1: Cardiometabolic risk profile of the study sample (N = 325) at the time of MRI examination ("current", 3rd examination cycle), at the time point of the 2nd examination cycle, ("recent") and at baseline ("remote", 1st examination cycle).

	1st examination cycle (1999-2001)	**2nd examination cycle (2006-2008)**	**3rd examination cycle (2013-2014)**	**p-value**
Men	193 (59.4%)	193 (59.4%)	193 (59.4%)	
Age, years	42.2 ± 9.2	49.2 ± 9.2	56.2 ± 9.2	
Systolic BP, mmHg	126.5 ± 16.4	121.3 ± 16.5	121.1 ± 16.4	<0.01
Diastolic BP, mmHg	81.6 ± 10.5	76.4 ± 9.6	75.6 ± 10.1	<0.01
Hypertension, # of individuals	94 (28.9%)	80 (24.6%)	109 (33.5%)	<0.01
Antihypertensive Treatment, # of individuals	25 (7.7%)	43 (13.2%)	77 (23.7%)	<0.01
BMI, kg/m^2	26.6 ± 3.8	27.3 ± 4.2	28.0 ± 4.7	<0.01
Weight, kg	78.8 ± 13.3	81.4 ± 14.8	82.9 ± 16.0	<0.01
Waist Circumference, cm	90.4 ± 11.5	93.6 ± 12.9	98.3 ± 13.8	<0.01
Hip Circumference, cm	104.4 ± 6.8	106.0 ± 7.7	106.6 ± 8.5	<0.01
Waist-To-Hip-Ratio	0.9 ± 0.1	0.9 ± 0.1	0.9 ± 0.1	<0.01
Total Cholesterol, mg/dL	223.8 ± 40.1	214.6 ± 36.7	218.4 ± 36.9	<0.01
LDL Cholesterol, mg/dL	134.0 ± 39.0	137.6 ± 32.8	140.4 ± 33.0	n.s
HDL Cholesterol, mg/dL	56.1 ± 17.2	53.6 ± 14.2	61.7 ± 18.1	<0.01
Ratio Total Cholesterol/HDL	4.4 ± 1.6	4.2 ± 1.2	3.8 ± 1.3	<0.01
Ratio LDL/HDL	2.7 ± 1.2	2.7 ± 1.0	2.5 ± 1.0	0.01
Lipid-lowering Medication, # of individuals	5 (1.5%)	20 (6.2%)	32 (9.8%)	<0.01
Diabetes mellitus, self-reported, # of individuals	3 (0.9%)	14 (4.3%)	27 (8.3%)	<0.01
HbA1c, %	5.5 ± 0.5	5.5 ± 0.5	5.6 ± 0.7	0.02
Antidiabetic Medication, # of individuals	3 (0.9%)	8 (2.5%)	24 (7.4%)	<0.01
Alcohol consumption, g/day	19.5 ± 25.3	17.9 ± 23.5	18.3 ± 22.2	n.s
Smoking, # of individuals				0.04
never-smoker	121 (37.2%)	121 (37.2%)	121 (37.2%)	
ex-smoker	116 (35.7%)	133 (40.9%)	140 (43.1%)	
smoker	88 (27.1%)	71 (21.8%)	64 (19.7%)	
Physically active, # of individuals	161 (49.5%)	192 (59.1%)	198 (60.9%)	<0.01

Continuous variables are presented as mean and standard deviation with p-values calculated by repeated measures ANOVA, indicating whether the mean values differ significantly in at least two time points. Categorical variables are presented as counts and percentages with p-values

calculated by Cochrans Q Test, indicating whether the percentage of subjects differ significantly in at least two time points.

Table 2: MRI-derived adipose tissue measures of the study sample (N = 325), obtained at the 3rd examination cycle.

	N = 325
TAT, l	12.6 ± 5.3
VAT, l	4.5 ± 2.7
SAT, l	8.1 ± 3.6
RSFF, %	63.9 ± 9.9
HFF, % (median[IQR])	5.7 [3.0, 11.7]
PFF, % (median[IQR])	5.4 [3.4, 9.2]

TAT: Total adipose tissue, VAT: Visceral adipose tissue, SAT: Subcutaneous adipose tissue, RSFF: Renal sinus fat fraction, HFF: Hepatic fat fraction, PFF: Pancreatic fat fraction

Table 3: Association of longitudinal risk profile trajectory clusters with different adipose tissue traits. Cluster I served as referent for all comparisons.

		Cluster II			Cluster III			
outcome	**Model**	**estimate**	**95%-CI**	**p-value**	**estimate**	**95%-CI**	**p-value**	
TAT	1	3.90	[2.89, 4.91]	<0.01	9.49	[8.20, 10.78]	<0.01	R^2 = 0.54
	2	3.21	[2.14, 4.29]	<0.01	6.25	[4.73, 7.77]	<0.01	R^2 = 0.65
	3	0.39	[-0.26, 1.04]	n.s	0.96	[0.09, 1.82]	0.03	R^2 = 0.89
VAT	1	1.30	[0.84, 1.75]	<0.01	3.32	[2.74, 3.90]	<0.01	R^2 = 0.63
	2	1.16	[0.63, 1.69]	<0.01	2.62	[1.87, 3.37]	<0.01	R^2 = 0.66
	3	0.17	[-0.30, 0.65]	n.s	0.90	[0.26, 1.53]	<0.01	R^2 = 0.76
SAT	1	2.60	[1.87, 3.34]	<0.01	6.16	[5.23, 7.10]	<0.01	R^2 = 0.48
	2	2.05	[1.30, 2.81]	<0.01	3.63	[2.56, 4.70]	<0.01	R^2 = 0.63
	3	0.22	[-0.26, 0.70]	n.s	0.06	[-0.59, 0.71]	n.s	R^2 = 0.87
RSFF	1	3.39	[1.02, 5.76]	<0.01	3.20	[0.18, 6.22]	0.04	R^2 = 0.29
	2	2.47	[-0.41, 5.35]	n.s	0.31	[-3.77, 4.39]	n.s	R^2 = 0.29
	3	0.19	[-2.80, 3.18]	n.s	-2.28	[-6.28, 1.72]	n.s	R^2 = 0.33
HFF	1	1.54	[1.27, 1.86]	<0.01	2.48	[1.93, 3.16]	<0.01	R^2 = 0.43
	2	1.51	[1.21, 1.90]	<0.01	2.23	[1.62, 3.03]	<0.01	R^2 = 0.47
	3	1.14	[0.91, 1.43]	n.s	1.32	[0.98, 1.79]	n.s	R^2 = 0.53
PFF	1	1.52	[1.26, 1.84]	<0.01	2.20	[1.73, 2.80]	<0.01	R^2 = 0.24
	2	1.52	[1.21, 1.92]	<0.01	1.82	[1.32, 2.51]	<0.01	R^2 = 0.26
	3	1.40	[1.10, 1.79]	<0.01	1.58	[1.15, 2.20]	<0.01	R^2 = 0.27

Estimates are derived from linear regression model. Estimates for TAT, VAT; SAT and renal sinus fat are given as β-coefficients. Estimates for hepatic and pancreatic fat are back-transformed from log-transformation and are therefore given as %change of the geometric mean. Model 1: adjusted for age, sex, antihypertensive medication (3rd examination cycle), lipid-lowering medication (3rd examination cycle), smoking status (3rd examination cycle), validated diabetes (3rd examination cycle). Model 2: as Model 1, plus adjusted for remote (1st examination cycle) risk profile. Model 3: as Model 1, plus adjusted for current (3rd examination cycle) risk profile.

Supplementary Table S1: Cardiometabolic risk profile of the study sample (N = 325) at the time of MRI examination ("current", 3rd examination cycle), at the time point of the 2nd examination cycle, ("recent") and at baseline ("remote", 1st examination cycle), stratified by men and women.

	S4 (1999-2001)	**F4 (2006-2008)**	**FF4 (2013-2014)**	**p-value**
Men	193 (59.4%)	193 (59.4%)	193 (59.4%)	
Age, years	42.2 ± 9.2	49.2 ± 9.2	56.2 ± 9.2	
Men	42.1 ± 9.3	49.1 ± 9.3	56.1 ± 9.3	
Women	42.4 ± 9.0	49.4 ± 9.0	56.4 ± 9.0	
p-value men/women	n.s	n.s	n.s	
Systolic BP, mmHg	126.5 ± 16.4	121.3 ± 16.5	121.1 ± 16.4	<0.01
Men	131.4 ± 14.7	125.8 ± 15.4	125.9 ± 16.2	<0.01
Women	119.4 ± 16.3	114.7 ± 15.9	114.1 ± 14.2	0.01
p-value men/women	<0.01	<0.01	<0.01	
Diastolic BP, mmHg	81.6 ± 10.5	76.4 ± 9.6	75.6 ± 10.1	<0.01
Men	83.8 ± 10.2	78.2 ± 9.4	77.6 ± 10.6	<0.01
Women	78.4 ± 10.0	73.8 ± 9.3	72.6 ± 8.4	<0.01
p-value men/women	<0.01	<0.01	<0.01	
Hypertension, # of subjects (%)	94 (28.9%)	80 (24.6%)	109 (33.5%)	<0.01
Men	63 (32.6%)	52 (26.9%)	73 (37.8%)	<0.01
Women	31 (23.5%)	28 (21.2%)	36 (27.3%)	n.s
p-value men/women	n.s	n.s	n.s	
Antihypertensive Treatment, # of subjects (%)	25 (7.7%)	43 (13.2%)	77 (23.7%)	<0.01
Men	8 (4.1%)	23 (11.9%)	43 (22.3%)	<0.01
Women	17 (12.9%)	20 (15.2%)	34 (25.8%)	<0.01
p-value men/women	<0.01	n.s	n.s	
BMI, kg/m2	26.6 ± 3.8	27.3 ± 4.2	28.0 ± 4.7	<0.01
Men	26.9 ± 3.1	27.6 ± 3.7	28.3 ± 4.1	<0.01
Women	26.1 ± 4.7	26.8 ± 4.9	27.5 ± 5.4	n.s
p-value men/women	n.s	n.s	n.s	
Weight, kg	78.8 ± 13.3	81.4 ± 14.8	82.9 ± 16.0	<0.01
Men	85.0 ± 10.1	88.0 ± 12.4	89.6 ± 13.5	<0.01
Women	69.6 ± 12.2	71.9 ± 12.7	73.1 ± 14.3	n.s
p-value men/women	<0.01	<0.01	<0.01	
Waist Circumference, cm	90.4 ± 11.5	93.6 ± 12.9	98.3 ± 13.8	<0.01
Men	95.8 ± 8.5	98.7 ± 10.3	103.2 ± 11.6	<0.01
Women	82.5 ± 10.9	86.3 ± 12.7	91.1 ± 13.6	<0.01
p-value men/women	<0.01	<0.01	<0.01	
Hip Circumference, cm	104.4 ± 6.8	106.0 ± 7.7	106.6 ± 8.5	<0.01
Men	104.8 ± 5.5	106.5 ± 6.7	106.7 ± 7.1	<0.01
Women	103.7 ± 8.3	105.3 ± 9.0	106.6 ± 10.2	0.04
p-value men/women	n.s	n.s	n.s	
Waist-To-Hip-Ratio	0.9 ± 0.1	0.9 ± 0.1	0.9 ± 0.1	<0.01

Men	0.9 ± 0.1	0.9 ± 0.1	1.0 ± 0.1	<0.01
Women	0.8 ± 0.1	0.8 ± 0.1	0.9 ± 0.1	<0.01
p-value men/women	<0.01	<0.01	<0.01	
Total Cholesterol, mg/dL	223.8 ± 40.1	214.6 ± 36.7	218.4 ± 36.9	<0.01
Men	227.1 ± 40.5	213.0 ± 35.9	217.5 ± 38.8	<0.01
Women	218.9 ± 39.3	216.9 ± 37.9	219.7 ± 33.9	n.s
p-value men/women	n.s	n.s	n.s	
LDL Cholesterol, mg/dL	134.0 ± 39.0	137.6 ± 32.8	140.4 ± 33.0	n.s
Men	140.0 ± 38.5	139.4 ± 31.2	143.3 ± 34.0	n.s
Women	125.1 ± 38.1	134.9 ± 35.0	136.3 ± 31.1	0.02
p-value men/women	<0.01	n.s	n.s	
HDL Cholesterol, mg/dL	56.1 ± 17.2	53.6 ± 14.2	61.7 ± 18.1	<0.01
Men	49.9 ± 13.6	48.3 ± 11.4	55.0 ± 14.9	<0.01
Women	65.1 ± 17.9	61.4 ± 14.4	71.3 ± 18.1	<0.01
p-value men/women	<0.01	<0.01	<0.01	
Ratio Total Cholesterol/HDL	4.4 ± 1.6	4.2 ± 1.2	3.8 ± 1.3	<0.01
Men	4.9 ± 1.7	4.6 ± 1.2	4.2 ± 1.4	<0.01
Women	3.6 ± 1.1	3.7 ± 1.0	3.3 ± 0.9	<0.01
p-value men/women	<0.01	<0.01	<0.01	
Ratio LDL/HDL	2.7 ± 1.2	2.7 ± 1.0	2.5 ± 1.0	0.01
Men	3.0 ± 1.2	3.0 ± 0.9	2.8 ± 1.1	0.05
Women	2.1 ± 1.0	2.3 ± 0.9	2.1 ± 0.8	0.02
p-value men/women	<0.01	<0.01	<0.01	
Lipid-lowering Medication, # of subjects (%)	5 (1.5%)	20 (6.2%)	32 (9.8%)	<0.01
Men	3 (1.6%)	16 (8.3%)	19 (9.8%)	<0.01
Women	2 (1.5%)	4 (3.0%)	13 (9.8%)	<0.01
p-value men/women	n.s	n.s	n.s	
Diabetes mellitus, # of subjects (%)	3 (0.9%)	14 (4.3%)	27 (8.3%)	<0.01
Men	1 (0.5%)	8 (4.1%)	17 (8.8%)	<0.01
Women	2 (1.5%)	6 (4.5%)	10 (7.6%)	<0.01
p-value men/women	n.s	n.s	n.s	
HbA1c, %	5.5 ± 0.5	5.5 ± 0.5	5.6 ± 0.7	0.02
Men	5.4 ± 0.5	5.5 ± 0.6	5.6 ± 0.9	0.05
Women	5.5 ± 0.4	5.5 ± 0.5	5.6 ± 0.5	n.s
p-value men/women	n.s	n.s	n.s	
Antidiabetic Medication, # of subjects (%)	3 (0.9%)	8 (2.5%)	24 (7.4%)	<0.01
Men	1 (0.5%)	5 (2.6%)	14 (7.3%)	<0.01
Women	2 (1.5%)	3 (2.3%)	10 (7.6%)	<0.01
p-value men/women	n.s	n.s	n.s	
Alcohol consumption, g/day	19.5 ± 25.3	17.9 ± 23.5	18.3 ± 22.2	n.s.
Men	26.6 ± 28.6	25.0 ± 26.9	25.3 ± 24.8	n.s.
Women	9.0 ± 13.9	7.5 ± 10.9	8.1 ± 11.7	n.s
p-value men/women	<0.01	<0.01	<0.01	
Smoking, # of subjects (%)				0.04
never-smoker	121 (37.2%)	121 (37.2%)	121 (37.2%)	

Men	65 (33.7%)	65 (33.7%)	65 (33.7%)	
Women	56 (42.4%)	56 (42.4%)	56 (42.4%)	
ex-smoker	116 (35.7%)	133 (40.9%)	140 (43.1%)	
Men	74 (38.3%)	84 (43.5%)	90 (46.6%)	
Women	42 (31.8%)	49 (37.1%)	50 (37.9%)	
smoker	88 (27.1%)	71 (21.8%)	64 (19.7%)	
Men	54 (28.0%)	44 (22.8%)	38 (19.7%)	
Women	34 (25.8%)	27 (20.5%)	26 (19.7%)	
p-value men/women	n.s	n.s	n.s	
Physically active, # of subjects (%)	161 (49.5%)	192 (59.1%)	198 (60.9%)	<0.01
Men	99 (51.3%)	115 (59.6%)	110 (57.0%)	n.s.
Women	62 (47.0%)	77 (58.3%)	88 (66.7%)	<0.01
p-value men/women	n.s	n.s	n.s	

Supplementary Figure S1: Association of individual risk factor measurements, obtained at the 1st , 2nd and 3rd examination cycle, with different MRI derived adipose tissues (obtained at the 3rd examination cycle).

Displayed are β-coefficients from a linear regression model adjusted for age, sex, smoking, intake of hypertensive or lipid-lowering medication and all risk profile variables at the respective time point. Risk profile variables were standardized (risk factor – mean(risk factor))/sd(risk factor) before analysis.

Supplementary Figure S1a: Associations of individual risk factor measurements at the 1st, 2nd and 3rd examination cycle with Total adipose tissue (TAT).

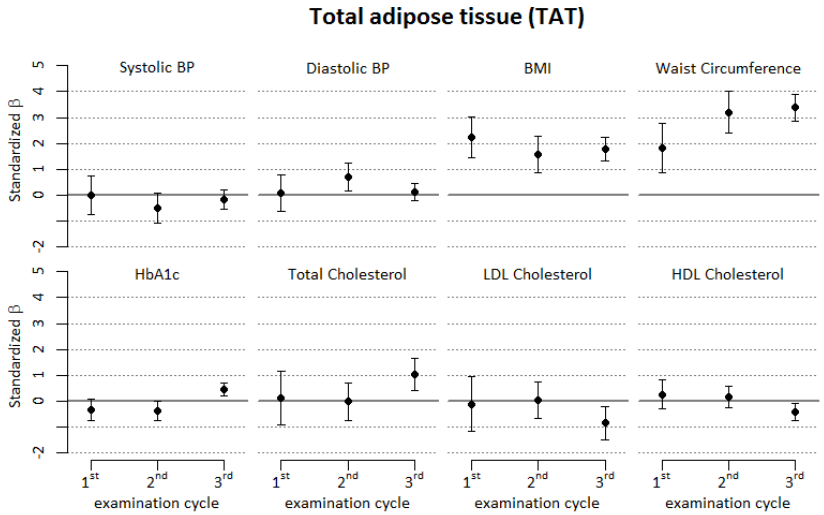

Supplementary Figure S1b: Associations of individual risk factor measurements at the 1st, 2nd and 3rd examination cycle with Visceral adipose tissue (VAT).

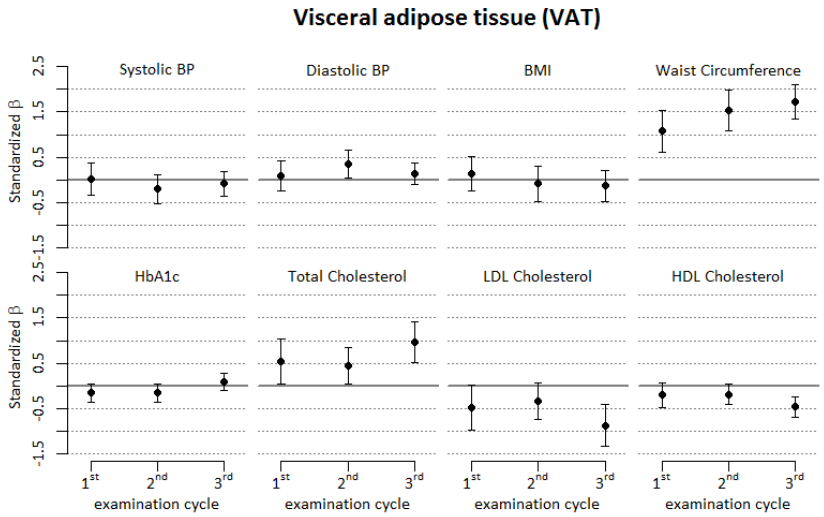

Supplementary Figure S1c: Associations of individual risk factor measurements at the 1st, 2nd and 3rd examination cycle with Subcutaneous adipose tissue (SAT).

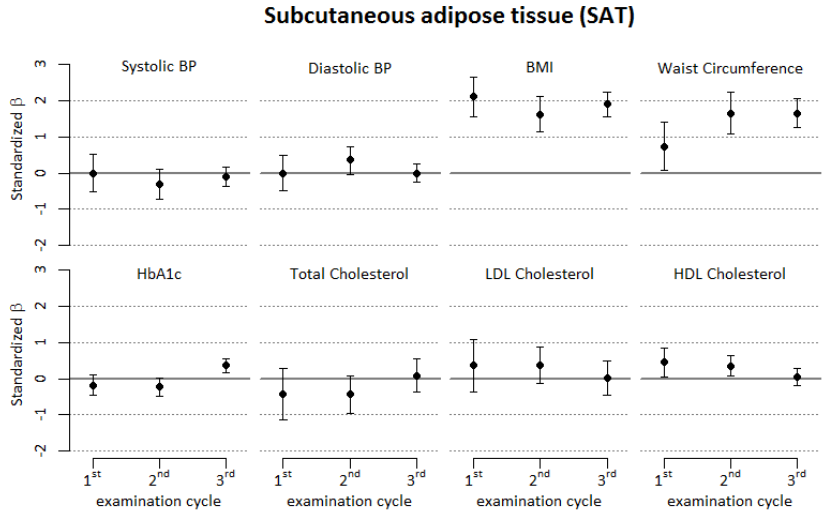

Supplementary Figure S1d: Associations of individual risk factor measurements at the 1st , 2nd and 3rd examination cycle with Renal sinus fat fraction (RSFF).

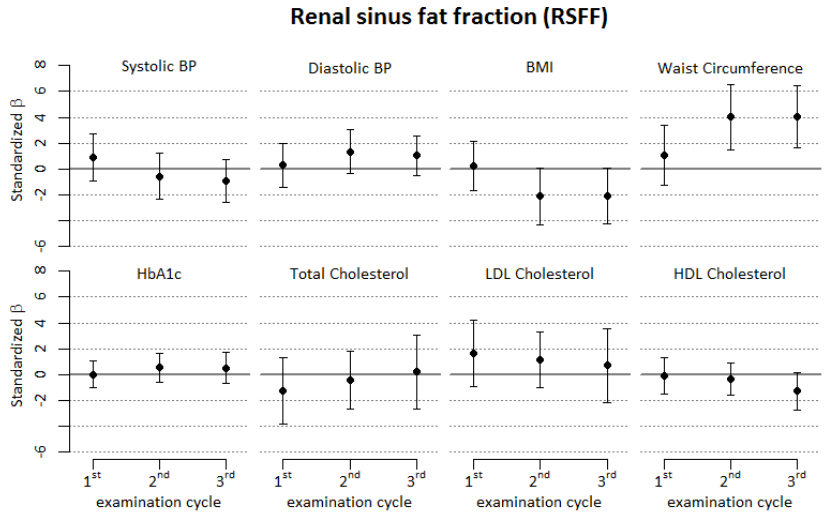

Supplementary Figure S1e: Associations of individual risk factor measurements at the 1st , 2nd and 3rd examination cycle with hepatic fat fraction (HFF).

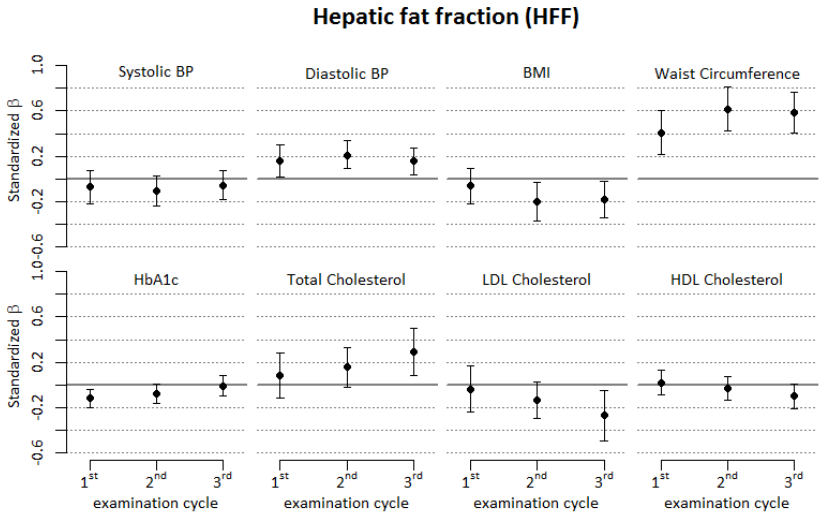

Supplementary Figure S1f: Associations of individual risk factor measurements at the 1st , 2nd and 3rd examination cycle with pancreatic fat fraction (PFF).

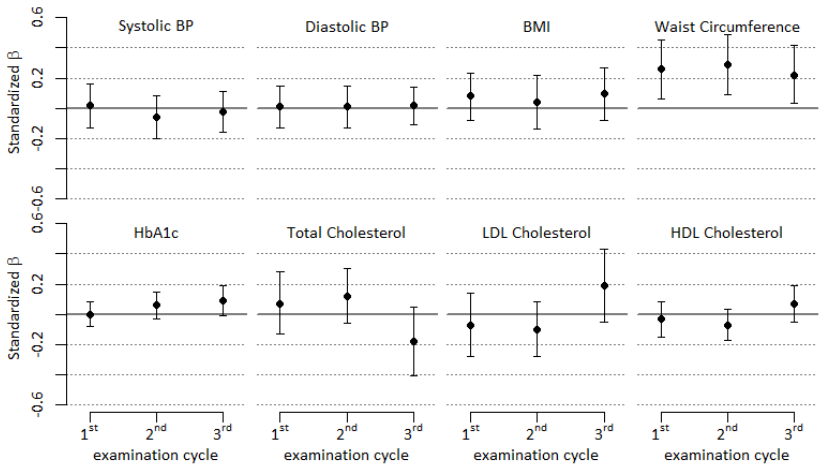

Supplementary Figure S2: Association of six individual risk factor measurements, obtained at the 1st , 2nd and 3rd examination cycle, with different MRI derived adipose tissues and BMI and WC (obtained at the 3rd examination cycle).

Displayed are β-coefficients from a linear regression model adjusted for age, sex, smoking, intake of hypertensive or lipid-lowering medication and the following risk profile variables at the respective time point: systolic blood pressure, diastolic blood pressure, HbA1c, total cholesterol, HDL cholesterol, LDL cholesterol. Risk profile variables were standardized (risk factor – mean(risk factor))/sd(risk factor) before analysis.

Supplementary Figure S2a: Associations of individual risk factor measurements at the 1st, 2nd and 3rd examination cycle with Total adipose tissue (TAT).

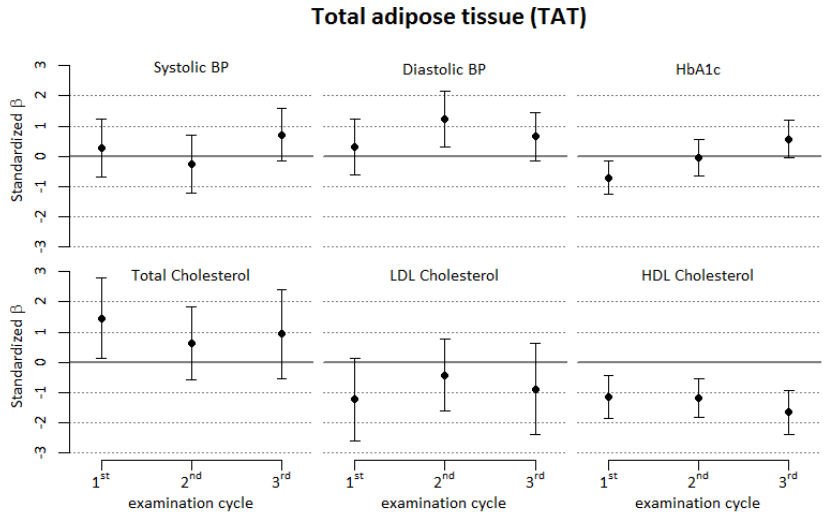

Supplementary Figure S2b: Associations of individual risk factor measurements at the 1st, 2nd and 3rd examination cycle with Visceral adipose tissue (VAT).

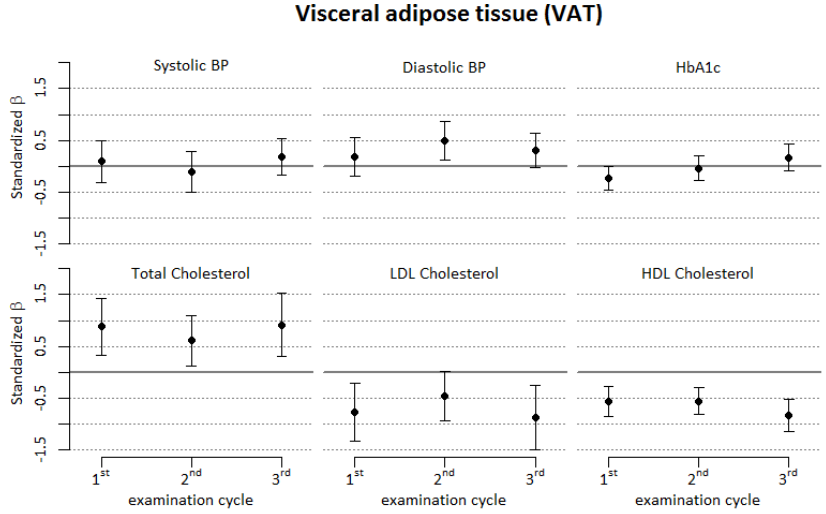

Supplementary Figure S2c: Associations of individual risk factor measurements at the 1st, 2nd and 3rd examination cycle with Subcutaneous adipose tissue (SAT).

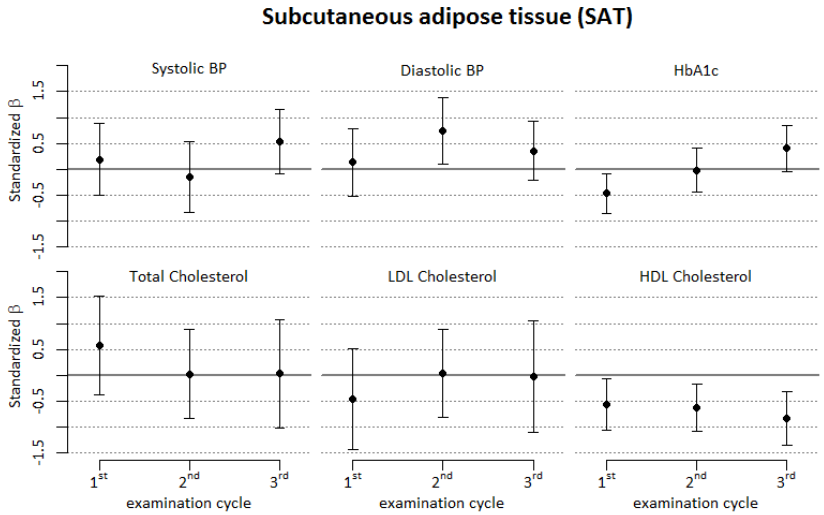

Supplementary Figure S2d: Associations of individual risk factor measurements at the 1st , 2nd and 3rd examination cycle with Renal sinus fat fraction (RSFF).

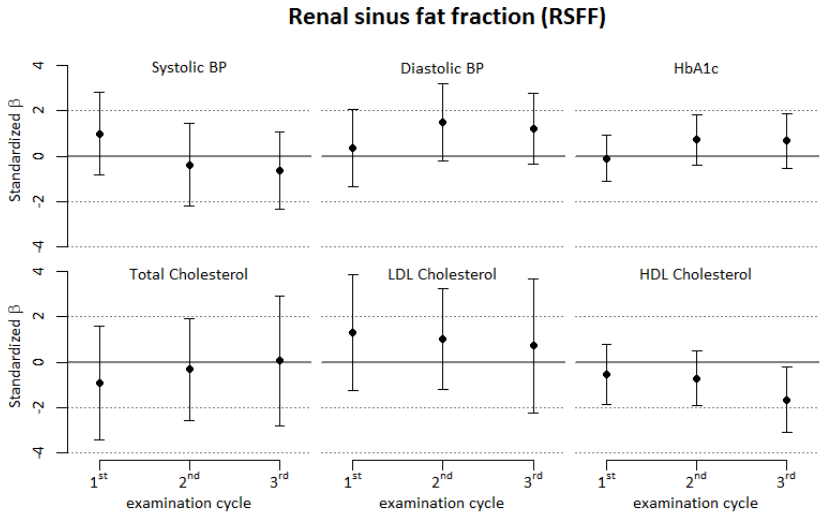

Supplementary Figure S2e: Associations of individual risk factor measurements at the 1st , 2nd and 3rd examination cycle with hepatic fat fraction (HFF).

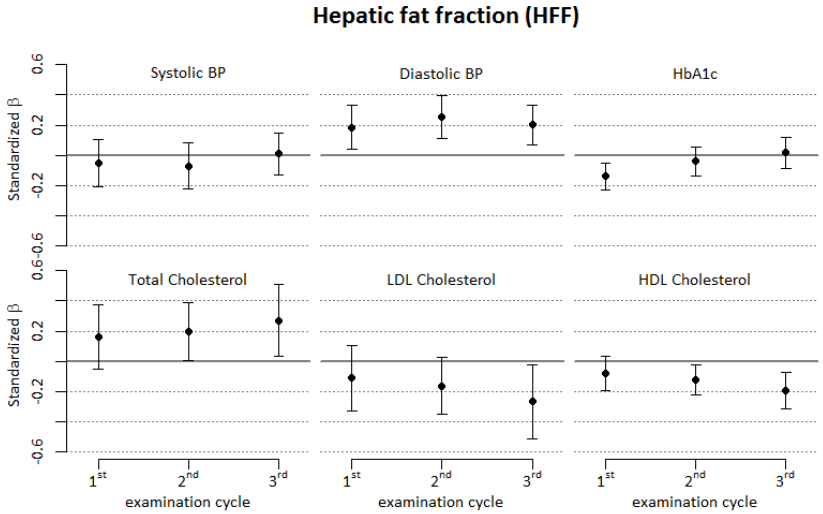

Supplementary Figure S2f: Associations of individual risk factor measurements at the 1st , 2nd and 3rd examination cycle with pancreatic fat fraction (PFF).

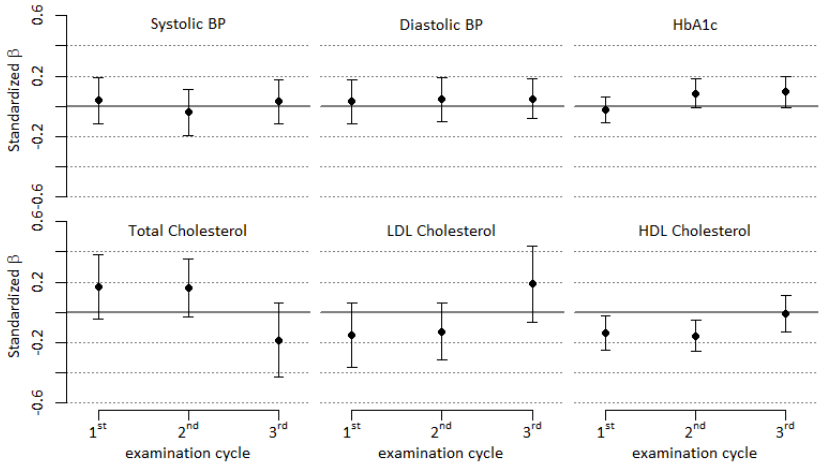

Supplementary Figure S2g: Associations of individual risk factor measurements at the 1st , 2nd and 3rd examination cycle with Body Mass Index (BMI).

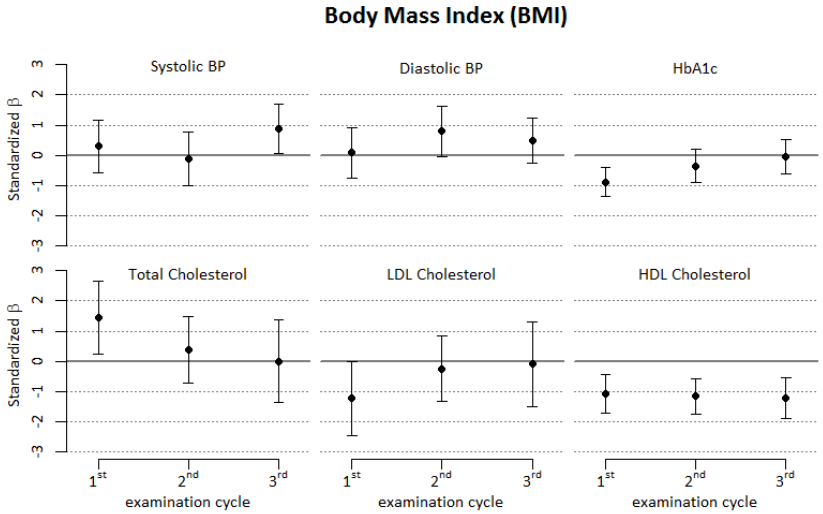

Supplementary Figure S2h: Associations of individual risk factor measurements at the 1st , 2nd and 3rd examination cycle with Waist Circumference (WC).

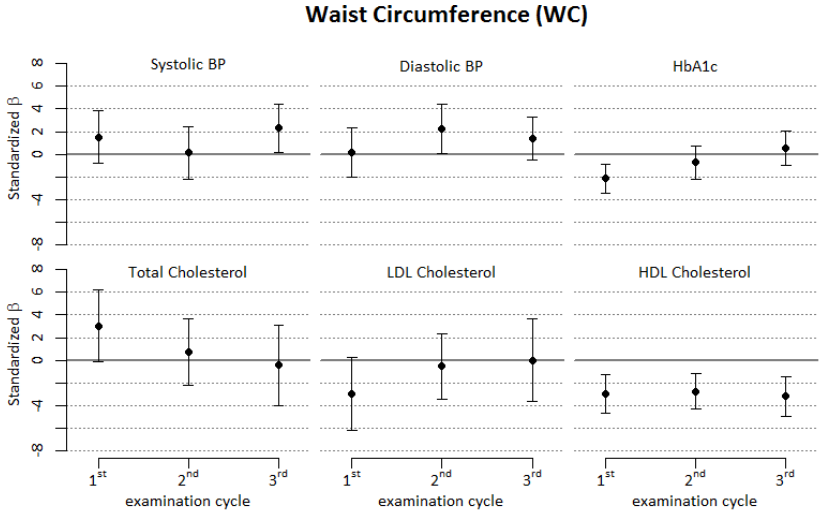

Supplementary Table S2: Risk factor values at (3rd examination cycle; contemporary to the MRI measurement), at the 2nd examination cycle (recent) and at the 1st examination cycle (remote) in the three longitudinal risk profile trajectory clusters.

	Exam cycle	Cluster I N = 114	Cluster II N = 129	Cluster III N = 82	p-value
%male	3rd	48 (42.1%)	82 (63.6%)	63 (76.8%)	< 0.01
Age, years	3rd	51.6 ± 7.9	58.4 ± 8.9	59.2 ± 8.9	< 0.01
Systolic BP, mmHg	1st	117.3 ± 13.8	127.8 ± 12.1	137.4 ± 18.4	< 0.01
	2nd	112.4 ± 14.1	122.2 ± 14.3	132.2 ± 16.0	< 0.01
	3rd	110.6 ± 12.8	123.8 ± 14.6	131.4 ± 15.6	< 0.01
	Δ%	-5.6 [-11.7, 1.1]	-3.2 [-10.5, 3.1]	-3.1 [-9.6, 3.2]	n.s
Diastolic BP, mmHg	1st	76.2 ± 8.9	82.0 ± 8.3	88.6 ± 11.3	< 0.01
	2nd	71.2 ± 8.1	77.3 ± 8.8	82.3 ± 9.0	< 0.01
	3rd	70.1 ± 7.2	77.4 ± 9.5	80.3 ± 11.0	< 0.01
	Δ%	-6.1 [-13.5, -0.6]	-6.5 [-13.1, 2.6]	-8.0 [-16.9, 0.9]	n.s
Total Cholesterol, mg/dL	1st	194.0 ± 29.0	244.6 ± 35.6	232.3 ± 35.4	< 0.01
	2nd	190.2 ± 28.3	237.6 ± 30.0	212.3 ± 34.1	< 0.01
	3rd	199.6 ± 28.4	241.0 ± 32.6	209.0 ± 35.0	< 0.01
	Δ%	3.8 [-4.3, 12.8]	0.8 [-9.0, 8.6]	-9.9 [-16.8, -0.4]	< 0.01
LDL, mg/dL	1st	104.6 ± 26.3	155.1 ± 35.8	141.6 ± 33.3	< 0.01
	2nd	113.7 ± 23.4	158.7 ± 25.5	137.4 ± 31.5	< 0.01
	3rd	120.5 ± 22.7	161.8 ± 28.2	134.5 ± 32.3	< 0001
	Δ%	17.1 [2.0, 35.2]	7.6 [-5.4, 22.8]	-3.1 [-12.4, 9.1]	< 0.01
HDL, mg/dL	1st	62.1 ± 18.7	57.3 ± 15.2	45.8 ± 12.8	< 0.01
	2nd	58.4 ± 16.4	54.4 ± 12.1	45.8 ± 10.4	< 0.01
	3rd	69.5 ± 20.2	61.2 ± 14.4	51.4 ± 14.9	< 0.01
	Δ%	14.6 [0.7, 26.0]	8.4 [-6.9, 23.3]	11.0 [-2.0, 22.3]	n.s
BMI, kg/m^2	1st	23.9 ± 2.8	26.2 ± 2.3	30.8 ± 3.2	< 0.01
	2nd	24.4 ± 2.9	26.9 ± 2.8	32.0 ± 3.6	< 0.01
	3rd	24.9 ± 3.3	27.6 ± 3.2	32.9 ± 4.3	< 0.01
	Δ%	3.2 [-2.4, 8.8]	4.3 [0.7, 8.8]	7.1 [0.2, 13.5]	0.04
Waist Circumference, cm	1st	81.8 ± 9.5	90.1 ± 7.7	102.7 ± 7.4	< 0.01
	2nd	83.8 ± 10.1	93.0 ± 7.2	108.3 ± 9.2	< 0.01
	3rd	87.9 ± 10.7	98.0 ± 8.5	113.3 ± 10.1	< 0.01
	Δ%	6.3 [1.1, 12.0]	7.9 [3.7, 13.1]	10.2 [4.8, 16.3]	0.03
HbA1c, %	1st	5.4 ± 0.4	5.4 ± 0.3	5.6 ± 0.7	< 0.01
	2nd	5.3 ± 0.3	5.4 ± 0.3	5.8 ± 0.8	< 0.01
	3rd	5.3 ± 0.4	5.5 ± 0.4	6.1 ± 1.2	< 0.01
	Δ%	-1.1 [-6.0, 4.0]	1.4 [-4.4, 6.2]	5.9 [-2.4, 12.4]	< 0.01
LDL to HDL ratio	1st	1.9 ± 0.8	2.9 ± 1.1	3.4 ± 1.3	< 0.01
	2nd	2.1 ± 0.8	3.1 ± 0.9	3.1 ± 0.9	< 0.01
	3rd	1.9 ± 0.7	2.8 ± 1.0	2.8 ± 1.1	< 0.01
	1st	3.4 ± 1.0	4.6 ± 1.4	5.5 ± 1.8	< 0.01

Total Cholesterol to HDL ratio	2nd	3.5 ± 0.9	4.6 ± 1.1	4.8 ± 1.2	< 0.01
	3rd	3.1 ± 0.8	4.2 ± 1.2	4.4 ± 1.4	< 0.01
Lipid-lowering Medication	1st	1 (0.9%)	2 (1.6%)	2 (2.4%)	n.s
	2nd	2 (1.8%)	9 (7.0%)	9 (11.0%)	0.02
	3rd	3 (2.6%)	14 (10.9%)	15 (18.3%)	<0.01
Antihypertensive medication	1st	1 (0.9%)	9 (7.0%)	15 (18.3%)	<0.01
	2nd	6 (5.3%)	15 (11.6%)	22 (26.8%)	<0.01
	3rd	13 (11.4%)	29 (22.5%)	35 (42.7%)	<0.01
Validated Glycemic Status					<0.01
Normoglycemic	3rd	102 (89.5%)	81 (62.8%)	22 (26.8%)	
Prediabetes	3rd	10 (8.8%)	37 (28.7%)	30 (36.6%)	
Diabetes	3rd	2 (1.8%)	11 (8.5%)	30 (36.6%)	

Risk factor values at each time point are presented as arithmetic mean with standard deviation. Δ% is calculated as (value_[3rd examination cycle]–value_[1stexamination cycle])/value_[1stexamination cycle]*100 and is presented as median with 1st and 3rd quartile. P-values from t-test or Wilcoxon rank test, where appropriate. Additional information for lipid-lowering medication, antihypertensive medication and validated glycemic status at the time point of the 3rd examination cycle is given as counts and percentages.

Supplementary Figure S3: Mean risk factor levels at the 3rd examination cycle (contemporary to the MRI adipose tissue measurement), at the 2nd examination cycle (recent) and at the 1st examination cycle (remote) in the three longitudinal risk profile trajectory clusters, when BMI and WC are not used to derive the clusters.

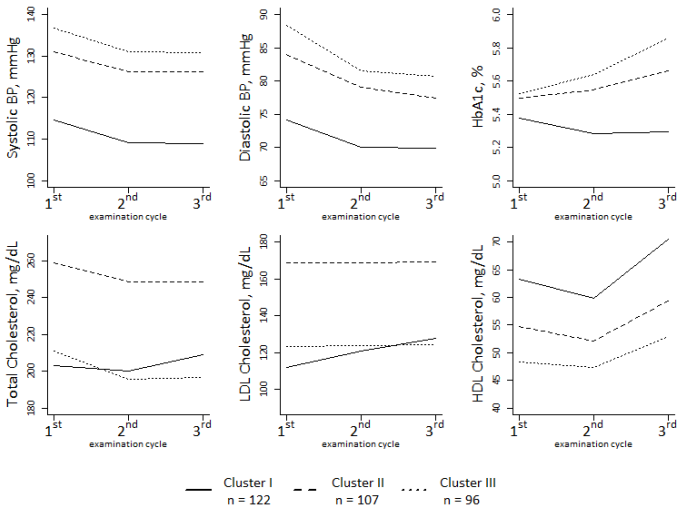

Supplementary Figure S4: Box plots, reflecting key measures of the distribution of the respective adipose tissue traits in the three longitudinal risk profile trajectory clusters, when BMI and WC are not used to derive the clusters, but counted as outcomes. TAT: Total adipose tissue, VAT: Visceral adipose tissue, SAT: Subcutaneous adipose tissue, RSFF: Renal sinus fat fraction, HFF: Hepatic fat fraction, PFF: Pancreatic fat fraction, BMI: Body Mass Index, WC: Waist Circumference.

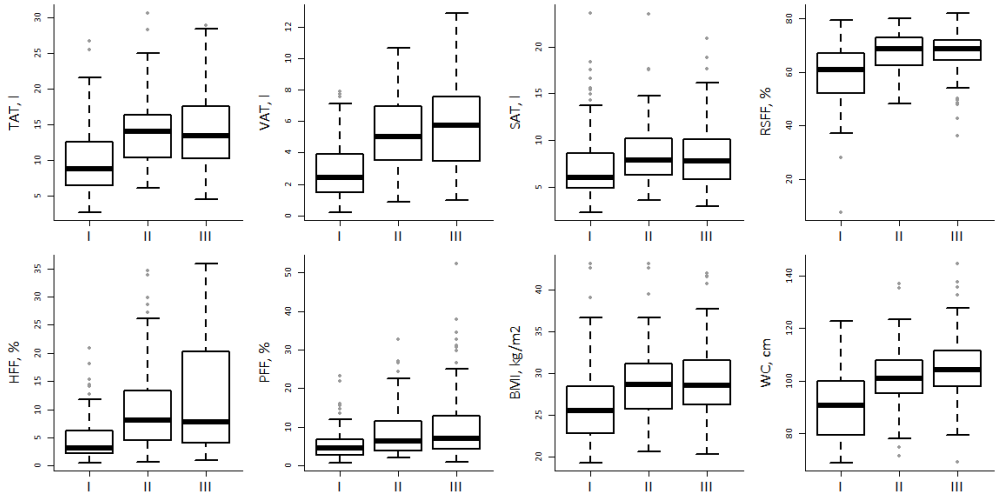

Supplementary Table S3: Key measures of the different adipose tissue traits in the three longitudinal risk profile trajectory clusters.

Values are presented as arithmetic mean +/- SD or median with IQR: interquartile range (1st quartile, 3rd quartile).

	Cluster I	**Cluster II**	**Cluster III**	**p-value**
TAT, l	8.6 ± 3.4	12.3 ± 3.5	18.4 ± 4.6	< 0.01
VAT, l	2.5 ± 1.7	4.6 ± 1.9	7.3 ± 2.2	< 0.01
SAT, l	6.2 ± 2.4	7.8 ± 2.9	11.1 ± 4.1	< 0.01
RSFF, %	59.2 ± 11.2	65.9 ± 8.1	67.3 ± 8.1	< 0.01
HFF, % (median[IQR])	2.9 [2.0, 4.9]	5.9 [3.9, 10.8]	13.4 [7.9, 23.0]	< 0.01
PFF, % (median [IQR])	3.7 [2.3, 5.7]	5.9 [4.3, 9.2]	10.7 [5.0, 16.3]	< 0.01

TAT: Total adipose tissue, VAT: Visceral adipose tissue, SAT: Subcutaneous adipose tissue, RSFF: Renal sinus fat fraction, HFF: Hepatic fat fraction, PFF: Pancreatic fat fraction

Supplementary Table S4: Association of longitudinal risk profile trajectory clusters with different adipose tissue traits, when BMI and WC are not used to derive the clusters. Cluster I served as referent for all comparisons.

		Cluster II			Cluster III			
outcome	**Model**	**estimate**	**95%-CI**	**p-value**	**estimate**	**95%-CI**	**p-value**	**R^2**
TAT	1	2.67	[1.30, 4.03]	<0.01	2.80	[1.33, 4.28]	<0.01	0.28
	2	2.56	[0.91, 4.22]	<0.01	2.46	[0.83, 4.09]	<0.01	0.30
	3	0.94	[-0.65, 2.54]	0.25	0.14	[-1.50, 1.79]	0.86	0.36
VAT	1	1.09	[0.53, 1.66]	<0.01	1.09	[0.48, 1.70]	<0.01	0.51
	2	1.00	[0.32, 1.68]	<0.01	0.83	[0.16, 1.51]	0.02	0.53
	3	0.52	[-0.14, 1.18]	0.12	0.15	[-0.53, 0.83]	0.66	0.56
SAT	1	1.57	[0.62, 2.53]	<0.01	1.71	[0.68, 2.74]	<0.01	0.24
	2	1.57	[0.40, 2.74]	0.01	1.63	[0.48, 2.78]	0.01	0.25
	3	0.42	[-0.71, 1.56]	0.46	-0.01	[-1.18, 1.16]	0.99	0.30
RSFF	1	4.30	[1.77, 6.83]	<0.01	2.92	[0.19, 5.65]	0.04	0.29
	2	4.14	[1.01, 7.26]	0.01	1.80	[-1.28, 4.89]	0.25	0.29
	3	2.75	[-0.36, 5.86]	0.08	1.27	[-1.93, 4.46]	0.44	0.31
HFF	1	0.34	[0.12, 0.55]	<0.01	0.34	[0.10, 0.57]	0.01	0.36
	2	0.29	[0.03, 0.55]	0.03	0.26	[0.01, 0.52]	0.05	0.38
	3	0.17	[-0.09, 0.42]	0.21	0.02	[-0.24, 0.29]	0.87	0.41
PFF	1	0.21	[-0.01, 0.42]	0.06	0.31	[0.07, 0.54]	0.01	0.16
	2	0.16	[-0.11, 0.42]	0.24	0.27	[0.01, 0.53]	0.04	0.16
	3	0.10	[-0.17, 0.36]	0.48	0.19	[-0.08, 0.46]	0.17	0.16
BMI	1	1.90	[0.64, 3.17]	<0.01	2.27	[0.91, 3.64]	<0.01	0.21
	2	1.83	[0.31, 3.34]	0.02	2.05	[0.55, 3.54]	0.01	0.25
	3	0.36	[-1.13, 1.84]	0.64	-0.12	[-1.64, 1.40]	0.88	0.29
WC	1	6.48	[3.24, 9.73]	<0.01	8.13	[4.62, 11.63]	<0.01	0.39

2	6.96	[3.06, 10.86]	<0.01	7.30	[3.46, 11.15]	<0.01	0.42
3	2.99	[-0.85, 6.82]	0.13	2.04	[-1.91, 5.98]	0.31	0.45

Estimates are derived from linear regression model. Estimates for TAT, VAT; SAT and renal sinus fat are given as β-coefficients. Estimates for hepatic and pancreatic fat are back-transformed from log-transformation and are therefore given as %change of the geometric mean. Model 1: adjusted for age, sex, antihypertensive medication (3rd examination cycle), lipid-lowering medication (3rd examination cycle), smoking status (3rd examination cycle), validated diabetes (3rd examination cycle). Model 2: as Model 1, plus adjusted for remote (1st examination cycle) risk profile. Model 3: as Model 1, plus adjusted for current (3rd examination cycle) risk profile.

Supplementary Table S5: Goodness of Fit as measured by explained variance (adjusted R^2) of different models.

	Predictor variables in model					
outcome	**remote risk profile alone**	**recent risk profile alone**	**current risk profile alone**	**traj clusters alone**	**traj clusters + remote risk profile**	**traj clusters + current risk profile**
TAT	0.57855	0.74993	0.88847	0.54222	0.65176	0.88946
VAT	0.61280	0.69311	0.75721	0.62927	0.66006	0.76312
SAT	0.57030	0.73082	0.86844	0.48148	0.63180	0.86804
RSFF	0.28550	0.31595	0.32937	0.28467	0.28631	0.33040
HFF	0.43344	0.50097	0.53093	0.43124	0.47394	0.53285
PFF	0.21882	0.25570	0.25369	0.24432	0.25740	0.27140

All models are adjusted for age, sex, antihypertensive medication, lipid-lowering medication and smoking. Note that the values in the first three columns are graphically displayed in Figure 1 in the main document. TAT: Total adipose tissue, VAT: Visceral adipose tissue, SAT: Subcutaneous adipose tissue, RSFF: Renal sinus fat fraction, HFF: Hepatic fat fraction, PFF: Pancreatic fat fraction

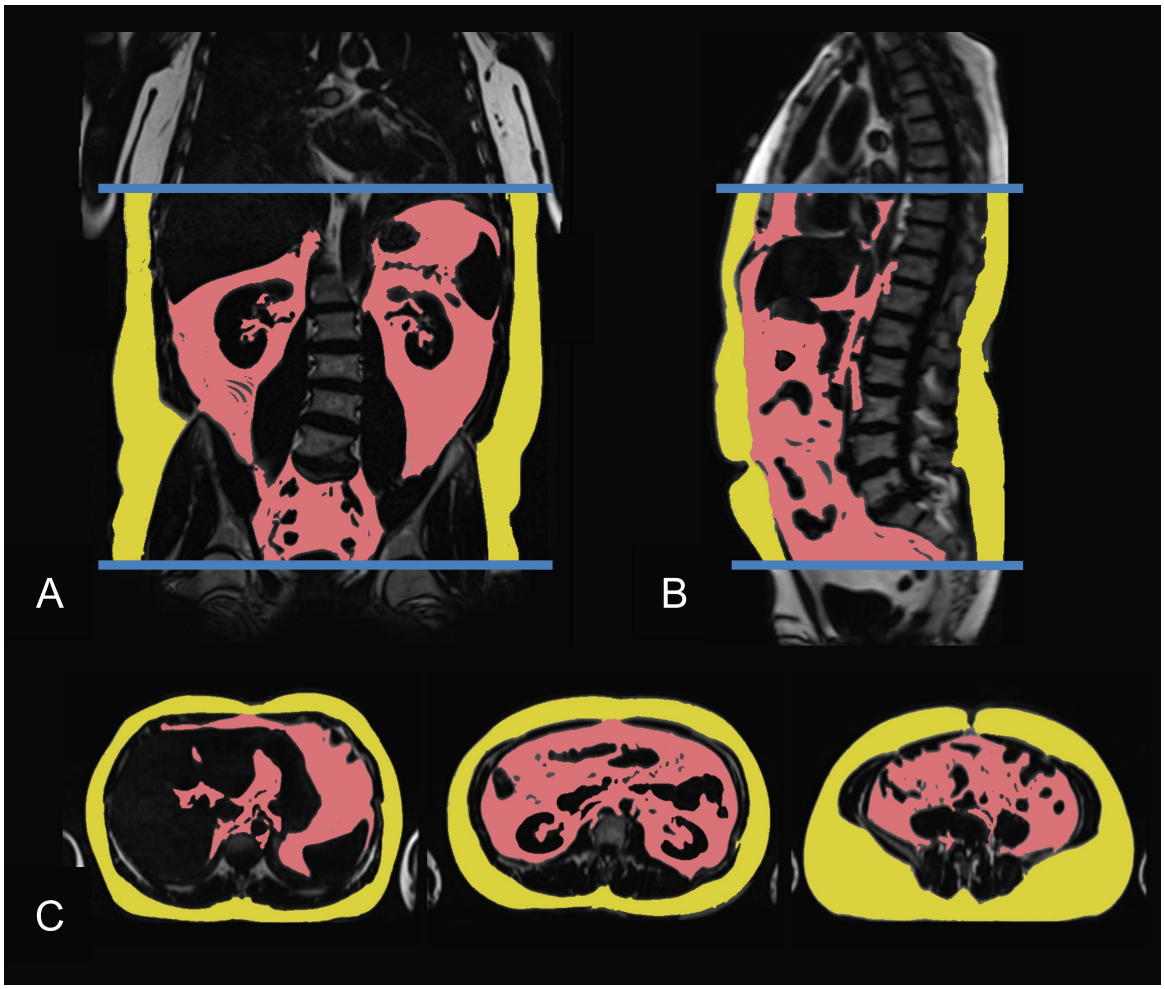
A
B
C

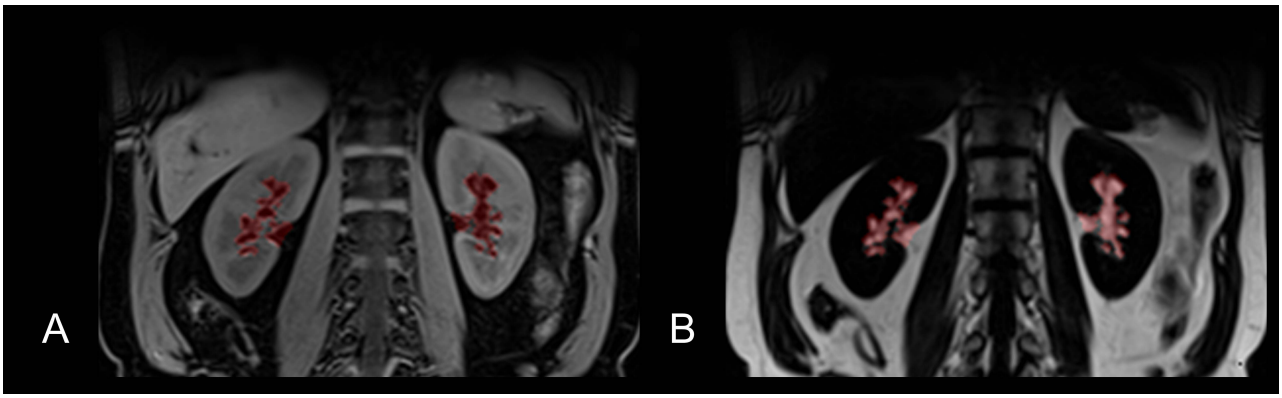
A
B

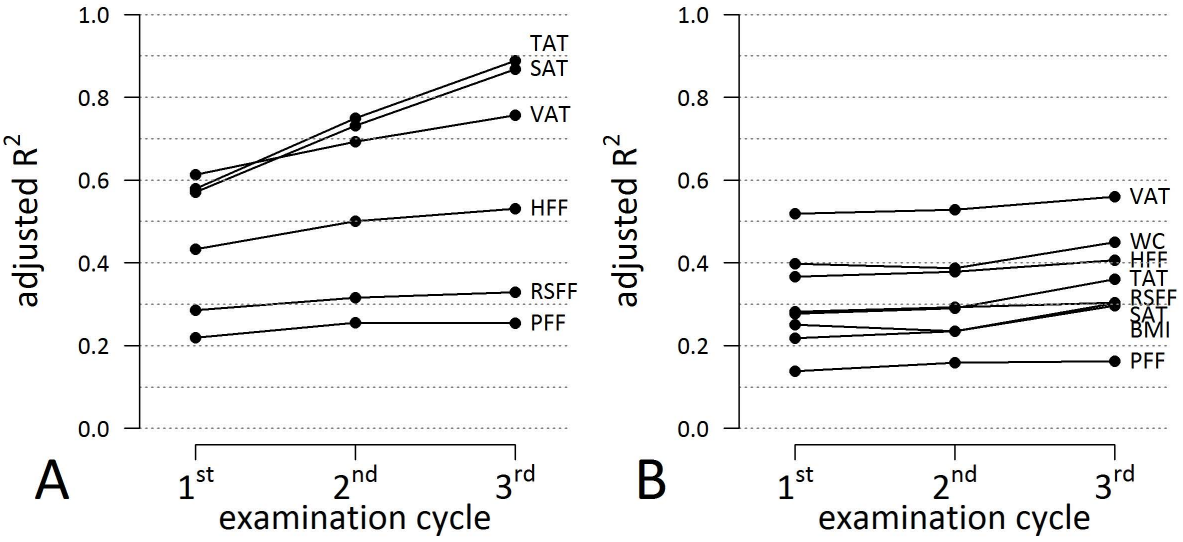
1.0
0.8
0.6
0.4
0.2
0.0
adjusted R^2
TAT
SAT
VAT
HFF
RSFF
PFF
A
1st
2nd
3rd
examination cycle
B
WC
BMI

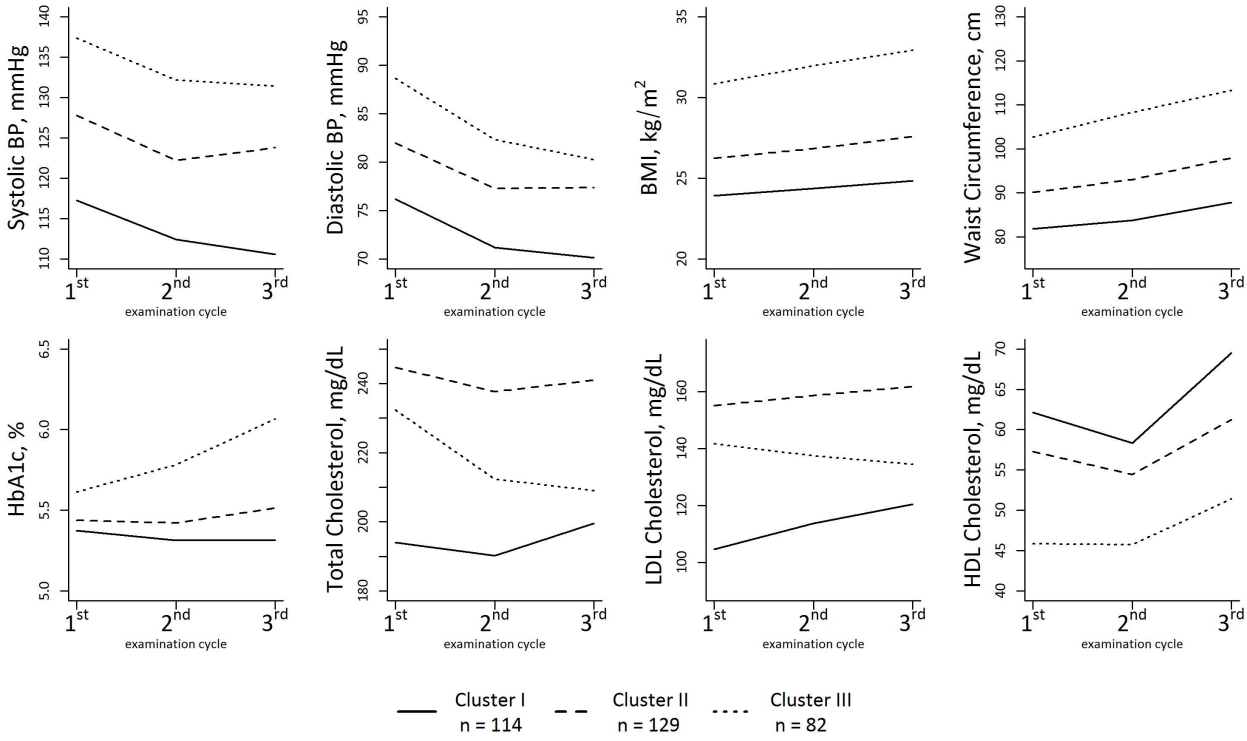
Systolic BP, mmHg
110 115 120 125 130 135 140
Diastolic BP, mmHg
70 75 80 85 90 95
BMI, kg/m2
20 25 30 35
Waist Circumference, cm
80 90 100 110 120 130
HbA1c, %
5.0 5.5 6.0 6.5
Total Cholesterol, mg/dL
180 200 220 240
LDL Cholesterol, mg/dL
100 120 140 160
HDL Cholesterol, mg/dL
40 45 50 55 60 65 70
1st 2nd 3rd
examination cycle
Cluster I
n = 114
Cluster II
n = 129
Cluster III
n = 82

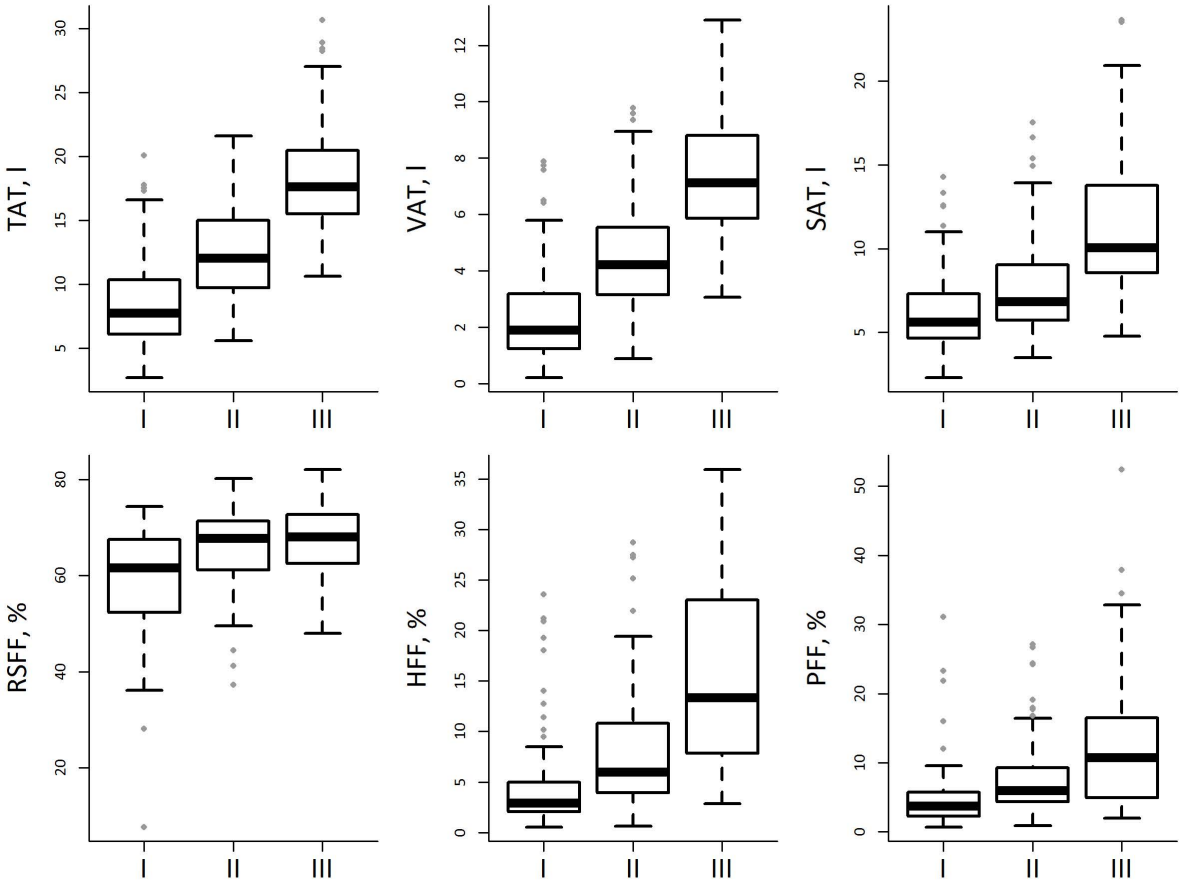
TAT, l
VAT, l
SAT, l
RSFF, %
HFF, %
PFF, %
I
II
III

Manuscript III

Title: Association of glycemic status and segmental left ventricular wall thickness in subjects without prior cardiovascular disease: a cross-sectional study

Authors: Susanne Rospleszcz,
Anina Schafnitzel,
Wolfgang Koenig,
Roberto Lorbeer,
Sigrid Auweter,
Cornelia Huth,
Wolfgang Rathmann,
Margit Heier,
Birgit Linkohr,
Christa Meisinger,
Holger Hetterich,
Fabian Bamberg,
Annette Peters

Journal: BMC Cardiovascular Disorders
Status: Published
doi: 10.1186/s12872-018-0900-7

Rospleszcz et al. BMC Cardiovascular Disorders (2018) 18:162
https://doi.org/10.1186/s12872-018-0900-7

BMC Cardiovascular Disorders

RESEARCH ARTICLE Open Access

Association of glycemic status and segmental left ventricular wall thickness in subjects without prior cardiovascular disease: a cross-sectional study

Susanne Rospleszcz[1*], Anina Schafnitzel[2], Wolfgang Koenig[3,4,5], Roberto Lorbeer[2], Sigrid Auweter[2], Cornelia Huth[1,6], Wolfgang Rathmann[6,7], Margit Heier[1,8], Birgit Linkohr[1], Christa Meisinger[1,6,8], Holger Hetterich[2], Fabian Bamberg[2,9] and Annette Peters[1,5,6]

Abstract

Background: Left ventricular (LV) hypertrophy and changes in LV geometry are associated with increased cardiovascular mortality. Subjects with type 2 diabetes have an increased risk of such alterations in cardiac morphology. We sought to assess the association of glycemic status and LV wall thickness measured by cardiac magnetic resonance (CMR), and potential interactions of hypertension and diabetes.

Methods: CMR was performed on 359 participants from a cross-sectional study nested in a population-based cohort (KORA FF4) free of overt cardiovascular disease. Participants were classified according to their glycemic status as either control (normal glucose metabolism), prediabetes or type 2 diabetes. Segmentation of the left ventricle was defined according to the American Heart Association (AHA) 16-segment model. Measurements of wall thickness were obtained at end-diastole and analyzed by linear regression models adjusted for traditional cardiovascular risk factors.

Results: LV wall thickness gradually increased from normoglycemic controls to subjects with prediabetes and subjects with diabetes (8.8 ± 1.4 vs 9.9 ± 1.4 vs 10.5 ± 1.6 mm, respectively). The association was independent of hypertension and traditional cardiovascular risk factors (β-coefficient: 0.44 mm for prediabetes and 0.70 mm for diabetes, *p*-values compared to controls: $p = 0.007$ and $p = 0.004$, respectively). Whereas the association of glycemic status was strongest for the mid-cavity segments, the association of hypertension was strongest for the basal segments.

Conclusion: Abnormal glucose metabolism, including pre-diabetes, is associated with increased LV wall thickness independent of hypertension.

Keywords: Cardiac magnetic resonance imaging, Prediabetes, Diabetes, Left ventricular wall thickness, 16-segment model

* Correspondence: susanne.rospleszcz@helmholtz-muenchen.de
[1]Institute of Epidemiology, Helmholtz Zentrum München, German Research Center for Environmental Health, Ingolstaedter Landstrasse 1, 85764 Neuherberg, Germany
Full list of author information is available at the end of the article

Background

Abnormal cardiac morphology, such as left ventricular (LV) hypertrophy and altered geometry, represents a risk factor for increased cardiovascular mortality and morbidity [1, 2].

Increased LV wall thickness is considered as an adaptive response to augmented wall stress caused by pressure overload. Short-term increase in wall thickness can therefore be regarded as a beneficial adaptation in order to maintain oxygen demand and contractile function of the heart [3]. However, a persistent increase in wall thickness leads to impaired myocardial relaxation and subsequently to decreased diastolic function, [4] which is associated with diastolic heart failure and other adverse cardiovascular outcomes [5]. The exact pathophysiological pathways of the transition from compensatory response to a detrimental chronic condition are not yet fully understood.

Chronic hypertension and the resulting increased hemodynamic load are a major risk factor for cardiac remodeling. However, metabolic factors, including diabetes status, play an important role [6–9]. Multiple studies have used echocardiography to analyze the potential impact of glycemic status on measures of LV mass and geometric patterns. Although most studies found higher values of LV mass in people with abnormal glucose metabolism, these associations were often attenuated by the presence of other traditional cardiovascular risk factors, especially elevated blood pressure [10–15]. Moreover, the prognostic utility of LV mass for CVD events in people with diabetes also depends on other metabolic factors [16–18].

These findings raise the question whether these measurements of LV mass and geometric patterns are detailed enough to describe the complex interplay between glycemic status and blood pressure on cardiac structure. Cardiac magnetic resonance imaging (CMR) has now become the gold standard for the measurement of myocardial mass and volumes [19, 20] and delivers a more detailed characterization of cardiac morphology than echocardiography, thereby allowing more precise insights into the mechanisms of LV remodeling.

In our initial analyses, using CMR to derive measures of LV geometry and function, we had observed an increased myocardial mass in subjects with abnormal glucose metabolism, but the difference disappeared after adjustment for major cardiovascular risk factors [21]. We therefore aim to elucidate the impact of glycemic status on regional LV remodeling and further analyze its potential interaction with blood pressure.

Methods

Study sample

The study sample is a subsample of the second follow-up of the population-based KORA ("Cooperative Health Research in the Region of Augsburg") S4 cohort (KORA FF4). The major focus of the substudy is the analysis of subclinical cardiovascular disease by whole-body magnetic resonance imaging (MRI).

Recruitment and eligibility criteria for the KORA studies have been described elsewhere [22]. The KORA FF4 study was conducted between 2013 and 2014 and included 2279 of the originally recruited 4261 KORA S4 participants. Of these, 400 subjects participated in the MRI substudy who were eligible and willing to undergo whole-body MRI. The detailed participant flow and exclusion criteria have been described previously [21].

Additionally, we excluded 31 subjects with incomplete measurements of any AHA segment due to low image quality and subsequently excluded 10 subjects with visible Late Gadolinium Enhancement.

Covariate assessment

Glycemic status was defined as known diabetes, either self-reported or defined by current use of glucose-lowering medication, and in participants without known diabetes, it was determined by a standard 2-h oral glucose tolerance test (OGTT). According to the 1999 WHO criteria [23], subjects with fasting serum glucose levels ≥7.0 mmol/l or OGTT 2-h serum glucose levels ≥11.1 mmol/l were also classified as having diabetes. Isolated impaired fasting glucose (iIFG) was defined as fasting glucose ≥6.1 but < 6.9 mmol/l and 2-h glucose < 7.8 mmol/l. Isolated impaired glucose tolerance (iIGT) was defined as fasting glucose < 6.1 mmol/l and 2-h glucose ≥7.8 but < 11.1 mmol/l. Subjects with iIFG, iIGT or with both conditions were classified as having prediabetes. Subjects with fasting glucose < 6.1 mmol/l and 2-h glucose < 7.8 mmol/l were considered controls.

Hypertension was defined as current antihypertensive treatment and/or systolic/diastolic blood pressure above 140/90 mmHg. Prehypertension was defined as systolic/diastolic blood pressure above 120/80 mmHg. Subjects were classified as smokers if they reported current regular or sporadic cigarette smoking. Cholesterol, serum glucose, serum insulin and Hba1c were determined by standard methods as described in Additional file 1: Text S1.

CMR outcome assessment

Magnetic resonance imaging was performed at a 3 Tesla Magnetom Skyra (Siemens AG, Healthcare Sector, Erlangen Germany) using a 18 channel body coil in combination with the table-mounted spine matrix coil. The whole-body MRI protocol comprised several sequences as described previously [21].

Imaging of cardiac function and morphology was performed using cine steady-state free precession (cine-SSFP) sequences in the short axis with a stack of

10 layer and 25 phases per cardiac cycle as well as in a 4-chamber view (echo time 1.46 ms, repetition time 29.97 ms, in-plane voxel size 1.5 × 1.5 mm, flip angle 62–63°, field-of-view 297 × 360 mm, matrix size 240 × 160 mm, slice thickness 8 mm).

The cine-SSFP sequences were then analyzed semi-automatically using cvi42 software (Circle Cardiovascular Imaging, Calgary, Canada) by two readers unaware of the subject's glycemic status and all other clinical covariates. In the 4-chamber view, apex and base of the LV were first manually selected, followed by automatic border detection of the LV endocardial and epicardial border in the short axis. Borders were corrected manually, if necessary. The basal slice was selected when at least 50 % of the LV cavity was surrounded by myocardium at end-diastole. Papillary muscles and trabeculations were excluded from the myocardial area and included in the blood pool. To assess intraobserver agreement, measurements of 25 randomly chosen subjects were repeated by the first reader. Interobserver agreement was assessed on 52 subjects who were measured by the first and the second reader. Intra- and Interobserver agreement were calculated by the Intraclass Correlation Coefficient (ICC).

Mean wall thickness was measured at the end of diastole for each segment according to the American Heart Association (AHA) 16-segment model [24]. Measurements of the single segments are visualized in a polar plot according to glycemic status. For further statistical analysis, segments are grouped according to level (basal: AHA segments 1–6; mid-cavity: AHA segments 7–12; apical: AHA segments 12–16) and region (lateral: AHA segments 5, 6, 11, 12 and 16; septal: AHA segments 2, 3, 8 and 9; anterior: AHA segments 1, 7 and 13; inferior: AHA segments 4, 10 and 15) [24].

Statistical analysis

Main demographic and cardiovascular characteristics of the participants are reported as arithmetic means with standard deviations for continuous variables and counts and percentages for categorical variables. Differences in wall thickness between the glycemic groups were assessed by one-way ANOVA. A linear regression model including glycemic status, age, sex, Body Mass Index (BMI), systolic blood pressure, total cholesterol, use of antihypertensive medication and smoking status was calculated to determine the association of glycemic status to the respective wall thickness variable. The same model without adjustment for systolic blood pressure was calculated for hypertension. Additionally, linear regression models with multiplicative terms between glycemic status and systolic blood pressure were computed to discover any interaction effects.

As the MRI sample is a non-representative subsample of a population based cohort, we used appropriate sampling weights to render the sample more representative of the full eligible underlying cohort. Weighting was based on glycemic status, age and sex. Details of the weighting procedure are presented in Additional file 1: Text S2.

P-values < 0.05 were considered to denote statistical significance. All analyses were done with R version 3.2.1 (R Core Team, Vienna, Austria).

The KORA FF4 study was approved by the ethics committee of the Bavarian Chamber of Physicians, Munich; the MRI substudy by the institutional review board of the Ludwig-Maximilians-University Munich. The investigations were carried out in accordance with the Declaration of Helsinki, including written informed consent of all participants.

Results

Study population

The sample of 359 subjects comprised 223 normoglycemic controls (62%), 92 subjects with prediabetes (26%) and 44 subjects with diabetes (12%) as presented in Table 1. Of those, 15 diabetes cases were diagnosed based on the results of OGTT. In subjects with established diabetes the median duration of diabetes was 7.0 years.

Intra- and Interobserver agreement

The ICCs for intraobserver and interobserver agreement were 0.93 and 0.94 for mean wall thickness, respectively. ICCs for single segments are presented in Additional file 1: Figure S1.

Comparison of wall thickness according to glycemic status

Mean wall thickness of all AHA segments in the whole sample was 9.1 mm (± standard deviation: 1.5 mm). The polar plots in Fig. 1 display the wall thickness of the individual AHA segments for the three glycemic groups.

We found a gradual increase in wall thickness from controls through prediabetes to diabetes for all classes of segments grouped by level and region. The differences between the glycemic groups were statistically significant in univariate analysis for all analyzed segment classes (Table 2).

Association of glycemic status and wall thickness independent of confounding factors

After adjustment for additional covariates as detailed above, prediabetes and diabetes were independently associated to increased wall thickness (prediabetes: β: 0.44 mm, 95%-CI: [0.12 mm, 0.75 mm], diabetes: β: 0.70 mm, 95%-CI: [0.23 mm, 1.17 mm]). Associations held true for most segment classes according to level and region as

Table 1 Demographic characteristics of study participants

	All	Control	Prediabetes	Type 2 diabetes
	N = 359	*N* = 223	*N* = 92	*N* = 44
Age (years)	56.1 ± 9.1	54.3 ± 8.9	58.1 ± 8.8	61.4 ± 8.3
Male gender	205 (57.1%)	115 (51.6%)	58 (63.0%)	32 (72.7%)
BMI (kg/m^2)	27.9 ± 4.8	26.5 ± 4.2	30.3 ± 4.6	30.2 ± 5.1
Systolic blood pressure (mmHg)	120.3 ± 16.9	116.5 ± 15.2	124.7 ± 15.5	130.1 ± 21.2
Diastolic blood pressure (mmHg)	75.3 ± 10.1	73.7 ± 9.2	78.0 ± 9.7	78.0 ± 13.2
Prehypertension	94 (26.2%)	61 (27.4%)	26 (28.3%)	7 (15.9%)
Hypertension	117 (32.6%)	45 (20.2%)	41 (44.6%)	31 (70.5%)
Fasting glucose (mmol/L)	5.7 ± 1.3	5.2 ± 0.4	5.9 ± 0.6	8.0 ± 2.3[a]
Fasting insulin (pmol/L)	65.4 ± 41.1	51.6 ± 26.7	86.9 ± 44.6	91.7 ± 60.0[b]
HbA1c (%)	5.6 ± 0.7	5.3 ± 0.3	5.6 ± 0.3	6.7 ± 1.4
Total cholesterol (mmol/L)	5.6 ± 1.0	5.6 ± 0.9	5.8 ± 0.8	5.5 ± 1.2
HDL cholesterol (mmol/L)	1.6 ± 0.5	1.7 ± 0.5	1.5 ± 0.4	1.4 ± 0.4
LDL cholesterol (mmol/L)	3.6 ± 0.9	3.6 ± 0.8	3.7 ± 0.8	3.5 ± 1.1
Triglycerides (mmol/L)	1.5 ± 1.0	1.2 ± 0.7	1.7 ± 1.0	2.3 ± 1.4
Smoking				
Never-smoker	130 (36.2%)	88 (39.5%)	28 (30.4%)	14 (31.8%)
Ex-smoker	156 (43.5%)	87 (39.0%)	46 (50.0%)	23 (52.3%)
Smoker	73 (20.3%)	48 (21.5%)	18 (19.6%)	7 (15.9%)
Antihypertensive medication	85 (23.7%)	35 (15.7%)	28 (30.4%)	22 (50.0%)

Values are arithmetic means ± standard deviations for continuous variables and number of subjects (percentage of respective group) for categorical outcomes
[a]Based on *N* = 43 subjects with type 2 diabetes
[b]Based on *N* = 42 subjects with type 2 diabetes

presented in Table 3. The strongest associations were found for the mid-cavity segments and the anterior segments.

Effects of weighting

Additional file 1: Table S1 shows the characteristics of the underlying eligible cohort that was used for the calculation of sampling weights.

Comparing the MRI sample to the whole cohort, there was an overrepresentation of subjects with prediabetes (26% in the sample vs 12% in the cohort) and subjects with diabetes (12% in the sample vs 10% in the cohort). Additionally, the proportion of males was higher in the MRI sample compared to the underlying cohort, whereas mean age was similar.

Results of the unweighted analysis are presented in Additional file 1: Table S2. Associations that were statistically significant in the weighted analysis were also significant in the unweighted analysis. The size of the estimates was comparable; however as sampling weights

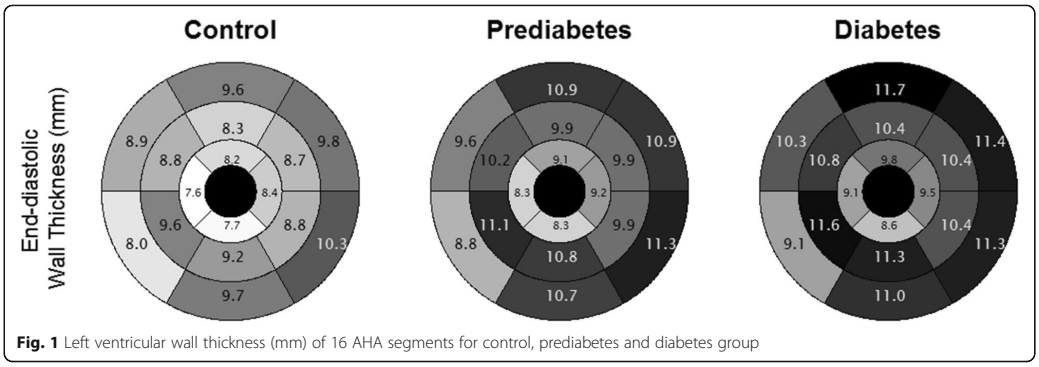

Fig. 1 Left ventricular wall thickness (mm) of 16 AHA segments for control, prediabetes and diabetes group

Table 2 Mean wall thickness grouped by level and region and myocardial mass

	All	Control	Prediabetes	*P*-value	Type 2 diabetes	*P*-value
	N = 359	*N* = 223	*N* = 92		*N* = 44	
Wall thickness (mm): arithmetic mean of						
All segments	9.1 ± 1.5	8.8 ± 1.4	9.9 ± 1.4	**< 0.001**	10.5 ± 1.6	**< 0.001**
Basal segments	9.6 ± 1.6	9.4 ± 1.6	10.4 ± 1.6	**< 0.001**	10.8 ± 1.7	**< 0.001**
Mid segments	9.2 ± 1.8	8.9 ± 1.6	10.3 ± 1.8	**< 0.001**	10.9 ± 2.1	**< 0.001**
Apical segments	8.2 ± 1.5	8.0 ± 1.4	8.7 ± 1.5	**< 0.001**	9.3 ± 1.6	**< 0.001**
Lateral segments	9.8 ± 1.6	9.3 ± 1.5	10.3 ± 1.4	**< 0.001**	10.8 ± 1.8	**< 0.001**
Septal segments	9.1 ± 1.6	8.7 ± 1.5	9.7 ± 1.4	**< 0.001**	10.3 ± 1.6	**< 0.001**
Anterior segments	9.4 ± 1.9	8.8 ± 1.7	10.0 ± 1.7	**< 0.001**	10.8 ± 2.2	**< 0.001**
Inferior segments	9.4 ± 1.5	9.0 ± 1.5	9.9 ± 1.4	**< 0.001**	10.4 ± 1.4	**< 0.001**
Myocardial mass (g/m^2)	70.0 ± 13.9	69.0 ± 13.6	72.3 ± 13.0	0.1	75.9 ± 16.0	**0.019**

P-values are obtained from one-way ANOVA and Bonferroni corrected for the repeated comparisons to the control group

introduce additional variation in the data, confidence intervals for the weighted analysis were wider than for the unweighted analysis. Model diagnostics such as residual distribution were similar between the weighted and unweighted analysis. Taken together, the evidence suggests that the analytical model was correctly specified [25] and although the weighted estimates are conceptually more precise, as they relate to the underlying cohort, the actual differences between weighted and unweighted estimates were small.

Association of specific prediabetes subgroups and wall thickness

We further differentiated prediabetes status into subjects with iIFG (*N* = 35, 9.7% of total sample and 38.1% of subjects with prediabetes), iIGT (*N* = 41, 11.4% of total sample and 44.6% of subjects with prediabetes) and both IFG + IGT (*N* = 16, 4.5% of total sample and 17.4% of subjects with prediabetes). Though there were differences in mean wall thickness according to segment classes between the prediabetes subgroups there was no gradual increase from iIFG to iIGT and IFG + IGT (See Additional file 1: Figure S2 and Table S3).

Association of hypertension and wall thickness independent of confounding factors

Prehypertension and hypertension were significantly associated with increased wall thickness (prehypertension: β: 0.48 mm, 95%-CI: [0.17 mm, 0.79 mm], hypertension: β: 0.67 mm, 95%-CI: [0.31 mm, 1.02 mm]) after adjustment for additional covariates. The strongest associations were seen for the basal segments and the septal segments as presented in Table 4. Notably, there was also a significant association of hypertension to myocardial mass.

Interaction of glycemic status and blood pressure

As displayed in Fig. 2 we found no interaction of glycemic status and systolic blood pressure for mean wall thickness averaged over all segments. Marginal effects of glycemic status, i.e. associations of prediabetes and

Table 3 Association of glycemic status and wall thickness

	Prediabetes			Diabetes		
	Estimate	95%-CI	*P*-value	Estimate	95%-CI	*P*-value
Wall thickness (mm): arithmetic mean of						
All segments	0.44	[0.12, 0.75]	**0.007**	0.70	[0.23, 1.17]	**0.004**
Basal segments	0.33	[−0.05, 0.70]	0.087	0.51	[0.02, 0.99]	**0.040**
Mid segments	0.61	[0.20, 1.02]	**0.004**	0.86	[0.28, 1.45]	**0.004**
Apical segments	0.34	[−0.04, 0.73]	0.080	0.74	[0.23, 1.24]	**0.005**
Lateral segments	0.46	[0.09, 0.83]	**0.014**	0.65	[0.14, 1.16]	**0.013**
Septal segments	0.35	[0.05, 0.65]	**0.023**	0.64	[0.18, 1.10]	**0.006**
Anterior segments	0.52	[0.10, 0.93]	**0.015**	0.98	[0.38, 1.59]	**0.002**
Inferior segments	0.45	[0.11, 0.79]	**0.009**	0.58	[0.11, 1.04]	**0.016**
Myocardial mass (g/m^2)	−0.11	[−3.51, 3.28]	0.948	0.56	[−4.94, 6.07]	0.841

Estimates from linear regression models adjusted for age, sex, BMI, systolic blood pressure, total cholesterol, use of antihypertensive medication and smoking status

Table 4 Association of hypertension and wall thickness

	Prehypertension			Hypertension		
	Estimate	95%-CI	*P*-value	Estimate	95%-CI	*P*-value
Wall thickness (mm): arithmetic mean of						
All segments	0.48	[0.17, 0.79]	**0.003**	0.67	[0.31, 1.02]	**< 0.001**
Basal segments	0.63	[0.28, 0.98]	**< 0.001**	0.83	[0.42, 1.24]	**< 0.001**
Mid segments	0.35	[−0.01, 0.71]	0.057	0.70	[0.26, 1.14]	**0.002**
Apical segments	0.44	[0.02, 0.86]	**0.043**	0.38	[−0.01, 0.77]	0.060
Lateral segments	0.37	[0.03, 0.71]	**0.036**	0.52	[0.12, 0.92]	**0.012**
Septal segments	0.59	[0.29, 0.89]	**< 0.001**	0.84	[0.48, 1.19]	**< 0.001**
Anterior segments	0.44	[0.02, 0.86]	**0.039**	0.77	[0.34, 1.19]	**< 0.001**
Inferior segments	0.51	[0.14, 0.88]	**0.007**	0.54	[0.16, 0.92]	**0.006**
Myocardial mass (g/m^2)	3.18	[−0.02, 6.39]	0.053	6.16	[2.19, 10.12]	**0.003**

Estimates from linear regression models adjusted for age, sex, BMI, glycemic status, total cholesterol, use of antihypertensive medication and smoking status

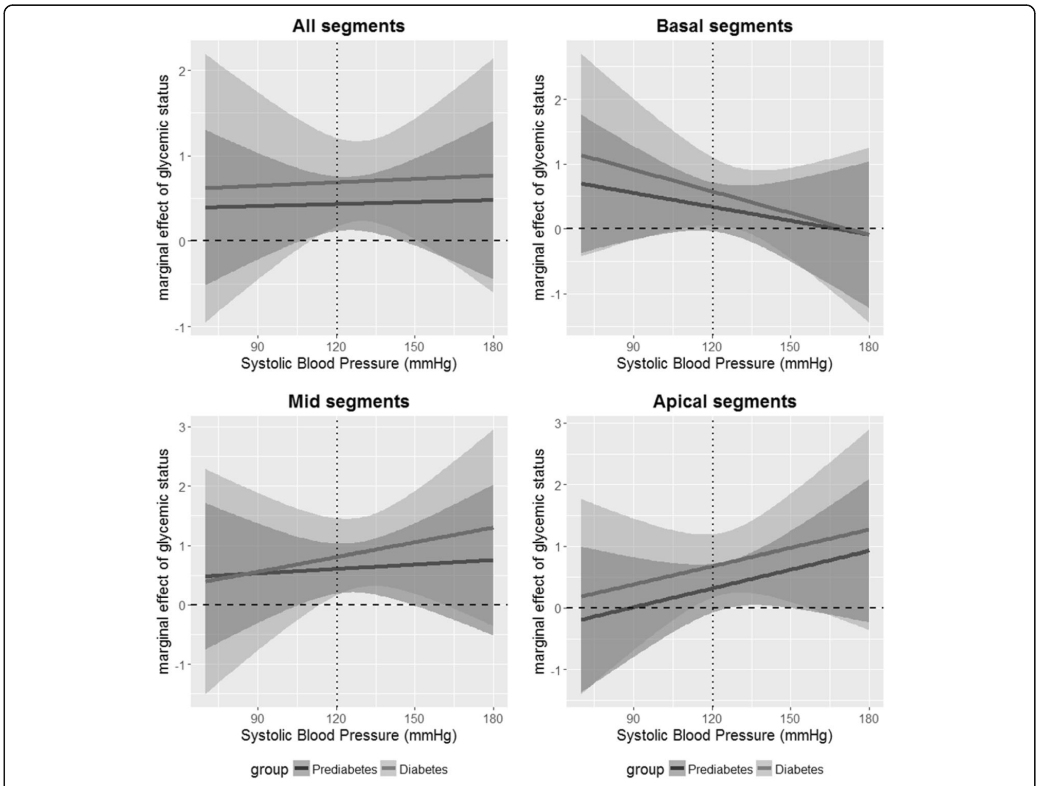

Fig. 2 Marginal effects of glycemic status on wall thickness for multiplicative interactions with systolic blood pressure. Marginal effects indicate the size of the association of the respective group (prediabetes or diabetes) with wall thickness for a specific value of systolic blood pressure. Displayed are the marginal effects of prediabetes (solid line, dark grey) and diabetes (solid line, light grey) and the respective 95% confidence interval for a grid of possible values of systolic blood pressure (range in data: 73–179.5 mmHg). The arithmetic mean is indicated by a dotted line. The dashed line indicates the line of no effect

diabetes with wall thickness for a specific value of systolic blood pressure, remained constant over the range of possible blood pressure values. However, for basal segments, there was a decreasing marginal effect of glycemic status with rising blood pressure, whereas for mid-cavity and apical segments the marginal effect of glycemic status was increasing with rising blood pressure.

Discussion

Increased LV wall thickness is associated with a higher risk for cardiovascular outcomes. Recent findings from the Framingham study showed that a 0.1 unit increase in relative wall thickness was accompanied by a 59% increase in the hazard for cardiovascular disease [1]. A detailed assessment of LV geometry based on regional wall thickness can predict risk of incident cardiovascular disease [26]. Given these implications, it is of major importance to determine modifiable risk factors for increased wall thickness.

Our findings from this cross-sectional study show that (i) type 2 diabetes is associated to increased LV wall thickness, independent of traditional cardiovascular risk factors and especially independent of hypertension, (ii) the independent association of abnormal glucose homeostasis to cardiac structure is already present in prediabetes, (iii) individual LV segments are differently affected by hypertension and glycemic status. Thereby, we could demonstrate that the more specific evaluation of CMR derived regional LV wall thickness unveils associations that cannot be detected when assessing LV mass alone.

Our results therefore support and extend findings from other established population-based studies. In the Atherosclerosis Risk in the Community (ARIC) study, Skali et al. found that mean and relative LV wall thickness were elevated in subjects with diabetes independent of systolic blood pressure. To a certain extent, wall thickness was already increased in subjects with prediabetes [27]. In the Framingham Offspring Cohort, Velageti et al. [28] found an increasing CMR derived relative wall thickness across glycemia categories. After multivariable adjustment, the association remained significant in men. In the Multiethnic Study of Atherosclerosis (MESA), an association between CMR-derived LV mass and diabetes was found that was independent of blood pressure; however no measurements of segmental wall thickness were taken [29]. On the other hand, Bertoni et al. measured mid-cavity segments and found an increasing wall thickness for Caucasian subjects with normal glucose metabolism to subjects with iIFG and type 2 diabetes. The differences were not significant after adjustment for other cardiovascular risk factors [30]. Another study found an association of glycemic status to LV mass, but not to (relative or mean) wall thickness [31]. In our sample, we showed that the increased LV mass in subjects with diabetes was attributable to hypertension but there are independent regional associations of diabetes and blood pressure in segmental wall thickness.

Regarding the prediabetic state, recent evidence from the CARDIA study implies that longer exposure to abnormal glucose tolerance, longer duration of diabetes, and early onset of diabetes leads to more unfavorable remodeling [32]. Analyses from the Strong Heart Study demonstrated increased LV mass in Native Americans with impaired glucose tolerance, however the finding was less definitive for measures of wall thickness [33]. Our findings corroborate that prediabetes, defined as either iIGT, iIFG or IFG + IGT, is independently associated to increased wall thickness. Our sample size was probably too small to detect gradual effects of these different prediabetic groups.

Disentangling the associations of blood pressure and glycemic status proves to be complicated. In the Strong Heart Study, LV mass of subjects with diabetes but without hypertension was significantly lower compared to those subjects with both conditions, whereas relative wall thickness was not different [34]. In the HyperGEN study comprising only hypertensive subjects, diabetes was independently associated to increased LV mass [35]. A recent Chinese study suggested additive effects of diabetes and hypertension to LV remodeling [36]. Although blood pressure reduction appears to be an effective way of lowering the risk of cardiovascular disease in hypertensive patients with increased LV mass, [37] these treatments do not seem to be as effective in patients with diabetes [38]. In our study, we found a decreasing marginal effect of both prediabetes and diabetes with rising blood pressure for the basal segments, whereas the marginal effect for apical and mid segments was increasing. Thus we could further characterize the complex interplay of blood pressure and glycemic status and its impact on cardiac geometry.

The exact mechanisms of impaired glucose metabolism on LV geometry remain to be identified. Increased LV stiffness, induced by an accumulation of collagen and advanced glycation end products and subsequent fibrosis in diabetic cardiomyopathy have been suggested to contribute to LV remodeling [39, 40]. Also, a decreased myocardial perfusion reserve in subjects with diabetes induced by an impaired myocardial blood flow has been shown to be correlated with LV torsion and strain [41]. Recent findings imply that myocardial steatosis, excess storage of cardiac triglycerides, and impaired myocardial energetics are associated with concentric LV remodeling [42]. However, our study is limited in this respect as it cannot explain the pathophysiological mechanisms behind the association of glycemic status on regional LV geometry.

The values of LV wall thickness reported here, as measured by short-axis cine SSFP, substantially exceed the reference values according to the 16-segment model suggested by other groups [43, 44]. These reference values have been obtained from healthy subjects with a low-risk profile for developing cardiovascular disease, excluding smokers, and people with hypertension or diabetes. Given the major impact of these risk factors on wall thickness, it is plausible that our study found larger values for the control group.

For this nested cross-sectional study, we used a well-characterized population-based cohort. Highly standardized measurements and validation allowed us to precisely define covariates and glycemic status. Furthermore, using adequate sampling weights we were able to relate our results to the full underlying cohort.

Limitations of our study include its cross-sectional design that precludes causal inference. Further longitudinal follow-up of this study sample is mandated to determine the prognostic potential of segmental wall thickness.

Conclusion

Our findings highlight the role of glycemic status as a potential risk factor and implicate prediabetes as unfavorably associated to LV wall thickness. Measurements of regional wall thickness provides a more precise picture than assessing overall myocardial mass. Delaying or halting progression from impaired fasting glucose to diabetes might prevent further thickening of the ventricular walls and subsequent cardiovascular complications.

Additional file

Additional file 1: Text S1. Description of laboratory measurements. **Figure S1.** Intra-and interobserver agreement. **Text S2.** Description of the underlying eligible cohort. **Table S1.** Characteristics of study subjects from the full eligible cohort used for the calculation of sampling weights. **Table S2.** Associations of glycemic status with wall thickness from weighted and unweighted linear regression models. **Figure S2.** Mean wall thickness according to prediabetic glycemic status. **Table S3.** Association of prediabetic glycemic status and mean wall thickness. (DOCX 57 kb)

Abbreviations

(i)IFG: (isolated) impaired fasting glucose; (i)IGT: (isolated) impaired glucose tolerance; AHA: American Heart Association; BMI: Body Mass Index; CI: Confidence interval; CMR: Cardiac magnetic resonance; KORA: Cooperative Health Research in the Region of Augsburg; LV: Left ventricular; MRI: Magnetic resonance imaging; OGTT: Oral glucose tolerance test; SSFP: Steady-state free precession; WHO: World Health Organization

Acknowledgements

The authors wish to thank Mainsi Marowsky-Köppl and Andrea Wulff for expert data handling.

Funding

The KORA study was initiated and financed by the Helmholtz Zentrum München – German Research Center for Environmental Health, which is funded by the German Federal Ministry of Education and Research (BMBF) and by the State of Bavaria. Furthermore, KORA research was supported within the Munich Center of Health Sciences (MC-Health), Ludwig-Maximilians-Universität, as part of LMUinnovativ.

Availability of data and materials

The informed consent given by KORA study participants does not cover data posting in public databases. However, data are available upon request from KORA-gen (http://epi.helmholtz-muenchen.de/kora-gen/) by means of a project agreement. Requests should be sent to kora.passt@helmholtz-muenchen.de and are subject to approval by the KORA Board.

Authors' contributions

SR performed the statistical analyses, evaluated the results and drafted the paper. AS, HH and FB collected the CMR data and analyzed the images. CH, WR, WK, MH, CM, RL, BL, SA and HH contributed substantially to data preparation and quality assurance. FB, AP, HH and SA participated in the conception and design of the study. WK, WR, CH, RL, BL, MH, CM, HH and AP revised the paper for important intellectual content. All authors have read and approved the final manuscript.

Ethics approval and consent to participate

The KORA FF4 study was approved by the ethics committee of the Bavarian Chamber of Physicians, Munich; the MRI substudy by the institutional review board of the Ludwig-Maximilians-University Munich. The investigations were carried out in accordance with the Declaration of Helsinki, including written informed consent of all participants.

Consent for publication

Not applicable.

Competing interests

The authors declare that they have no competing interests.

Publisher's Note

Author details

[1]Institute of Epidemiology, Helmholtz Zentrum München, German Research Center for Environmental Health, Ingolstaedter Landstrasse 1, 85764 Neuherberg, Germany. [2]Department of Radiology, Ludwig-Maximilians-University Hospital, Munich, Germany. [3]Department of Internal Medicine II – Cardiology, University of Ulm Medical Center, Ulm, Germany. [4]Deutsches Herzzentrum München, Technische Universität München, Munich, Germany. [5]German Centre for Cardiovascular Research (DZHK e.V.), Munich, Germany. [6]German Center for Diabetes Research (DZD), München-Neuherberg, Germany. [7]Institute for Biometrics and Epidemiology, German Diabetes Center, Duesseldorf, Germany. [8]KORA Myocardial Infarction Registry, Central Hospital of Augsburg, Augsburg, Germany. [9]Department of Diagnostic and Interventional Radiology, University of Tuebingen, Tuebingen, Germany.

Received: 29 January 2018 Accepted: 31 July 2018
Published online: 09 August 2018

References

1. Tsao CW, Gona PN, Salton CJ, Chuang ML, Levy D, Manning WJ, O'Donnell CJ. Left ventricular structure and risk of cardiovascular events: a Framingham heart study cardiac magnetic resonance study. J Am Heart Assoc. 2015;4(9):e002188.
2. Bluemke DA, Kronmal RA, Lima JAC, Liu K, Olson J, Burke GL, Folsom AR. The relationship of left ventricular mass and geometry to incident cardiovascular events. J Am Coll Cardiol. 2008;52(25):2148–55.
3. Burchfield JS, Xie M, Hill JA. Pathological ventricular remodeling: mechanisms: part 1 of 2. Circulation. 2013;128(4):388–400.
4. Edvardsen T, Rosen BD, Pan L, Jerosch-Herold M, Lai S, Hundley WG, Sinha S, Kronmal RA, Bluemke DA, Lima JA. Regional diastolic dysfunction in

individuals with left ventricular hypertrophy measured by tagged magnetic resonance imaging--the multi-ethnic study of atherosclerosis (MESA). Am Heart J. 2006;151(1):109–14.
5. Kuznetsova T, Thijs L, Knez J, Herbots L, Zhang Z, Staessen JA. Prognostic Value of Left Ventricular Diastolic Dysfunction in a General Population. J Am Heart Assoc. 2014;3(3):e000789.
6. Devereux RB, Roman MJ. Left ventricular hypertrophy in hypertension: stimuli, patterns, and consequences. Hypertens Res. 1999;22(1):1–9.
7. De Simone G, Palmieri V, Bella JN, Celentano A, Hong Y, Oberman A, Kitzman DW, Hopkins PN, Arnett DK, Devereux RB. Association of left ventricular hypertrophy with metabolic risk factors: the HyperGEN study. J Hypertens. 2002;20(2):323–31.
8. Al-Daydamony MM, El-Tahlawi M. What is the effect of metabolic syndrome without hypertension on left ventricular hypertrophy? Echocardiography. 2016;33(9):1284–9.
9. Cuspidi C, Sala C, Negri F, Mancia G, Morganti A. Prevalence of left-ventricular hypertrophy in hypertension: an updated review of echocardiographic studies. J Hum Hypertens. 2012;26(6):343–9.
10. Rutter MK, Parise H, Benjamin EJ, Levy D, Larson MG, Meigs JB, Nesto RW, Wilson PWF, Vasan RS. Impact of glucose intolerance and insulin resistance on cardiac structure and function: sex-related differences in the Framingham heart study. Circulation. 2003;107(3):448–54.
11. Palmieri V, Okin PM, de Simone G, Bella JN, Wachtell K, Gerdts E, Boman K, Nieminen MS, Dahlöf B, Devereux RB. Electrocardiographic characteristics and metabolic risk factors associated with inappropriately high left ventricular mass in patients with electrocardiographic left ventricular hypertrophy: the LIFE study. J Hypertens. 2007;25(5):1079–85.
12. Gerdts E, Okin PM, Omvik P, Wachtell K, Dahlöf B, Hildebrandt P, Nieminen MS, Devereux RB. Impact of diabetes on treatment-induced changes in left ventricular structure and function in hypertensive patients with left ventricular hypertrophy. The LIFE study. Nutr Metab Cardiovasc Dis. 2009;19(5):306–12.
13. Pareek M, Aharaz A, Nielsen ML, Gerke O, Leósdóttir M, Møller JE, Andersen NH, Nilsson PM, Olsen MH. Untreated diabetes mellitus, but not impaired fasting glucose, is associated with increased left ventricular mass and concentric hypertrophy in an elderly, healthy, Swedish population. IJC Metabolic Endocrine. 2015;9:39–47.
14. Lorber R, Gidding SS, Daviglus ML, Colangelo LA, Liu K, Gardin JM. Influence of systolic blood pressure and body mass index on left ventricular structure in healthy African-American and white young adults: the CARDIA study. J Am Coll Cardiol. 2003;41(6):955–60.
15. Demmer RT, Allison MA, Cai J, Kaplan RC, Desai AA, Hurwitz BE, Newman JC, Shah SJ, Swett K, Talavera GA, et al. Association of Impaired Glucose Regulation and Insulin Resistance With Cardiac Structure and Function: Results From ECHO-SOL (Echocardiographic Study of Latinos). Circ Cardiovasc Imaging. 2016;**9**(10).
16. Cioffi G, Rossi A, Zoppini G, Targher G, de Simone G, Devereux RB, Vassanelli C, Bonora E. Inappropriate left ventricular mass independently predicts cardiovascular mortality in patients with type 2 diabetes. Int J Cardiol. 2013;168(5):4953–6.
17. Hoang K, Zhao Y, Gardin JM, Carnethon M, Mukamal K, Yanez D, Wong ND. LV mass as a predictor of CVD events in older adults with and without metabolic syndrome and diabetes. JACC Cardiovasc Imaging. 2015;8(9): 1007–15.
18. Eguchi K, Ishikawa J, Hoshide S, Ishikawa S, Pickering TG, Schwartz JE, Homma S, Shimada K, Kario K. Differential impact of left ventricular mass and relative wall thickness on cardiovascular prognosis in diabetic and nondiabetic hypertensive subjects. Am Heart J. 2007;154(1):79 e79–15.
19. Armstrong AC, Gidding S, Gjesdal O, Wu C, Bluemke DA, Lima JA. LVM assessed by echocardiography and cardiac magnetic resonance, cardiovascular outcomes, and medical practice. JACC Cardiovascular Imaging. 2012;5(8):837.
20. Bottini PB, Carr AA, Prisant LM, Flickinger FW, Allison JD, Gottdiener JS. Magnetic resonance imaging compared to echocardiography to assess left ventricular mass in the hypertensive patient. Am J Hypertens. 1995;8(3):221–8.
21. Bamberg F, Hetterich H, Rospleszcz S, Lorbeer R, Auweter SD, Schlett CL, Schafnitzel A, Bayerl C, Schindler A, Saam T, et al. Subclinical Disease Burden as Assessed by Whole-Body MRI in Subjects With Prediabetes, Subjects With Diabetes, and Normal Control Subjects From the General Population: The KORA-MRI Study. Diabetes 2017;66(1):158–69
22. Holle R, Happich M, Löwel H, Wichmann H. KORA--a research platform for population based health research. Gesundheitswesen. 2005;67:S19–25.
23. World Health Organization (WHO). Definition, diagnosis and classification of diabetes mellitus and its complications. In: Report of a WHO Consultation, Department of Noncommunicable Disease Surveillance. Geneva: World Health Organization; 1999.
24. Cerqueira MD, Weissman NJ, Dilsizian V, Jacobs AK, Kaul S, Laskey WK, Pennell DJ, Rumberger JA, Ryan T, Verani MS. Standardized myocardial segmentation and nomenclature for tomographic imaging of the heart a statement for healthcare professionals from the cardiac imaging committee of the council on clinical cardiology of the American Heart Association. Circulation. 2002;105(4):539–42.
25. Solon G, Haider SJ, Wooldridge JM. What are we weighting for? J Hum Resour. 2015;50(2):301–16.
26. Lieb W, Gona P, Larson MG, Aragam J, Zile MR, Cheng S, Benjamin EJ, Vasan RS. The natural history of left ventricular geometry in the community: clinical correlates and prognostic significance of change in LV geometric pattern. JACC Cardiovasc Imaging. 2014;7(9):870–8.
27. Skali H, Shah A, Gupta DK, Cheng S, Claggett B, Liu J, Bello N, Aguilar D, Vardeny O, Matsushita K. Cardiac structure and function across the glycemic Spectrum in elderly men and women free of prevalent heart disease the atherosclerosis risk in the community study. Circ Heart Fail. 2015;8(3):448–54.
28. Velagaleti RS, Gona P, Chuang ML, Salton CJ, Fox CS, Blease SJ, Yeon SB, Manning WJ, O'Donnell CJ. Relations of insulin resistance and glycemic abnormalities to cardiovascular magnetic resonance measures of cardiac structure and function: the Framingham heart study. Circ Cardiovasc Imaging. 2010;3(3):257–63.
29. Heckbert SR, Post W, Pearson GD, Arnett DK, Gomes AS, Jerosch-Herold M, Hundley WG, Lima JA, Bluemke DA. Traditional cardiovascular risk factors in relation to left ventricular mass, volume, and systolic function by cardiac magnetic resonance imaging: the multiethnic study of atherosclerosis. J Am Coll Cardiol. 2006;48(11):2285–92.
30. Bertoni AG, Goff DC, D'Agostino RB, Liu K, Hundley WG, Lima JA, Polak JF, Saad MF, Szklo M, Tracy RP. Diabetic cardiomyopathy and subclinical cardiovascular disease the multi-ethnic study of atherosclerosis (MESA). Diabetes Care. 2006;29(3):588–94.
31. Henry RMA, Kamp O, Kostense PJ, Spijkerman AMW, Dekker JM, van Eijck R, Nijpels G, Heine RJ, Bouter LM, Stehouwer CDA. Left ventricular mass increases with deteriorating glucose tolerance, especially in women: independence of increased arterial stiffness or decreased flow-mediated dilation: the Hoorn study. Diabetes Care. 2004;27(2):522–9.
32. Kishi S, Gidding SS, Reis JP, Colangelo LA, Venkatesh BA, Armstrong AC, Isogawa A, Lewis CE, Wu C, Jacobs DR Jr, et al. Association of Insulin Resistance and Glycemic Metabolic Abnormalities with LV structure and function in middle age: the CARDIA study. JACC Cardiovasc Imaging. 2017;10(2):105–14.
33. Capaldo B, Di Bonito P, Iaccarino M, Roman MJ, Lee ET, Devereux RB, Riccardi G, Howard BV, de Simone G. Cardiovascular characteristics in subjects with increasing levels of abnormal glucose regulation: the strong heart study. Diabetes Care. 2013;36(4):992–7.
34. Bella JN, Devereux RB, Roman MJ, Palmieri V, Liu JE, Paranicas M, Welty TK, Lee ET, Fabsitz RR, Howard BV. Separate and joint effects of systemic hypertension and diabetes mellitus on left ventricular structure and function in American Indians (the strong heart study). Am J Cardiol. 2001;87(11):1260–5.
35. Palmieri V, Bella JN, Arnett DK, Liu JE, Oberman A, Schuck M-Y, Kitzman DW, Hopkins PN, Morgan D, Rao D. Effect of type 2 diabetes mellitus on left ventricular geometry and systolic function in hypertensive subjects. Circulation. 2001;103(1):102–7.
36. Li T, Chen S, Guo X, Yang J, Sun Y. Impact of hypertension with or without diabetes on left ventricular remodeling in rural Chinese population: a cross-sectional study. BMC Cardiovasc Disord. 2017;17(1):206.
37. Pierdomenico SD, Cuccurullo F. Risk reduction after regression of echocardiographic left ventricular hypertrophy in hypertension: a meta-analysis. Am J Hypertens. 2010;23(8):876–81.
38. Lonnebakken MT, Izzo R, Mancusi C, Gerdts E, Losi MA, Canciello G, Giugliano G, De Luca N, Trimarco B, de Simone G. Left Ventricular Hypertrophy Regression During Antihypertensive Treatment in an Outpatient Clinic (the Campania Salute Network). J Am Heart Assoc. 2017; 6(3):e004152.

39. Asbun J, Villarreal FJ. The pathogenesis of myocardial fibrosis in the setting of diabetic cardiomyopathy. J Am Coll Cardiol. 2006;47(4):693–700.
40. Van Heerebeek L, Hamdani N, Handoko ML, Falcao-Pires I, Musters RJ, Kupreishvili K, Ijsselmuiden AJ, Schalkwijk CG, Bronzwaer JG, Diamant M. Diastolic stiffness of the failing diabetic heart. Circulation. 2008;117(1):43–51.
41. Larghat AM, Swoboda PP, Biglands JD, Kearney MT, Greenwood JP, Plein S. The microvascular effects of insulin resistance and diabetes on cardiac structure, function, and perfusion: a cardiovascular magnetic resonance study. European Heart Journal-Cardiovascular Imaging. 2014;15(12):1368–76.
42. Levelt E, Mahmod M, Piechnik SK, Ariga R, Francis JM, Rodgers CT, Clarke WT, Sabharwal N, Schneider JE, Karamitsos TD, et al. Relationship between left ventricular structural and metabolic remodeling in type 2 diabetes. Diabetes. 2016;65(1):44–52.
43. Kawel N, Turkbey EB, Carr JJ, Eng J, Gomes AS, Hundley WG, Johnson C, Masri SC, Prince MR, van der Geest RJ, et al. Normal left ventricular myocardial thickness for middle-aged and older subjects with steady-state free precession cardiac magnetic resonance: the multi-ethnic study of atherosclerosis. Circulation: Cardiovascular Imaging. 2012;5(4):500–8.
44. Le Ven F, Bibeau K, De Larochelliere E, Tizon-Marcos H, Deneault-Bissonnette S, Pibarot P, Deschepper CF, Larose E. Cardiac morphology and function reference values derived from a large subset of healthy young Caucasian adults by magnetic resonance imaging. Eur Heart J Cardiovasc Imaging. 2015;17(9):981–90.

Additional file

Text S1: Description of laboratory measurements

Glucose, total cholesterol, HDL cholesterol, LDL cholesterol as well as triglyceride levels were measured in fresh serum by enzymatic, colorimetric methods using GLU, CHOL, LDLC, HDLC, and TRIG Flex assays, respectively, on a Dimension Vista 1500 instrument (Siemens Healthcare Diagnostics Inc., Newark, USA) or using GLUC3, CHOL2, LDL_C, HDLC3, and TRIGL assays, respectively, on a Cobas c702 instrument (Roche Diagnostics GmbH, Mannheim, Germany). Insulin was measured in fresh serum by an solid-phase enzyme-labeled chemiluminescent immunometric assay on an Immulite 2000 systems analyzer (Siemens) or by an electrochemiluminescence immunoassay on a Cobas e602 instrument (Roche). The measurement instrument and assays changed from Siemens to Roche halfway during the study. Calibration formulas were developed using 122 (194 for insulin) KORA FF4 samples which were measured with both methods during the time of the change. The Siemens measurement results were calibrated to the Roche measurements using the following formulas [insulin in µU/mL; all other units in mg/dL]: Total_Cholesterol_Roche = 3.00 + Total_Cholesterol_Siemens * 1.00; HDL_Cholesterol_Roche = 2.40 + HDL_Cholesterol_Siemens * 1.12; LDL_Cholesterol_Roche = antilog (-0.13328 + log LDL_Cholesterol_Siemens * 1.03051); Triglycerides_Roche = 4.97073 + Triglycerides_Siemens * 0.90732; Insulin_Roche = 1.307 + Insulin_Siemens * 1.016. No calibration was needed for glucose because the double measurements were very similar so that the intercept and the slope of the Passing-Bablok regression used for calibration were estimated to be zero and one, respectively. HbA1c was measured in hemolyzed whole blood using the cation-exchange high performance liquid chromatographic, photometric VARIANT II TURBO HbA1c Kit - 2.0 assay on a VARIANT II TURBO Hemoglobin Testing System (Bio-Rad Laboratories Inc., Hercules, USA).

Figure S1: Intra-and interobserver agreement

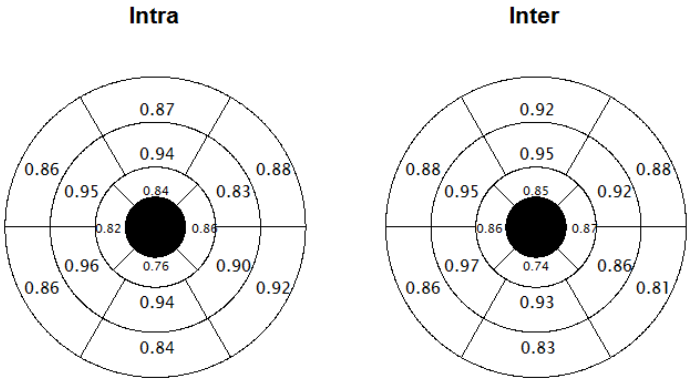

Intraclass Correlation Coefficients for intra- and interobserver agreement for end-diastolic wall thickness. Intraobserver agreement was based on 25 subjects and interobserver agreement based on 52 subjects.

Text S2: Description of the underlying eligible cohort

The original KORA FF4 cohort comprises N = 2279 participants, whereas the MRI study sample comprises N = 400 participants. Due to the sampling design of the MRI study, not all subjects from the cohort can be represented by a subject from the MRI sample. The underlying eligible cohort comprises n = 1652 subjects: not eligible were subjects older than 72 years (n = 428), subjects with indeterminable glycemic status (n = 69), a history of myocardial infarction or stroke (n = 63), subjects with implanted medical devices (n = 11) and subjects with impaired renal function (n = 56). We treated the remaining n = 1652 subjects as the underlying cohort for the calculation of sampling weights. The difference to the n = 1282 subjects as presented in (1) arises because we considered the exclusion criteria claustrophobia, pregnancy, inability to hold breath, tattoos and allergy to contrast agents as unrelated to a subject's glycemic status and cardiac morphology. Therefore, all subjects for whom these exclusion criteria would apply can nevertheless be represented in their glycemic status and cardiac morphology by subjects who participated in the MRI study. Base weights were calculated by inverse-probability cell weighting in 12 cells defined by glycemic status and age category (38-47 years, 48 – 57 years, 58 – 67 years, 68- 72 years) (2) and were then further modified by post-stratification according to sex (3). Weighted variances and standard errors were computed by Taylor series linearization.

Table S1: Characteristics of study subjects from the full eligible cohort used for the calculation of sampling weights.

	all N = 1652	Control N = 1240	Prediabetes N = 250	Type 2 Diabetes N = 162
Age (years)	56.1 ± 9.4	54.3 ± 9.0	60.5 ± 8.9	62.7 ± 8.4
Male gender n (%)	763 (46.2%)	538 (43.4%)	136 (54.4%)	89 (54.9%)
BMI (kg/m^2)	27.6 ± 5.1	26.5 ± 4.5	30.2 ± 5.2	31.5 ± 5.6
Systolic BP (mmHg)	118.0 ± 16.9	115.5 ± 15.8	123.9 ± 16.4	127.6 ± 19.7
Hypertension n (%)	497 (30.1%)	272 (21.9%)	116 (46.4%)	109 (67.3%)
Total Cholesterol (mg/dL)	219.2 ± 37.6	219.2 ± 37.0	224.4 ± 37.5	211.0 ± 40.4
Smoking n (%)				
never-smoker	726 (43.9%)	555 (44.8%)	98 (39.2%)	73 (45.1%)
ex-smoker	625 (37.8%)	449 (36.2%)	107 (42.8%)	69 (42.6%)
smoker	301 (18.2%)	236 (19.0%)	45 (18%)	20 (12.3%)

Table S2: Associations of glycemic status with wall thickness from weighted and unweighted linear regression models.

		Prediabetes			Diabetes		
		estimate	95%-CI	p-value	estimate	95%-CI	p-value
Diastole							
Wall thickness (mm): arithmetic mean of							
all segments	unweighted	0.36	[0.07, 0.65]	**0.014**	0.69	[0.31, 1.08]	**<0.001**
	weighted	0.44	[0.12, 0.75]	**0.007**	0.70	[0.23, 1.17]	**0.004**
basal segments	unweighted	0.32	[-0.02, 0.66]	0.065	0.53	[0.08, 0.98]	**0.022**
	weighted	0.33	[-0.05, 0.70]	0.087	0.51	[0.02, 0.99]	**0.040**
mid segments	unweighted	0.49	[0.13, 0.85]	**0.007**	0.86	[0.39, 1.34]	**<0.001**
	weighted	0.61	[0.20, 1.02]	**0.004**	0.86	[0.28, 1.45]	**0.004**
apical segments	unweighted	0.24	[-0.11, 0.60]	0.178	0.69	[0.22, 1.17]	**0.004**
	weighted	0.34	[-0.04, 0.73]	0.080	0.74	[0.23, 1.24]	**0.005**
lateral segments	unweighted	0.38	[0.05, 0.71]	**0.024**	0.64	[0.20, 1.08]	**0.005**
	weighted	0.46	[0.09, 0.83]	**0.014**	0.65	[0.14, 1.16]	**0.013**
septal segments	unweighted	0.31	[0.02, 0.61]	**0.035**	0.66	[0.27, 1.05]	**0.001**
	weighted	0.35	[0.05, 0.65]	**0.023**	0.64	[0.18, 1.10]	**0.006**
anterior segments	unweighted	0.44	[0.05, 0.83]	**0.027**	1.00	[0.48, 1.52]	**<0.001**
	weighted	0.52	[0.10, 0.93]	**0.015**	0.98	[0.38, 1.59]	**0.002**
inferior segments	unweighted	0.35	[0.04, 0.66]	**0.028**	0.54	[0.13, 0.96]	**0.011**
	weighted	0.45	[0.11, 0.79]	**0.009**	0.58	[0.11, 1.04]	**0.016**
myocardial mass (g/m^2)	unweighted	-1.37	[-4.52, 1.77]	0.392	0.00	[-4.20, 4.20]	1
	weighted	-0.11	[-3.51, 3.28]	0.948	0.56	[-4.94, 6.07]	0.841

Figure S2: Mean wall thickness according to prediabetic glycemic status.

iIFG: isolated impaired fasting glucose. iIGT: isolated impaired glucose tolerance. IFG+IGT: both impaired fasting glucose and impaired glucose tolerance.

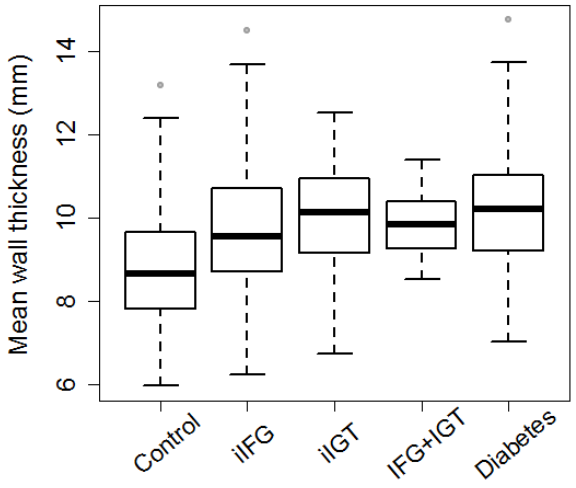

Table S3: Association of prediabetic glycemic status on mean wall thickness.

	isolated IFG (N = 35)			**isolated IGT (N = 41)**			**IFG + IGT (N = 16)**		
	estimate	95%-CI	p-value	estimate	95%-CI	p-value	estimate	95%-CI	p-value
Wall thickness (mm): arithmetic mean of									
all segments	0.50	[-0.03, 1.04]	0.067	0.39	[0.02, 0.76]	0.038	0.41	[0.01, 0.81]	0.047
basal segments	0.28	[-0.23, 0.80]	0.278	0.17	[-0.31, 0.64]	0.490	0.77	[0.04, 1.50]	0.118
mid segments	0.75	[0.09, 1.41]	0.082	0.61	[0.05, 1.17]	0.098	0.33	[-0.20, 0.86]	0.326
apical segments	0.46	[-0.24, 1.15]	0.278	0.41	[-0.03, 0.84]	0.099	-0.03	[-0.51, 0.46]	0.911
lateral segments	0.45	[-0.23, 1.12]	0.193	0.48	[0.04, 0.91]	0.133	0.46	[-0.04, 0.97]	0.149
septal segments	0.44	[-0.01, 0.90]	0.092	0.29	[-0.10, 0.68]	0.141	0.31	[-0.17, 0.79]	0.207
anterior segments	0.68	[-0.05, 1.41]	0.092	0.46	[-0.03, 0.94]	0.133	0.33	[-0.17, 0.83]	0.207
inferior segments	0.51	[0.02, 0.99]	0.092	0.36	[-0.08, 0.80]	0.141	0.56	[0.10, 1.03]	0.074
myocardial mass (g/m^2)	0.88	[-4.81, 6.57]	0.762	-0.89	[-4.92, 3.14]	0.665	-0.27	[-5.69, 5.15]	0.923

Estimates from linear regression models adjusted for age, sex, BMI, systolic BP, total cholesterol, use of antihypertensive medication and smoking status.CI: Confidence Interval. Results of the diabetes group are not displayed as the interpretation remains unchanged compared to Table 3 in the main manuscript

1. Bamberg F, Hetterich H, Rospleszcz S, Lorbeer R, Auweter SD, Schlett CL, et al. Subclinical Disease in Subjects with Prediabetes, Diabetes and Normal Controls from the General Population: the KORA MRI-Study. Diabetes. 2016.
2. Kalton G, Flores-Cervantes I. Weighting methods. Journal of Official Statistics. 2003;19(2):81.
3. Little RJ. Post-stratification: a modeler's perspective. Journal of the American Statistical Association. 1993;88(423):1001-12.

Manuscript IV

Title: Phenotypic Multiorgan Involvement of Subclinical Disease as Quantified by Magnetic Resonance Imaging in Subjects with Prediabetes, Diabetes, and Normal Glucose Tolerance

Authors: Corinna Storz,
Susanne Rospleszcz,
Roberto Lorbeer,
Holger Hetterich,
Sigrid Auweter,
Wieland Sommer,
Jürgen Machann,
Sergios Gatidis,
Wolfgang Rathmann,
Margit Heier,
Birgit Linkohr,
Christa Meisinger,
Maximilian Reiser,
Udo Hoffmann,
Annette Peters,
Christopher L. Schlett,
Fabian Bamberg

Journal: Investigative Radiology
Status: Published
doi: 10.1097/rli.0000000000000451

ORIGINAL ARTICLE

Phenotypic Multiorgan Involvement of Subclinical Disease as Quantified by Magnetic Resonance Imaging in Subjects With Prediabetes, Diabetes, and Normal Glucose Tolerance

Corinna Storz, MD, Susanne Rospleszcz, MSc,† Roberto Lorbeer, PhD,‡§ Holger Hetterich, MD,‡§ Sigrid D. Auweter, PhD,‡ Wieland Sommer, MD,‡ Jürgen Machann, PhD,*||¶# Sergios Gatidis, MD,* Wolfgang Rathmann, MD,** Margit Heier, MD,† Birgit Linkohr, PhD,† Christa Meisinger, MD, MPH,††† Maximilian Reiser, MD,‡ Udo Hoffmann, MD, MPH,‡‡ Annette Peters, PhD,†§§§ Christopher L. Schlett, MD, MPH,|||| and Fabian Bamberg, MD, MPH*‡§*

Introduction: Detailed mechanisms in the pathophysiology of diabetes disease are poorly understood, but structural alterations in various organ systems incur an elevated risk for cardiovascular events and adverse outcome. The aim of this study was to compare multiorgan subclinical disease phenotypes by magnetic resonance (MR) imaging to study differences between subjects with prediabetes, diabetes, and normal controls.

Materials and Methods: Subjects without prior cardiovascular disease were enrolled in a prospective case-control study and underwent multiorgan MR for the assessment of metabolic and arteriosclerotic alterations, including age-related white matter changes, hepatic proton density fat fraction, visceral adipose tissue volume, left ventricular remodeling index, carotid plaque, and late gadolinium enhancement. Magnetic resonance features were summarized in a phenotypic-based score (range, 0–6). Univariate, multivariate correlation, and unsupervised clustering were performed.

Results: Among 243 subjects with complete multiorgan MR data sets included in the analysis (55.6 ± 8.9 years, 62% males), 48 were classified as subjects with prediabetes and 38 as subjects with diabetes. The MR phenotypic score was significantly higher in subjects with prediabetes and diabetes as compared with controls (mean score, 3.00 ± 1.04 and 2.69 ± 0.98 vs 1.22 ± 0.98, $P < 0.001$ respectively), also after adjustment for potential confounders. We identified 2 clusters of MR phenotype patterns associated with glycemic status ($P < 0.001$), independent of the MR score (cluster II–metabolic specific: odds ratio, 2.49; 95% CI, 1.00–6.17; $P = 0.049$).

Discussion: Subjects with prediabetes and diabetes have a significantly higher phenotypic-based score with a distinctive multiorgan phenotypic pattern, which may enable improved disease characterization.

Key Words: epidemiology, prediabetes and diabetes, magnetic resonance imaging, risk assessment

(*Invest Radiol* 2018;53: 357–364)

Prevalence of diabetes is steadily increasing throughout developed and developing countries worldwide, representing one of the most common noncommunicable diseases globally with prevalence rates of 7.9% and 9.0% in women and men, respectively.[1,2] As a precursor stage of diabetes, prediabetes affects a substantial proportion of individuals and is defined as an impaired glucose metabolism not satisfying diabetes criteria but also incurring an elevated risk for cardiovascular events and adverse outcome.[3]

Detailed mechanisms in the pathophysiology of prediabetes and diabetes are poorly understood, but structural alterations in various organs are related to the development of impaired glucose metabolism, which in itself is a major risk factor.[4,5] In addition, previous studies found that nonalcoholic fatty liver disease (NAFLD) may be associated with low-grade chronic inflammatory state, affecting adipose tissue and resulting in abnormal glucose metabolism, increased oxidative stress, dyslipidemia, and endothelial dysfunction with progression of atherosclerosis.[6,7] Visceral adipose tissue (VAT), in turn, seems to be associated with an increased risk for hypertension, dyslipidemia, and prediabetes.[8] Furthermore, multiple prior studies demonstrated a correlation between metabolic risk factors and VAT as well as hepatic steatosis in prediabetes and diabetes.[9–12] In addition to that, white matter changes were previously shown to be associated with cardiovascular risk, cognitive decline, and impaired glucose metabolism and can be detected in patients with metabolic diseases.[13–15] Thus, the variety of metabolic and organ changes clarify the complex interrelationship of metabolic processes and the development of adverse outcome.

Magnetic resonance (MR) imaging can be used to derive strong prognostic multiorgan phenotypic parameters for the occurrence of metabolic alterations and cardiovascular events in patients with prediabetes and diabetes.[9,16,17] Relevant parameters include quantification of hepatic fat content by proton density fat fraction (PDFF), VAT, the cerebral age-related white matter changes (ARWMC) score, the left ventricular remodeling index (LVRI), carotid atherosclerotic plaque, as well as post-ischemic changes to the myocardium as evident by late gadolinium enhancement (LGE).[15,18–21] The noninvasive detection of these MR

Received for publication November 7, 2017; and accepted for publication, after revision, December 30, 2017.

From the *Department of Diagnostic and Interventional Radiology University of Tuebingen, Tuebingen; †Institute of Epidemiology II, Helmholtz Zentrum Muenchen, German Research Center for Environmental Health, Neuherberg; ‡Department of Radiology, Ludwig-Maximilians-University-Hospital; §German Center for Cardiovascular Disease Research (DZHK e.V.), Munich; ||Institute for Diabetes Research and Metabolic Diseases of the Helmholtz Centre Munich at the University of Tuebingen; ¶German Centre for Diabetes Research (DZD); #Section on Experimental Radiology, Department of Diagnostic and Interventional Radiology, University Hospital Tuebingen, Tuebingen; **Department of Biometry and Epidemiology, German Diabetes Center, Duesseldorf; ††KORA Myocardial Infarction Registry, Central Hospital of Augsburg, Augsburg, Germany; ‡‡Cardiac MR PET CT Program, Massachusetts General Hospital, Harvard Medical School, Boston, MA; §§Institute for Cardiovascular Prevention, Ludwig-Maximilians-University-Hospital, Munich; and ||||Department of Diagnostic and Interventional Radiology, University Hospital Heidelberg, Heidelberg, Germany.

Conflicts of interest and sources of funding: This study was funded by the German Research Foundation (DFG, Bonn, Germany), the German Centre for Cardiovascular Disease Research (DZHK, Berlin, Germany), and the German Centre for Diabetes Research (DZD e.V., Neuherberg, Germany).

The KORA study was initiated and financed by the Helmholtz Zentrum München–German Research Center for Environmental Health, which is funded by the German Federal Ministry of Education and Research (BMBF) and by the State of Bavaria.

The authors report no conflicts of interest.

Supplemental digital contents are available for this article. Direct URL citations appear in the printed text and are provided in the HTML and PDF versions of this article on the journal's Web site (www.investigativeradiology.com).

Correspondence to: Fabian Bamberg, MD, MPH, Department of Diagnostic and Interventional Radiology, University of Tuebingen, Hoppe-Seyler-Straße 3, 72076 Tuebingen, Germany. E-mail: Fabian.Bamberg@uni-tuebingen.de.

ISSN: 0020-9996/18/5306–0357
DOI: 10.1097/RLI.0000000000000451

imaging–based parameter may, on one hand, enable a better understanding of the pathophysiology in patients with metabolic diseases, especially in precursor states of diabetes disease, and, on the other hand, allow for an early detection of organic alterations. Summarizing, comprehensive MR imaging provides a detailed assessment of multiorgan alterations in subclinical disease state, which were separately shown to be associated with higher risk profile for adverse cardiovascular outcome.[22,23] Accordingly, the purpose of our study was to compare multiorgan subclinical disease phenotypes as determined by MR imaging between subjects with prediabetes, diabetes, and controls with normal glucose tolerance and to identify diabetic specific MR pattern differing from subjects with normal glucose tolerance. Our hypothesis was that there is a distinguishable multiorgan phenotypic MR pattern in patients with impaired glucose metabolism compared with subjects with normal glucose tolerance.

MATERIALS AND METHODS

Study Design

The study was approved by the institutional review board and all participants provided written informed consent.

The study was designed as a prospective case control study nested in a cohort from the Cooperative Health Research in the Region of Augsburg (KORA). As described elsewhere, subjects were recruited from the FF4 follow-up of the KORA study, representing a large sample from the general population in the region of Augsburg, Germany.[22,24] Subjects, aged between 25 and 74 years and recruited between 1999 and 2001, were enrolled in an MR substudy and examined between June 2013 and September 2014 at the KORA study center.[22] Subjects were excluded if they had any contraindications to either MR or gadolinium contrast administration. In addition, we included only subjects in this specific subanalysis with a complete set of all analyzed MR parameters. Thus, of overall 400 subjects who underwent whole-body MR imaging examinations, 157 participants were excluded due to incomplete MR imaging data sets (Supplementary Figure 1, Supplemental Digital Content 1, http://links.lww.com/RLI/A370).

While differences in single imaging markers of the overall cohort have been published previously,[22] the current analysis is tailored to the assessment of comprehensive whole-body MR imaging phenotypic markers.

Covariates

Subjects of the KORA cohort were reexamined between June 2013 and September 2014 at the KORA study center.[22] An oral glucose tolerance test was performed to all participants who had not been diagnosed for type 2 diabetes. According to the World Health Organization guidelines[25] and as described previously,[22,24] subjects were stratified into prediabetes, diabetes, and controls. Subjects who had been diagnosed with diabetes ≥7 years ago were defined as long-term diabetes patients, based on the median duration of diabetes subjects in our study population (n = 25), subjects with diabetes below this period were assigned to the group of short-term diabetes.

Other established risk factors such as hypertension, smoking, or increased body mass index (BMI) were collected in standardized fashion as part of the KORA study design and are described elsewhere.[22,24]

Magnetic Resonance Imaging—Acquisition and Image Analysis

As described previously, MR scans were performed with a 3 T whole-body MR system (Magnetom Skyra; Siemens AG, Healthcare Sector, Erlangen, Germany).[22] Details on the MR protocol comprising sequences of the whole body including the brain, cardiovascular system, and adipose tissue compartments are provided in Supplementary Table 1, Supplemental Digital Content 2, http://links.lww.com/RLI/A371.[22] All analyses were performed in blinded fashion by 2 independent readers each (overall 6 independent readers with ≥3 years of experience) unaware of the diabetic group and clinical covariates on dedicated offline workstations. In case of discrepancy, a consensus reading was performed. To allow for improved interpretability, cut-points representing binary normal versus abnormal results of MR parameters per subject were derived individually and included either known pathologic thresholds (ie, LGE or hepatic PDFF), established grading systems (ie, ARWMC), or the highest 75th percentile of a similar population (ie, VAT).

Assessment of White Matter Lesions

According to the ARWMC rating scale adapted from the Fazekas scale, FLAIR sequences were evaluated for T2 hyperintense area ≥5 mm lesions in 5 brain areas per hemisphere.[18,26] A total ARWMC value ranging from 0 to 30 was derived. As severity of ARWMC and diabetes is associated with cognitive decline, all subjects with a severity of ARWMC ≥1 (mild/moderate) were categorized as abnormal.[15]

Gadolinium Enhancement of the Myocardium

Late gadolinium enhancement was acquired on fast low-angle shot inversion recovery sequences in short-axis stack and a 4-chamber view 10 minutes after administration of gadopentetate dimeglumine (0.2 mmol/kg, Gadovist; Bayer Healthcare, Berlin, Germany). For the assessment of the presence and distribution pattern of LGE, the 17-segment model of the American Heart Association was used.[27] As LGE seems to be associated with adverse outcome in cardiomyopathy, the presence of LGE in any myocardial segment was considered as abnormal.[21]

Assessment of Left Ventricular Function

Cine-SSFP sequences were evaluated semi-automatically using commercially available software (cvi42, Circle Cardiovascular Imaging, Calgary, Canada) providing established LV volumetric data. The LVRI was calculated by the ratio of the LV mass to the LV end-diastolic volume.[28] Left ventricular remodeling index >1.3 represents architectural and functional changes in myocardium and was considered as abnormal.[20]

Assessment of Carotid Plaque

Presence and measures of atherosclerotic plaque in the common carotid artery, at the carotid bulb, and in the proximal internal carotid artery on both sides were determined on black-blood T1-weighted fat-suppressed sequences.[29] Any type of carotid plaque (type I, type III, type IV/V and type VI/VII) was considered as abnormal.[29]

Assessment of Hepatic PDFF

For the purpose of quantification of the hepatic PDFF, a multi-echo VIBE T1-weighted sequence for determination of hepatic PDFF by accounting for confounding effects of T2* decay and the spectral complexity of fat were performed.[30]

Hepatic PDFF was classified according to the estimated hepatic PDFF thresholds for dichotomized hepatic steatosis scoring system for NAFLD from the nonalcoholic steatohepatitis clinical research network ancillary study: grade 0 (<6.4% hepatic PDFF), grade 1 (≥6.4 to <17.4%), grade 2 (≥17.4 to <22.1%), and grade 3 (≥22.1%)[8]; hepatic steatosis grade ≥1 were considered as abnormal.[6,31]

Assessment of Visceral Abdominal Adipose Tissue

Visceral adipose tissue volume was measured from the femoral head to the cardiac apex, indicated in liter. High VAT levels seem to be related to adverse metabolic risk profiles, but studies about threshold levels associated with higher risk profiles are lacking. Thus, the determined cutoff value in our generated score is related to the 75% percentile volume-based VAT level of the healthy control group identified within the large-scale UK Biobank Imaging Study (median, 1.32 [0.86–1.79] L/m^2).[32] Visceral adipose tissue levels ≥1.79 L/m^2 were considered as abnormal.

Multiorgan MR Phenotypic Score

An unweighted numeric summation score representing the extent of organ areas affected by subclinical disease as measured by MR was calculated by the sum of parameters exceeding the defined thresholds (range, 0–6). To characterize the distribution of the summation score, mean and standard deviation were calculated in addition to a categorization into low (score ≤ 1), intermediate (score = 2), and high (score ≥3).

Statistical Analysis

Subject demographics and cardiovascular risk factors are presented as arithmetic means and standard deviations for continuous variables and counts (percentages) for categorical variables. Differences in dichotomized MR features according to diabetes group were assessed by χ^2 test. Differences in continuous MR features and in the multiorgan MR phenotypic score among diabetes groups were evaluated by one-way analysis of variance (ANOVA). Pairwise comparisons of multiorgan MR phenotypic score between short-/long-term diabetes and prediabetes were Bonferroni adjusted. Correlation between diabetes groups and multiorgan MR phenotypic score was tested by Spearman rank correlation coefficient.

To assess the association between diabetes groups and multiorgan MR phenotypic score, predicted score means with 95% confidence intervals (CIs) were calculated and compared by linear regression models adjusting for age, sex, smoking, BMI, hypertension, high-density lipoprotein, low-density lipoprotein, and triglycerides. Diabetes groups entered the model as a categorical variable with the 3 levels—control, prediabetes, and diabetes, with the control group as the reference group. Differences in baseline characteristics according to different multiorgan MR phenotypic score categories (low, intermediate, high as detailed above) were assessed by one-way ANOVA or χ^2 test. The predictive power among the different MR parameters and the score was compared by fitting logistic regression models and comparing the c-statistics, which is equivalent to the area under the ROC curve[33] using DeLongs nonparametric test of areas under the curve.

For the purpose of deriving underlying MR phenotypic patterns of the specific combinations of the dichotomized outcomes, unsupervised fuzzy clustering with a dissimilarity matrix given by Gower coefficient was used (Supplementary Figure 2, Supplemental Digital Content 1, http://links.lww.com/RLI/A370).[34] Correlation between the resulting 2 clusters and glycemic status was assessed by χ^2 test. Combinations of dichotomized outcomes associated to glycemic status were identified by LASSO regression. Variables that remained in the model with a nonzero coefficient after shrinkage were considered to be associated to glycemic status.[35] The shrinkage parameter λ was chosen as the minimum value after 10-fold cross validation. Fuzzy clustering and LASSO regression were carried out with R version 3.3.1 and packages cluster (v2.0.4) and glmnet (2.0-5). A 2-sided P value of less than 0.05 was considered to indicate statistical significance.

RESULTS

Among 243 white subjects with complete MR data sets, 48 subjects were classified as prediabetes and 38 subjects had established diabetes mellitus (20% and 16%, respectively). They were predominantly middle-aged (55.6 ± 8.9 years) with a slightly higher proportion of males (62%). Further demographics and risk profiles are provided in Table 1.

Significantly higher ARWMC levels were found in subjects with diabetes and prediabetes compared with controls with normal glucose tolerance (3.9 ± 3.2 vs 3.7 ± 4.3 vs 2.4 ± 3.1, $P = 0.013$; respectively). Similar differences were found for LVRI, hepatic PDFF, and VAT (all $P < 0.001$). Carotid plaque was detected more often in subjects with

TABLE 1. Patient Demographic Characteristics and Cardiovascular Risk Factors

	All	Control	Prediabetes	Diabetes
Variable	**N = 243**	**n = 157**	**n = 48**	**n = 38**
Age, y	55.6 ± 8.9	54.2 ± 8.8	55.9 ± 8.9	61.3 ± 7.5
Male sex	151 (62.1%)	89 (56.7%)	34 (70.8%)	28 (73.7%)
Height, cm	172.5 ± 9.2	172.5 ± 9.5	173.2 ± 9.7	171.8 ± 7.4
Weight, kg	82.2 ± 14.7	78.6 ± 13.6	90.0 ± 11.6	86.9 ± 17.5
BMI, kg/m^2	27.5 ± 4.2	26.3 ± 3.6	30.1 ± 4.3	29.3 ± 4.7
Waist-to-hip ratio	0.9 ± 0.1	0.9 ± 0.1	1.0 ± 0.1	1.0 ± 0.1
Duration of diabetes, median [first quartile, third quartile], y	7.0 [5.0, 12.0]	NA	NA	7.0 [5.0, 12.0]
HbA1c, %	5.6 ± 0.8	5.3 ± 0.3	5.6 ± 0.3	6.7 ± 1.5
Smoking				
Never-smoker	85 (35.0%)	58 (36.9%)	16 (33.3%)	11 (28.9%)
Ex-smoker	108 (44.4%)	63 (40.1%)	23 (47.9%)	22 (57.9%)
Smoker	50 (20.6%)	36 (22.9%)	9 (18.8%)	5 (13.2%)
Systolic blood pressure, mm Hg	120.5 ± 17.1	116.9 ± 15.6	125.9 ± 14.9	128.2 ± 21.3
Diastolic blood pressure, mm Hg	75.4 ± 9.8	74.0 ± 9.2	78.9 ± 9.6	76.6 ± 11.5
Total cholesterol, mg/dL	217.1 ± 35.5	215.9 ± 34.7	228.0 ± 30.6	208.2 ± 41.9
HDL cholesterol, mg/dL	61.3 ± 17.5	64.3 ± 17.2	57.1 ± 13.8	54.1 ± 20.0
LDL cholesterol, mg/dL	139.6 ± 32.2	138.9 ± 30.4	150.1 ± 30.2	129.2 ± 38.3
Triglycerides, mg/dL	134.1 ± 87.1	111.3 ± 71.3	161.4 ± 93.4	193.8 ± 101.3
Hypertension	77 (31.7%)	30 (19.1%)	21 (43.8%)	26 (68.4%)
Antihypertensive medication	57 (23.5%)	23 (14.6%)	14 (29.2%)	20 (52.6%)
Antithrombotic medication	12 (4.9%)	2 (1.3%)	3 (6.2%)	7 (18.4%)
Lipid lowering medication	26 (10.7%)	8 (5.1%)	3 (6.2%)	15 (39.5%)

Data are presented as mean ± standard deviation for continuous variables and counts and percentages for categorical variables, unless otherwise indicated.
NA indicates not available; LDL, low-density lipoprotein; HDL, high-density lipoprotein.

TABLE 2. Overview of Affected Organ Systems Among Subjects With Prediabetes, Diabetes, and Controls and Differences in Multiorgan MR Phenotypic Score Among Groups

	All	Control	Prediabetes	Diabetes	
	N = 243	n = 157	n = 48	n = 38	*P*
Brain					
Total ARWMC Score, mean ± SD	2.9 ± 3.4	2.4 ± 3.1	3.7 ± 4.3	3.9 ± 3.2	0.013
Subjects with total ARWMC score ≥ 1, n (%)	151 (62.1%)	88 (56.1%)	32 (66.7%)	31 (81.6%)	0.01
Cardiac					
LVRI, mean ± SD	1.1 ± 0.3	1.0 ± 0.2	1.3 ± 0.3	1.4 ± 0.4	<0.001
Subjects with LVRI >1.3, n (%)	51 (21.0%)	17 (10.8%)	18 (37.5%)	16 (42.1%)	<0.001
Subjects with presence of LGE	5 (2.1%)	2 (1.3%)	1 (2.1%)	2 (5.3%)	0.3
AHA myocardial segments involved	1, 2, 4, 4, 4	2, 4	1	4, 4	
Atherosclerosis					
Subjects with presence of carotid plaque, n (%)	49 (20.2%)	26 (16.6%)	16 (33.3%)	7 (18.4%)	0.04
Visceral organ					
PDFF, mean ± SD	8.2 ± 8.2	4.9 ± 4.8	12.6 ± 7.9	16.2 ± 11.4	<0.001
Subjects with PDFF ≥ 6.4%, n (%)	95 (39.1%)	33 (21.0%)	33 (68.8%)	29 (76.3%)	<0.001
Subjects with grade 1 PDFF, n (%)	57 (23.5%)	25 (15.9%)	20 (41.7%)	12 (31.6%)	
Subjects with grade 2 PDFF, n (%)	15 (6.2%)	4 (2.5%)	4 (8.3%)	7 (18.4%)	
Subjects with grade 3 PDFF, n (%)	23 (9.5%)	4 (2.5%)	9 (18.8%)	10 (26.3%)	
Adipose tissue					
VAT, mean ± SD, L/m^2	4.4 ± 2.6	3.4 ± 2.1	5.8 ± 2.2	6.7 ± 2.6	<0.001
Subjects with VAT ≥ 1.79 L/m^2, n (%)	83 (34.2%)	25 (15.9%)	29 (60.4%)	29 (76.3%)	<0.001
Multiorgan MR phenotypic score, mean ± SD	1.79 ± 1.35	1.22 ± 0.98	2.69 ± 1.50	3.00 ± 1.04	<0.001

Data are presented as mean ± standard deviation for continuous variables and counts and percentages for categorical variables, unless indicated otherwise. *P* values are from χ^2 test or one-way ANOVA. PDFF grade 1: PDFF ≥ 6.4% but <17.4%. PDFF grade 2: PDFF ≥ 17.4% but < 22.1%. PDFF grade 3: PDFF ≥ 22.1%.

AHA indicates American Heart Association; MR, magnetic resonance; ARWMC, age-related white matter changes; LVRI, left ventricular remodeling index; LGE, late gadolinium enhancement; PDFF, proton density fat fraction of the liver; VAT, visceral adipose tissue.

prediabetes and diabetes compared with controls ($P = 0.04$). The presence of LGE was rare (2.1% of all 243 subjects).

The prevalence of these MR features, dichotomized based on previously published cutoffs, are detailed in Table 2.

Multiorgan MR Phenotypic Score

On average, the multiorgan MR phenotypic score was 1.79 ± 1.35 and ranged from 0 to 5. Subjects with prediabetes and diabetes had significantly higher scores compared with controls with normal glucose tolerance ($P < 0.001$; Table 2, Supplementary Figure 3, Supplemental Digital Content 1, http://links.lww.com/RLI/A370). These differences remained significant after multivariable adjustment for age, sex, smoking, BMI, hypertension, high-density lipoprotein, low-density lipoprotein, and triglycerides ($P < 0.001$, Fig. 1). The multiorgan MR phenotypic score provided the highest discriminatory power to predict prediabetes and diabetes as compared with single MR features (area under the curve, 0.824) and provided the highest risk estimate (odds ratio [OR], 25.92; 95% CI, 10.83–62.05, for high vs low score, Table 3).

When comparing subjects with long-term, short-term, and newly diagnosed diabetes mellitus, there were no differences in MR phenotypic score between the groups (MR phenotypic score: 3.1 ± 1.0 vs 2.9 ± 1.2 vs 2.8 ± 1.1, $P = 0.16$, for long-term vs short-term vs newly diagnosed diabetes mellitus; respectively).

MR Phenotype Pattern between Subgroups

The frequency distribution of MR features in controls and subjects with prediabetes and diabetes stratified by extent of multiorgan MR phenotypic score is shown in Figures 2 and 3. Among controls with low score, a high prevalence of elevated ARWMC was found (47,5%), while only in a small proportion of these subjects, hepatic PDFF, carotid

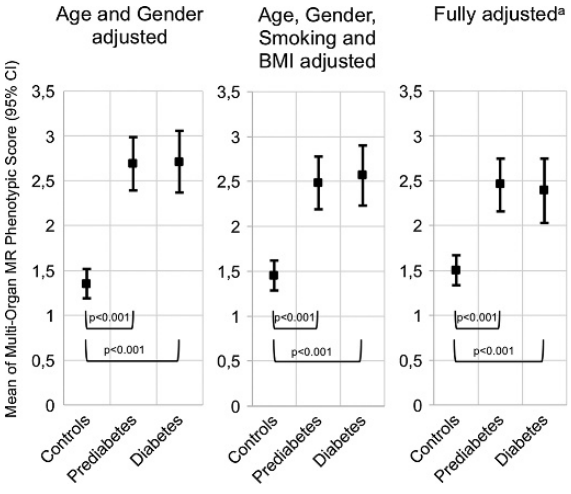

FIGURE 1. Predicted means of multiorgan MR phenotypic score after adjustment by linear regression analysis. Higher means of multiorgan MR phenotypic score were independently associated with impaired glucose metabolism ($P < 0.001$). *Adjusted for age, sex, smoking, body mass index, hypertension, high-density lipoprotein, low-density lipoprotein, and triglycerides.

TABLE 3. Risk and Discriminatory Power of MR Phenotypic Score and Single MR Parameters to Predict Metabolic Disease State (Prediabetes and Diabetes) Adjusted for Age and Sex

	OR	95% CI	*P*	AUC	*P**
MR Phenotypic Score					
Numeric	3.03	2.21–4.16	<0.001	0.824	
Intermediate vs low	2.38	1.04–5.42	0.0392	0.812	0.119
High vs low	25.92	10.83–62.05	<0.001		
Single MR parameters					
ARWMC	1.83	1–3.38	0.0513	0.674	<0.001
LVRI	4.64	2.34–9.21	<0.001	0.728	<0.001
Plaque	1.59	0.82–3.09	0.173	0.673	<0.001
LGE	2.12	0.34–13.31	0.422	0.670	<0.001
PDFF	8.99	4.68–17.26	<0.001	0.787	0.066
VAT	10.11	5.04–20.27	<0.001	0.774	0.017

**P* value from DeLongs test if AUC of MR phenotypic Score (numeric) is larger than AUC of each single parameter.

OR indicates odds ratio; CI, confidence interval; AUC, area under the curve; ARWMC, age-related white matter changes; LVRI, left ventricular remodeling index; LGE, late gadolinium enhancement; PDFF, proton density fat fraction of the liver; VAT, visceral adipose tissue.

plaque, VAT, or myocardial changes were detected (6.9%, 5.0%, 2.0%, 4.0%, and 0.0% for hepatic PDFF, carotid plaque, VAT, LVRI, and LGE, respectively). The prevalence increased continuously among controls resulting in highest prevalence of hepatic PDFF and VAT in control subjects with high multiorgan MR phenotypic score (85.7% and 78.6%, respectively). Similarly, among subjects with prediabetes and diabetes and low score, the prevalence of ARWMC and hepatic PDFF was highest (31.2% and 18.8%, respectively). Among subjects with prediabetes and diabetes and high score, the prevalence of hepatic PDFF and VAT was highest (91.1% and 92.9%, respectively). We found significantly higher ARWMC, LVRI, hepatic PDFF, and VAT levels in subjects with prediabetes and diabetes and high score compared with subjects with prediabetes and diabetes and low score (Fig. 3) (all $P < 0.001$).

MR-Based Cluster Analysis

Assessing the combination of normal and abnormal MR parameters (ARWMC, hepatic PDFF, VAT, LVRI, carotid plaque, and LGE) in each subject, unsupervised fuzzy clustering revealed 2 different

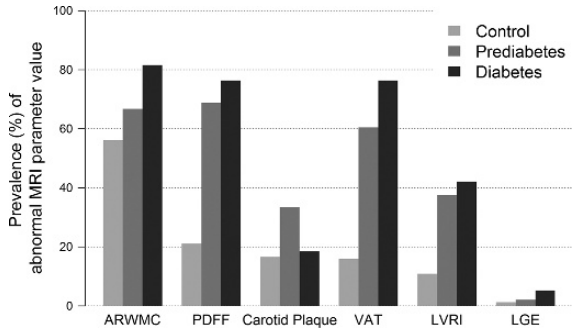

FIGURE 2. Prevalence of MR-based parameters among controls, prediabetes, and diabetes patients. ARWMC indicates age-related white matter changes; PDFF, hepatic proton density fat fraction; VAT, visceral adipose tissue; LVRI, left ventricular remodeling index; LGE, late gadolinium enhancement.

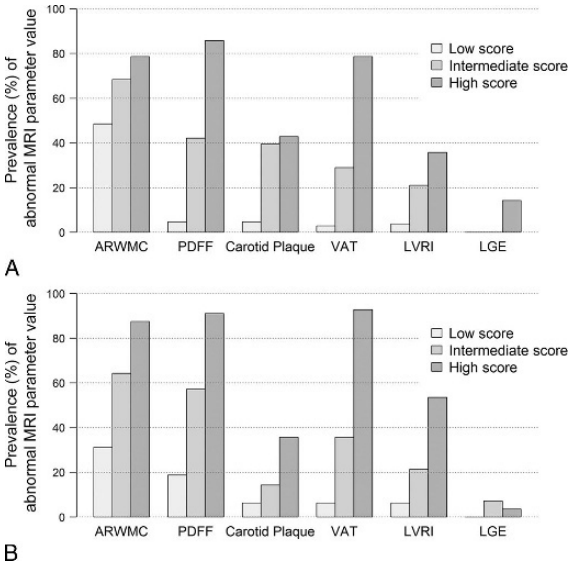

FIGURE 3. Frequency distribution of MR-based parameters among low-, intermediate-, and high-score ranges (0–1, 2, and ≥3, respectively) between controls (A) and patients with prediabetes and diabetes (B). ARWMC denotes age-related white matter changes; PDFF, hepatic proton density fat fraction; VAT, visceral adipose tissue volume; LVRI, left ventricular remodeling index; LGE, late gadolinium enhancement.

multiorgan phenotypic clusters (Supplementary Figure 2, Supplemental Digital Content 1, http://links.lww.com/RLI/A370) which were significantly associated with glycemic status ($P < 0.001$). After adjustment for high multiorgan MR phenotypic score, cluster II was still independently associated with prediabetes/diabetes group (OR, 10.05; 95% CI, 3.75–27.00, $P = <0.001$). Within the group with low multiorgan MR phenotypic score, cluster II was also significantly associated to diabetes status (OR, 2.49; 95% CI, 1.00–6.17, $P = 0.049$). No further prediabetes-specific cluster could be identified. Figure 4 presents the distribution of the observed 33 combinations of dichotomized MR parameters (of theoretically possible 64 combinations) that occurred in the sample according to glycemic status and cluster membership. LASSO regression revealed that the MR feature combinations of only abnormal ARWMC and of only abnormal ARWMC plus carotid plaque were associated with normal controls, while all MR feature combination patterns associated with prediabetes/diabetes included hepatic PDFF and VAT beside other abnormal MR parameters (Figs. 4, 5).

DISCUSSION

In this sample from the general population, we characterized multiorgan involvement of subclinical disease phenotypes between subjects with impaired glucose metabolism and controls. While our results demonstrate that the overall prevalence and distribution of MR variables representing metabolic alterations is significantly elevated among subjects with prediabetes and diabetes as compared with controls, our findings also indicate that metabolic organ alterations, such as elevated LVRI, hepatic PDFF, and increased VAT volumes, are mainly affected in subjects with higher scores. We also identified distinctive multiorgan phenotypic patterns in subjects with prediabetes or diabetes status, which are specific for metabolic disease.

Metabolic organ alterations, for example, the fatty degeneration of internal organs such as the liver (ie, NAFLD), seem to be associated with chronic inflammatory state, which affects the adipose tissue and

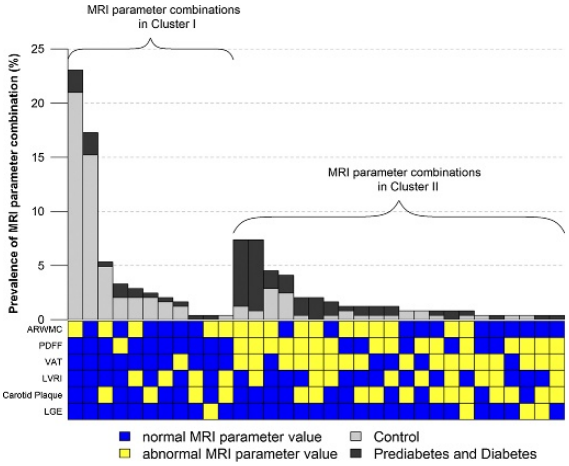

FIGURE 4. Distribution of specific combinations of dichotomized MR phenotypic parameters. Each MR phenotypic parameter is binary and may either be normal/negative (blue) or abnormal/positive (yellow). Among 64 possible combinations of MR phenotypic parameters, 33 combinations were observed. Each column in the figure represents the prevalence of a specific combination in the whole sample. The percentage of subjects with prediabetes/diabetes is shown as black; the gray columns display the control group. There were 2 clusters of MR phenotype patterns associated with glycemic status ($P < 0.001$), independent of the MR score. Cluster II was independently associated with diabetes state (odds ratio, 2.49; 95% confidence interval, 1.00–6.17; $P = 0.049$). ARWMC indicates age-related white matter changes; PDFF, hepatic proton density fat fraction; VAT, visceral adipose tissue volume; LVRI, left ventricular remodeling index; LGE, late gadolinium enhancement.

contribute to the complex pathomechanism of the development of an abnormal glucose metabolism, increased oxidative stress, dyslipidemia, and endothelial dysfunction with accelerated atherosclerosis and microangiopathy and macroangiopathy.[6] These changes lead to liver diseases and dysfunctional cardiometabolic phenotypes, which result in a higher risk for adverse cardiovascular events and mortality.[6,10] In addition, high levels of VAT are associated with cardiometabolic risk factors and are accompanied with the development of dyslipidemia and impaired glucose metabolism.[8,9,36]

In summarizing individual findings in multiple organs, we confirm earlier evidence pertaining to single findings. Specifically, hepatic PDFF is known to be associated with VAT and adverse metabolic risk profiles, independent of standard anthropometric indexes such as the BMI.[36] Similarly, white matter lesions, supposed as result of cerebrovascular origin, were found to be independent risk factors for cognitive decline and previous studies observed an association between changes in the white matter of the brain and diabetic disease.[15,37] In addition, LGE, representing myocardial fibrosis, and LVRI, a measure for structural changes in affected myocardium, were found to be reliable factors for the assessment of structural and functional changes[19,21] and represent strong predictors of adverse cardiovascular outcome and impaired cardiac function.[19,21] While we found that these specific MR phenotypes are elevated in subjects with diabetes and prediabetes, we found more subjects with higher LVRI indices in the high score as compared with subjects in the low-score group. However, we found a high percentage of ARWMC among controls with low MR score, which can be traced back to the fact that white matter lesions can also be caused by inflammatory vessel processes and hypertensive diseases, which may lead to the assumption that ARWMC represents an early detectable MR pattern with high prevalence in adult population, representing cardiovascular changes.[38,39] Interestingly, we found a substantially lower prevalence of 5.3% of LGE in our diabetic population as compared with a prior analysis in Korean population (15%), which may be attributable to the fact that these subjects underwent clinically indicated MR imaging due to suspected coronary artery disease and were retrospectively included.[40] Also, in contrast to Yoon et al, we excluded subjects with history of stroke or peripheral artery disease, which may further decrease likelihood of presence of disease. As such, our results may be generalizable to a general asymptomatic population without prior known cardiovascular disease only.

Our findings may indicate that risk factors such as high adipose tissue levels or fatty liver disease may occur relatively early within the course of diabetes disease and may lead to the end point of irreversible organic architectural and functional changes especially in the myocardium, caused by impaired glucose metabolism.[8–10] In addition, there was no difference in multiorgan MR phenotypes between subjects with long-term and short-term or newly diabetes mellitus, which may be attributable to the overall high effectiveness of currently available treatment options once diagnosed in this sample from a western European general population.

More importantly, by utilizing an MR imaging approach, we performed a multiparametric assessment of different clusters representing different combinations of phenotypic patterns that occurred in our study sample. This cluster analysis reveals a number of relevant findings. First, subjects with prediabetes and diabetes were assigned to the same cluster (Supplemental Figure 2, Supplemental Digital Content 1, http://links.lww.com/RLI/A370). In contrast, unsupervised cluster analysis could not identify a distinct phenotypic cluster for subjects with prediabetes, confirming the close metabolic relationship between the 2 hyperglycemic disease entities observed when applying the multiorgan MR phenotypic Score. Second, we identified distinctive clusters and specific phenotype patterns of healthy controls and subjects with prediabetes and diabetes. Subjects with normal glucose tolerance (healthy controls) mainly show MR parameter combinations of abnormal changes in ARWMC and carotid plaque only, with LVRI in higher score levels to some extent, whereas additional changes including hepatic PDFF and VAT are more likely in subjects with prediabetes and diabetes. This observation illustrates the distinctive multiorgan pattern in subjects with impaired glucose metabolism and outlines the importance of metabolic alterations such as hepatic PDFF and VAT representing the strongest contributors for the assessment of metabolic differences as compared with healthy controls. Third, the MR phenotypic cluster was associated with diabetes state, independent of a high multiorgan MR phenotypic score, thus providing incremental information in characterizing hyperglycemic disease manifestation as demonstrated by its superior discriminatory power compared with single MR parameter assessment. Overall, these results suggest that a comprehensive, detailed clustering-based assessment of subclinical MR phenotypes may provide incremental value in characterization of early metabolic changes and identifying the individual extent and risk profile of involvement of different organ systems, even in subclinical stages.

Our study has several limitations. First, our study assesses the cross-sectional association of imaging findings and clinical disease types. While this may be highly relevant for gaining more insights into the disease process, clinical relevance and consequence for patient management will need to be determined in longitudinal cohorts. Unfortunately, at this point in time, we have no outcome data available to determine the prognostic value of the MR phenotypic score. However, this MR phenotypic score provides a baseline for all subsequent analysis along the longitudinal course of our study and allows to integrate the multiorgan imaging into a sum estimate to display the extent of subclinical disease in patients with impaired glucose metabolism. Notably, studies on the definition of "normal versus abnormal" threshold levels of MR-based parameters derived from healthy cohorts are scarce, and there is a lack of uniform cutoff

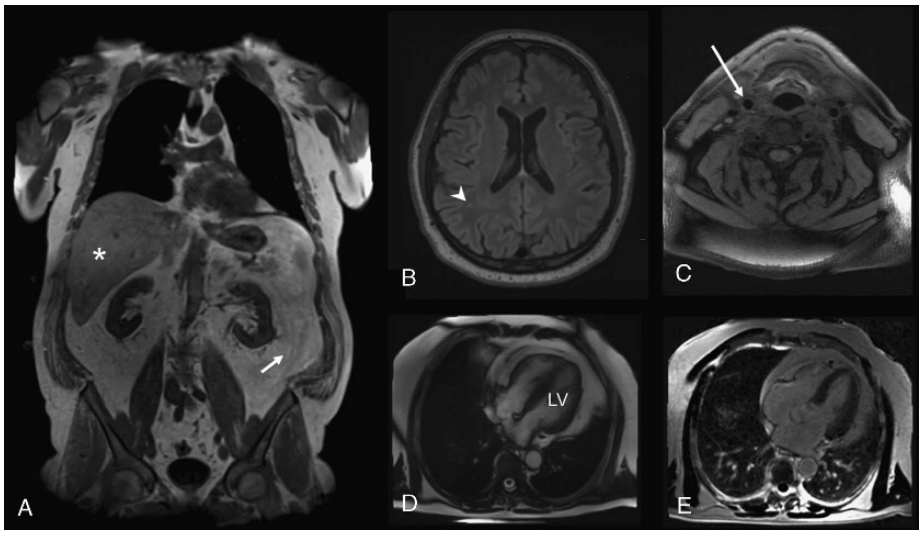

FIGURE 5. Imaging findings in a 61-year-old male as part of the study protocol. A, Two-point DIXON T1-weighted sequence for the assessment of visceral adipose tissue (VAT) volume from the femoral head to the cardiac apex (arrow) indicating high levels of VAT as well as hepatic proton density fat fraction (asterix, measured on multi-echo VIBE T1-weighted sequences). B, Fluid-attenuated inversion recovery sequences demonstrating mild white matter lesions (arrowhead). C, Atherosclerotic carotid plaque was determined on black-blood T1-weighted fat suppressed sequences in the common carotid artery (arrow), the carotid bulb, and the proximal internal carotid artery. D, Cine-SSFP sequences were evaluated for the calculation of volume and mass left ventricle (LV). F, late gadolinium enhancement was detected on fast-low-single-shot inversion recovery sequences 4-chamber view. The overall MR phenotypic score in this subject totaled 4.

levels associated with higher risk profiles. Thus, we applied heterogeneous definitions of thresholds, which were previously found to be strongly associated with impaired glucose metabolism and/or associated with higher cardiovascular risk and adverse outcome in an unweighted fashion.[22] For instance, the presence of LGE was previously found to be associated with an 8-fold increased risk of an adverse cardiovascular event, whereas an ARWMC score >1 is associated only with mild or moderate risk for adverse cardiovascular outcomes.[15,21] We applied 1.79 l/m^2 as a threshold level for VAT, which represents the 75th percentile in a large-scale population-based healthy sample from UK Biobank Imaging Study and was associated with increased of risk for adverse outcome and corresponds to the 84th percentile in our population.[32] It is clear that the thresholds we applied as well as the unweighting of parameters are preliminary and will require further adjustment once novel pertaining research findings occur. Thus, further research is clearly warranted but our findings may serve as a hypothesis-generating reference. Finally, the study was conducted in a southern German general population, and all subjects were white, thus the generation of our results to different settings is limited.

In our study population without prior cardiovascular disease, subjects with prediabetes and diabetes have significantly higher multiorgan involvement of subclinical disease as compared with subjects with normal glucose tolerance and feature a diabetes-specific pattern of MR imaging phenotypes. These specific disease patterns are accentuated when performing cluster analysis, which revealed distinctive hyperglycemic multiorgan phenotypic clusters of subclinical disease manifestation in subjects with impaired glucose metabolism, containing more metabolic organ alterations as compared with control subjects including elevated levels of hepatic PDFF and VAT volume as well as structural cardiac changes such as LVRI. With this study, we demonstrate that diabetes and prediabetes is associated with a multiorgan footprint that can be identified and quantified by MR imaging. Furthermore, MR imaging may provide a more detailed assessment of the extent of subclinical disease and multiorgan alterations, which were previously shown to be associated with higher risk for cardiovascular events and adverse outcome and may therefore justify a more complex and costly imaging procedure. As such, MR imaging may provide detailed insights into metabolic disease process and pathogenesis and thus may enable an individual characterization of disease states and improve risk stratification.

REFERENCES

1. NCD Risk Factor Collaboration (NCD-RisC). Worldwide trends in diabetes since 1980: a pooled analysis of 751 population-based studies with 4.4 million participants. *Lancet*. 2016;387:1513–1530.
2. King H, Aubert RE, Herman WH. Global burden of diabetes, 1995–2025: prevalence, numerical estimates, and projections. *Diabetes Care*. 1998;21:1414–1431.
3. Danaei G, Lawes CM, Vander Hoorn S, et al. Global and regional mortality from ischaemic heart disease and stroke attributable to higher-than-optimum blood glucose concentration: comparative risk assessment. *Lancet*. 2006;368:1651–1659.
4. Aneja A, Tang WH, Bansilal S, et al. Diabetic cardiomyopathy: insights into pathogenesis, diagnostic challenges, and therapeutic options. *Am J Med*. 2008;121:748–757.
5. Shah RV, Abbasi SA, Heydari B, et al. Insulin resistance, subclinical left ventricular remodeling, and the obesity paradox: MESA (Multi-Ethnic Study of Atherosclerosis). *J Am Coll Cardiol*. 2013;61:1698–1706.
6. Bhatia LS, Curzen NP, Calder PC, et al. Non-alcoholic fatty liver disease: a new and important cardiovascular risk factor? *Eur Heart J*. 2012;33:1190–1200.
7. Stefan N, Kantartzis K, Haring HU. Causes and metabolic consequences of fatty liver. *Endocr Rev*. 2008;29:939–960.
8. Tang L, Zhang F, Tong N. The association of visceral adipose tissue and subcutaneous adipose tissue with metabolic risk factors in a large population of Chinese adults. *Clin Endocrinol (Oxf)*. 2016;85:46–53.
9. Goodpaster BH, Krishnaswami S, Resnick H, et al. Association between regional adipose tissue distribution and both type 2 diabetes and impaired glucose tolerance in elderly men and women. *Diabetes Care*. 2003;26:372.
10. Cusi K. Nonalcoholic fatty liver disease in type 2 diabetes mellitus. *Curr Opin Endocrinol Diabetes Obes*. 2009;16:141–149.
11. Stefan N, Fritsche A, Schick F, et al. Phenotypes of prediabetes and stratification of cardiometabolic risk. *Lancet Diabetes Endocrinol*. 2016;4:789–798.
12. Kantartzis K, Machann J, Schick F, et al. The impact of liver fat vs visceral fat in determining categories of prediabetes. *Diabetologia*. 2010;53:882–889.

13. Hsu JL, Chen YL, Leu JG, et al. Microstructural white matter abnormalities in type 2 diabetes mellitus: a diffusion tensor imaging study. *Neuroimage*. 2012; 59:1098–1105.
14. van Harten B, de Leeuw FE, Weinstein HC, et al. Brain imaging in patients with diabetes: a systematic review. *Diabetes Care*. 2006;29:2539–2548.
15. Verdelho A, Madureira S, Moleiro C, et al. White matter changes and diabetes predict cognitive decline in the elderly: the LADIS study. *Neurology*. 2010;75: 160–167.
16. Idilman IS, Keskin O, Celik A, et al. A comparison of liver fat content as determined by magnetic resonance imaging-proton density fat fraction and MRS versus liver histology in non-alcoholic fatty liver disease. *Acta Radiol*. 2016;57: 271–278.
17. Wintersperger BJ, Bamberg F, De Cecco CN. Cardiovascular imaging: the past and the future, perspectives in computed tomography and magnetic resonance imaging. *Invest Radiol*. 2015;50:557–570.
18. Fazekas F, Chawluk JB, Alavi A, et al. MR signal abnormalities at 1.5 T in Alzheimer's dementia and normal aging. *AJR Am J Roentgenol*. 1987;149: 351–356.
19. Yoon JH, Son JW, Chung H, et al. Relationship between myocardial extracellular space expansion estimated with post-contrast T1 mapping MRI and left ventricular remodeling and neurohormonal activation in patients with dilated cardiomyopathy. *Korean J Radiol*. 2015;16:1153–1162.
20. Gaasch WH, Zile MR. Left ventricular structural remodeling in health and disease: with special emphasis on volume, mass, and geometry. *J Am Coll Cardiol*. 2011;58:1733–1740.
21. Wu KC, Weiss RG, Thiemann DR, et al. Late gadolinium enhancement by cardiovascular magnetic resonance heralds an adverse prognosis in nonischemic cardiomyopathy. *J Am Coll Cardiol*. 2008;51:2414–2421.
22. Bamberg F, Hetterich H, Rospleszcz S, et al. subclinical disease burden as assessed by whole-body MRI in subjects with prediabetes, subjects with diabetes, and normal control subjects from the general population: the KORA-MRI study. *Diabetes*. 2017;66:158–169.
23. Bamberg F, Kauczor HU, Weckbach S, et al. Whole-body MR imaging in the german national cohort: rationale, design, and technical background. *Radiology*. 2015;277:206–220.
24. Holle R, Happich M, Löwel H, et al. KORA—a research platform for population based health research. *Gesundheitswesen*. 2005;67(suppl 1):S19–S25.
25. Press W. World Health Organization. Definition and diagnosis of diabetes mellitus and intermediate hyperglycemia. In: *Publications of the World Health Organization*. Geneva, Switzerland: World Health Organization; 2006.
26. Wahlund L, Barkhof F, Fazekas F, et al. A new rating scale for age-related white matter changes applicable to MRI and CT. *Stroke*. 2001;32:1318–1322.
27. American College of Cardiology Foundation Task Force on Expert Consensus Documents, Hundley WG, Bluemke DA, Finn JP, et al. ACCF/ACR/AHA/NASCI/SCMR 2010 expert consensus document on cardiovascular magnetic resonance: a report of the American College of Cardiology Foundation Task Force on Expert Consensus Documents. *J Am Coll Cardiol*. 2010;55:2614–2662.
28. Lamb HJ, Beyerbacht HP, de Roos A, et al. Left ventricular remodeling early after aortic valve replacement: differential effects on diastolic function in aortic valve stenosis and aortic regurgitation. *J Am Coll Cardiol*. 2002;40:2182–2188.
29. Cai JM, Hatsukami TS, Ferguson MS, et al. Classification of human carotid atherosclerotic lesions with in vivo multicontrast magnetic resonance imaging. *Circulation*. 2002;106:1368–1373.
30. Hetterich H, Bayerl C, Peters A, et al. Feasibility of a three-step magnetic resonance imaging approach for the assessment of hepatic steatosis in an asymptomatic study population. *Eur Radiol*. 2015.
31. Kleiner DE, Brunt EM, Van Natta M, et al. Design and validation of a histological scoring system for nonalcoholic fatty liver disease. *Hepatology*. 2005;41: 1313–1321.
32. Dahlqvist Leinhard O, Linge J, West J, et al *Body composition profiling using MRI - normative data for subjects with diabetes extracted from the UK Biobank Imaging Cohort. Radiological Society of North America 2016 Scientific Assembly and Annual Meeting*. Chicago, IL: 2016.
33. Hanley JA, McNeil BJ. The meaning and use of the area under a receiver operating characteristic (ROC) curve. *Radiology*. 1982;143:29–36.
34. Gower JC. A general coefficient of similarity and some of its properties. *Biometrics*. 1971;27:857–871.
35. Friedman J, Hastie T, Tibshirani R. Regularization paths for generalized linear models via coordinate descent. *J Stat Softw*. 2010;33:1.
36. Fox CS, Massaro JM, Hoffmann U, et al. Abdominal visceral and subcutaneous adipose tissue compartments: association with metabolic risk factors in the Framingham Heart Study. *Circulation*. 2007;116:39–48.
37. Weckbach S, Findeisen HM, Schoenberg SO, et al. Systemic cardiovascular complications in patients with long-standing diabetes mellitus: comprehensive assessment with whole-body magnetic resonance imaging/magnetic resonance angiography. *Invest Radiol*. 2009;44:242–250.
38. de Leeuw FE, de Groot JC, Oudkerk M, et al. Hypertension and cerebral white matter lesions in a prospective cohort study. *Brain*. 2002;125(pt 4):765–772.
39. van Dijk EJ, Prins ND, Vermeer SE, et al. C-reactive protein and cerebral small-vessel disease: the Rotterdam Scan Study. *Circulation*. 2005;112:900–905.
40. Yoon YE, Kitagawa K, Kato S, et al. Prognostic value of unrecognised myocardial infarction detected by late gadolinium-enhanced MRI in diabetic patients with normal global and regional left ventricular systolic function. *Eur Radiol*. 2013; 23:2101–2108.

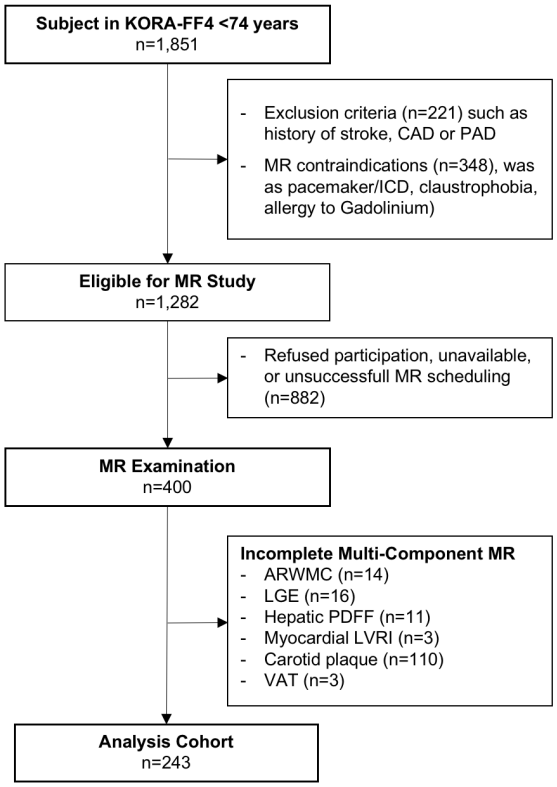

Supplemental Figure 1: Study flow chart. CAD, coronary artery disease; PAD peripheral artery disease; ARWMC, age-related white matter changes; PDFF, proton-density-fat-fraction; VAT, visceral adipose tissue volume; LVRI, left ventricular remodeling index; LGE, late gadolinium enhancement; MR, magnetic resonance.

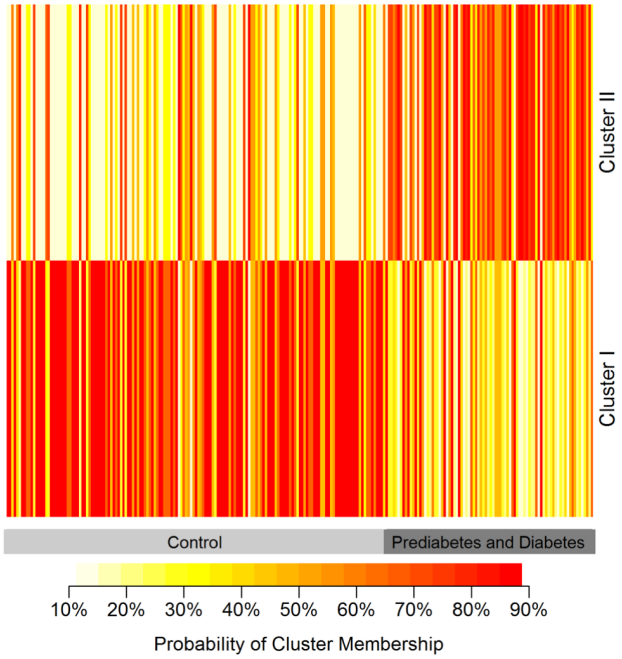

Supplemental Figure 2: Results of unsupervised fuzzy clustering by separation of two clusters. In general, subjects within a cluster are considered "similar" to each other with respect to the six dichotomized MRI parameters and "dissimilar" to the subjects in the other cluster. Unsupervised clustering includes no prior knowledge on glycemic status. The similarity/dissimilarity between the subjects is then calculated based the on the distances in their MRI parameters by Gower's general dissimilarity coefficient, which is appropriate for dichotomized data. Based on these distances, each subject is assigned a probability of membership to each cluster. The figure demonstrates the membership probabilities for both clusters for N = 243 individuals, sorted by glycemic status. The lower row displays the probability for each subject to belong to Cluster I whereas the upper row displays the probability to belong to Cluster II. Probabilities are color-coded according to the legend and always add up to one for a single subject. The figure shows that control subjects are more likely to belong to Cluster I, indicated by probabilities in darker red in the lower row, whereas subjects with prediabetes or diabetes are more likely to belong to Cluster II, indicated by

probabilities in darker red in the upper row. A χ^2 test reveals that the clusters are significantly associated to glycemic status (χ^2 statistic: 64.7, p-value < 0.001).

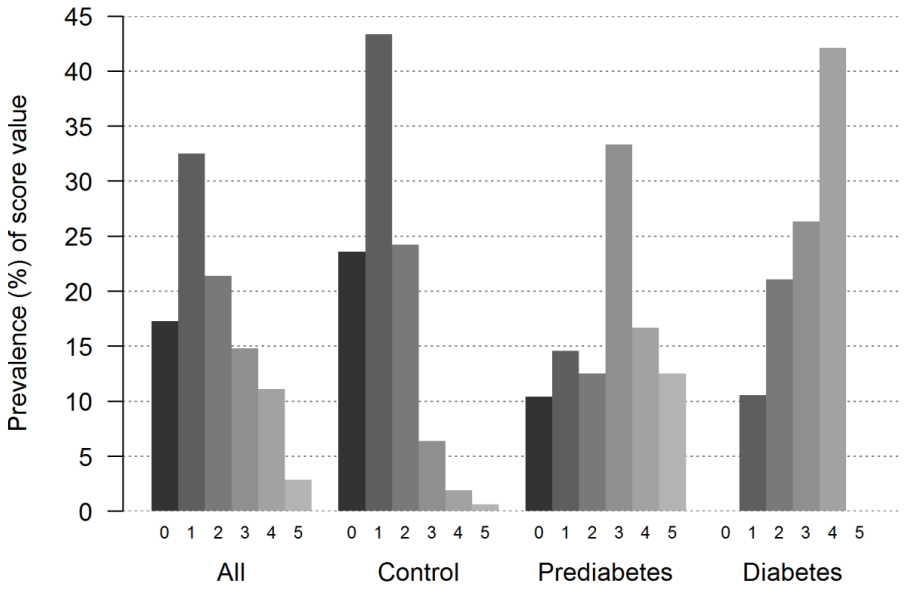

Supplemental Figure 3: Prevalence of MR phenotypic score among controls, patients with prediabetes and diabetes (score range: 0 to 6). There was no subject with maximum score.

Acknowledgements

Zunächst möchte ich ganz herzlich meiner Betreuerin Annette Peters danken, die es mir ermöglicht hat, in diesem spannenden Bereich meine Doktorarbeit zu schreiben und mir den Schatz der KORA-MRT Daten anvertraut hat. Ohne ihre geduldige Betreuung und Unterstützung, und ohne ihr unerschütterliches Vertrauen in meine Arbeit wäre dieses Projekt nicht zu bewerkstelligen gewesen.

Herzlicher Dank geht auch an Ulrich Mansmann und Wolfgang Koenig, die mir als TAC Mitglieder mit ihrem statistischen und medizinischen Fachwissen zur Seite standen.

Ein ganz großes Dankeschön an Roberto Lorbeer für die fantastische Zusammenarbeit von Anfang an, und die vielen spannenden statistischen Probleme, die wir zusammen gelöst haben.

Ich danke den "Radiologen": allen Koautorinnen und Koautoren aus diversen radiologischen Kliniken und Instituten, mit denen ich für so viele faszinierende Projekte zusammengearbeitet habe und von denen ich so viel gelernt habe. Zu danken habe ich besonders Corinna Storz, für die vielen interessanten Auswertungen und Einblicke in die unterschiedlichsten Bereiche, Christopher L. Schlett, für die Begeisterung für die statistische Modellierung, Sigrid Auweter, für die hilfreiche Einarbeitung ganz am Anfang, Sophia Stöcklein, für die tolle Zusammenarbeit bei den Machine-Learning Projekten, Holger Hetterich, für die Führung in Großhadern und die Erklärung wie ein MRT funktioniert, und natürlich Fabian Bamberg, der mich mit ins KORA-MRT Team aufgenommen hat.

Meinen Kolleginnen und Kollegen vom Institut für Epidemiologie am Helmholtz Zentrum München danke ich für die Unterstützung und die angenehme Arbeitsatmosphäre. Ganz ausdrücklich möchte ich Andrea Schneider, Mainsi Marowsky-Köppl und Andrea Wulff danken, die alle Datensätze für mich zusammengestellt haben und ohne deren Hilfe mir das wissenschaftliche Arbeiten nicht möglich gewesen wäre.

Außerdem danke ich Wolfgang Lieb für die gute Zusammenarbeit bei unserem gemeinsamen Projekt, Karoline Lukaschek für hilfreiche Gespräche und Diskussionen, und Konstantin Strauch, der mir meine ersten Schritte in der Epidemiologie möglich gemacht hat.

Ich danke meinen beiden Schwestern Eliana und Sabine, und meinen Freundinnen und Freunden, die während der Doktorarbeit immer für mich da waren, ohne die das alles viel weniger Spaß gemacht hätte, und die einfach ganz großartig sind.

Zum Schluss möchte ich meinen Eltern, Anke und Hans-Herbert Rospleszcz, danken, die mir so vieles ermöglicht haben, mir immer Rückhalt gegeben und mich immer unterstützt haben. Dafür bin ich unendlich dankbar. Ihnen ist diese Arbeit in Liebe gewidmet.